INVESTIGATING THE INTEGRITY OF THE VASCULATURE AND STRUCTURAL RELATIONSHIPS OF PERICYTES, ASTROCYTES AND THE ENDOTHELIAL GLYCOCALYX IN AN *EX VIVO* HYPERGLYCAEMIC RAT RETINAL MODEL

Dr Glory Chinuru Musa, *MBBS*

Student number: MSXGLO002

Dissertation Submitted for the Degree of Master of Science (MSc) in Medicine Specialising in Physiology (HUB5004W)

Department of Human Biology

Faculty of Health Sciences, University of Cape Town

Supervisor: A/Prof Elizabeth Van der Merwe

Co-supervisors: A/Prof Asfree Gwanyanya

Dr Ashwin Isaacs (Technical)

August 2022

DECLARATION

I, **Glory Chinuru Musa**, hereby declare that the work on which this dissertation is based is my original work (except where acknowledgements indicate otherwise) and that neither the whole work nor any part of it has been, is being, or is to be submitted for another degree in this or any other university. I empower the university to reproduce for the purpose of research either the whole or any portion of the contents in any manner whatsoever.

Signature: Signed by candidate

Date: 17 August 2022

ACKNOWLEDGEMENT

My sincere gratitude goes to my main supervisor A/Prof Elizabeth Van der Merwe, for her continuous mentoring, patience and enormous support throughout this project, and especially with imaging; you are much valued, Prof. I would like to express my most profound appreciation to my co-supervisor A/Prof Asfree Gwanyanya for his persistent guidance and knowledge impacting style; your assistance throughout this research journey has been credible. I could not have wished for better supervisors; I have tapped into your wealth of experience gained excellent research skills through their hearty tutelage. To Dr Ashwin Isaacs, my technical supervisor, I sincerely appreciate your kind assistance in the histology laboratory.

Special thanks to the South African Medical Research Council (SAMRC) for funding this research. Top up bursaries were also gratefully received from my supervisor's SAMRC and UCT URC grants. I appreciate the help of all the staff and support staff of the HUB department. Thank you to A-K Samuels, Thabisa in the research animal unit, for your prompt responses when due. To my colleagues, Viantha Naidoo, thank you for putting me through laboratory principles from the onset of my work. Many thanks to Hamida Agboalgalm for your kind support and time throughout my work in the laboratory. Deena, Amanda, Kauthar, Nikhil, Stephanie, Mayur, thank you all for making my stay in the lab memorable; your suggestions were valuable. Mrs Susan Cooper thanks for the training at the confocal. To Prof Lang, thank you for the support you provided to us during this project.

To my dear Husband, Dr Ezekiel Musa, words cannot express my heartfelt gratitude to you; your unending support to me has been enormous; thank you for your encouragement to venture into being a clinician-scientist, as I look back at the hustles and challenges, we passed through in this journey, I couldn't have wished for a better you. Thank you for particularly helping with

the statistical analysis of this work. To my beloved children, Shalom and Shadrach, thank you for your patience and your soft prayers even when you were too young to understand the reason for my seasonal absence and inattention throughout these years of study. I love you.

To my Parents, Dr and Mrs R.U Okoro, you set the pace for giant strides; I express my profound gratitude, thank you for your tender love and prayers; more is yet to come. Many thanks to my siblings, your kind words and prayers even amid uncertainties is highly appreciated, and to my extended family and in-laws, you are the best. To my family friends at JP Duminy Court, Mowbray, Cape Town, I appreciate your willingness to support in caring for my children while I was away on many occasions; may it be rewarded. DLCF University of Cape Town, I appreciate the spiritual support.

Above all, all glory be to God Almighty who has given me health and sound mind to go through this highly engaging academic process.

TABLE OF CONTENTS

LIST OF FIGURES

LIST OF TABLES

LIST OF ABBREVIATIONS

AEC	Animal ethics committee
AGES	Advanced glycation end products
BBB	Blood brain barrier
BCA	Bicinchoninic Acid
BRB	Blood Retinal Barrier
BSA	Bovine Serum Albumin
CNS	Central nervous system
DABCO	1, 4-diazabicyclo (2.2.2) octane
DCCT/EDIC	Diabetes Control and Complications Trial/Epidemiology of Diabetes Interventions and Complications
DM	Diabetes mellitus
DMEM	Dulbecco's Modified Eagle Medium
DR	Diabetic retinopathy
ELISA	Enzyme-linked immunosorbent assay
FBS	Foetal bovine serum
FITC	Fluorescein isothiocyanate

GFAP	Glial fibrillary acidic protein
HIF-1a	Hypoxia-inducible factor-1a
HRP	Horseradish peroxidase
HSF	Heat shock transcription factors
Hsps	Heat shock proteins
IDF	International Diabetes Federation
IGF-1	Insulin-like growth factor-1
K-H	Krebs-Henseleit
MDPK	Myotonic dystrophy protein kinase
mRNA	Messenger ribonucleic acid
NG2	Neuron-glial antigen 2
NPDR	Non-proliferative diabetic retinopathy
ODF	Outer dense fibre protein
PBS	Phosphate buffered saline
PBST	Phosphate-buffered saline tween
PDR	Proliferative diabetic retinopathy
PFA	Paraformaldehyde

PVDF	Polyvinylidene fluoride
RIPA	Radioimmunoprecipitation assay
ROI	Regions of interest
SAVC	South African Veterinary Council
SDS	Sodium deoxycholate sulphate
sHsps	small Heat shock proteins
UCT	University of Cape Town
UK	United Kingdom
UKPDS	United Kingdom Prospective Diabetes Study
USA	United States of America
VEGF	Vascular endothelial growth factor
αSMA	Alpha-smooth muscle actin

ABSTRACT

Background: Diabetes mellitus-induced retinopathy is the leading cause of adult-onset blindness. The retinopathy is characterised by the degeneration of the retinal microvascular and neural components that form the blood retinal barrier (BRB), and is due to diabetic metabolic derangements such as hyperglycaemia. The cellular components of the BRB include endothelial cells, pericytes and the glial cells (mainly astrocytes), which together maintain the integrity and barrier function of the retinal vasculature. However, there is limited data regarding the interconnecting biochemical pathways that lead to pericyte loss, astrocyte degeneration, and endothelial dysfunction as well as the thinning of the glycocalyx in the retinal vasculature of diabetics. As such, the underlying mechanism of how hyperglycaemia induces retinal damage is not fully understood, particularly at the early stages of the disease.

Aim and Objectives: To establish and validate an *ex vivo* rat retinal model and use a multi-immunolabelled approach on the retina to study the effects of hyperglycaemia on the vasculature and cellular components of the BRB, including effect of time and the retinal preparation type.

Methods: Eyes of euthanised Wistar and Sprague-Dawley adult rats (n = 68) were enucleated and the retinae were either dissected out (explant) or kept in situ after removal of the anterior segment, lens and vitreous (eyecup). Retinae were superfused continuously (for 1-, 2- or 3 hours) in a chamber with oxygenated Krebs-Henseleit buffer containing either physiological glucose (5.5 mmol/L; control group) or high glucose (25 mmol/L; hyperglycaemic group). For longer incubation (48 hours), explants were cultured in Dulbecco's Modified Eagle Medium containing the above glucose concentrations. Retinae were multi-immunolabelled to identify pericytes, astrocytes and the glycocalyx protein syndecan-1 with anti-neuron-glial 2 antigen

(NG2), anti-glial fibrillary acidic protein (GFAP), and anti-syndecan-1 antibodies respectively. Retinal blood vessels were detected with FITC-conjugated lycopersicon esculentum (Tomato) lectin. Fluorescent signals were detected using confocal microscopy imaging where Z-stack images were randomly sampled from the mid-peripheral retina. Images were analysed using Image J software. Additionally, western blotting was used to determine the abundance of syndecan-1 and heat shock proteins in the rat retina. P value < 0.05 was considered statistically significant.

Results: Retinal blood vessels, pericytes and astrocytes showed normal morphology in both explant and eyecup of normoglycaemia retinae, with no difference in fluorescence intensity between explant and eyecup preparations at each time point (1-3 hours). Similarly, there was no change in the vascular-associated syndecan-1 signal intensity over time. However, the syndecan-1 intensity was generally weak and localised mainly to the retinal arteries and their branches, but rarely in capillaries and was unevenly distributed throughout the entire retina in both retinal preparation types. Under hyperglycaemia, at the 3-hour time point of perfusion, the vessel width was reduced in the eyecup group, the neuron glial 2 (NG2) fluorescence intensity on pericytes was diminished with a noticeable reduction in number of pericyte nuclei bulge in the lower vascular bed in the explant and eyecup groups. Although the area coverage and fluorescence signal intensity of astrocytes did not change, retraction of astrocyte processes and signs of cellular disintegration were more evident in the hyperglycaemic eyecup group compared to that in the explant group. Syndecan-1 signal intensity was raised in hyperglycaemia compared to controls in the eyecup group. The preliminary investigation on retinae cultured for 48 hours showed signs of fragmentation and morphological deterioration of the BRB, which included narrowing of blood vessels, loss of pericytes and disintegration of astrocytes, especially in the hyperglycaemic group. Syndecan-1 signal intensity was also lower

in the hyperglycaemic groups compared to the control groups cultured for 48 hours . Syndecan-1 protein abundance in the 3-hour superfused retina using western blotting was significantly higher in the hyperglycaemic group than in control. Heat shock proteins showed higher expression in hyperglycaemic rat retina compared to the normoglycaemic group.

Conclusion: This study validated the suitability of the *ex vivo* rat retinal model to study the components of the BRB. The study revealed that there is no significant difference between the retinal preparations (explants vs eyecup) and that the BRB is still structurally intact up to 3 hours in normoglycaemic conditions. The subtle morphological changes of the BRB (blood vessels, pericytes and astrocytes) induced by hyperglycaemia which were more apparent in the lower vascular layers, suggests that this *ex vivo* model is suitable to study the early pathogenesis of diabetic retinopathy. Furthermore, this study showed that syndecan-1 levels were affected by hyperglycaemia *ex vivo,* and that this occurred prior to morphological changes to the other BRB structures, thus supporting the notion that syndecan-1 plays a role in the pathophysiology of DR. Preliminary data suggest that heat shock proteins may play a role in response to hyperglycemia-induced oxidative stress.

CHAPTER 1 INTRODUCTION

1.1 Definition and epidemiology of diabetes mellitus

Diabetes mellitus (DM) is a major health problem globally and is reported to be the leading cause of adult-onset blindness worldwide.[1, 2] The prevalence of DM is rapidly increasing globally, particularly in low and middle-income countries predominantly due to obesity, unhealthy diet, physical inactivity, poor health systems, increased ageing and genetic susceptibility.[3-5] According to the 2019 International Diabetes Federation (IDF) report, 463 million people are living with DM worldwide, with the low and middle-income countries accounting for the most incidences.[2] It is projected that the global prevalence of DM will rise to 700 million by 2045.[2] In Africa and South Africa, the prevalence of DM in 2019 is estimated to be 3.9% and 5.3%, according to the IDF report, respectively.[2] Alarmingly, it is estimated that half the number of people diagnosed with DM are undiagnosed, and two-thirds of diabetics are of working age (20-79 years), causing a significant negative social and economic impact.[2] This further suggests that a large proportion of the working age population, particularly those with type 2 DM, are likely to present for the first time with DM complications. DM is associated with chronic microvascular and macrovascular complications, especially in those with poor glycaemic control.[6] Landmark studies such as the United Kingdom Prospective Diabetes Study (UKPDS) and Diabetes Control and Complications Trial/Epidemiology of Diabetes Interventions and Complications (DCCT/EDIC) have demonstrated that intensive insulin treatment is associated with a reduction in microvascular complications in both type 1 and 2 DM.[7, 8] The duration of diabetes mellitus has been reported to have a directly proportional relationship with microvascular complications. Chawla et al. demonstrated the presence of microvascular disease in 25–40% of diabetic patients across different age groups with a duration of diabetes more than 5 years.[9]

Among the chronic microvascular complications of DM, diabetic retinopathy (DR) is the most common and has been reported to affect about 100 million people worldwide, amounting to a huge healthcare burden.[10, 11] Visual impairment caused by diabetic retinopathy is one of the earliest presenting signs for most diabetics.[12] Therefore, identifying early eye changes in the retina can lead to earlier therapeutic interventions to reduce this morbidity. Of interest to this study, are changes in the retinal vasculature and Blood Retinal Barrier (BRB) that are associated with the early onset of DR. The BRB is comprised of retinal blood vessels lined by a single layer of tightly adherent endothelial cells attached to a basal lamina, which is surrounded by smooth muscles cells in retinal arteries/arterioles and a continuous layer of pericytes that surround the retinal capillaries.[13, 14] In addition, glial cells (particularly astrocytes) have a close structural and functional association with the retinal capillaries. The following sections will review these key components that make up the BRB and important cellular relations and their structural characteristics and functions in DR.

1.2 Complications of diabetes mellitus

DM is a metabolic disorder characterised by chronic hyperglycaemia with disruption of carbohydrate, lipid and protein metabolism due to insulin secretory defect, insulin resistance or both.[15] Poorly controlled blood glucose leads to long term dysfunction and damage of organs such as the eyes, heart, kidneys, nerves and blood vessels, making DM the leading cause of adult-onset blindness, end-stage renal disease and lower limb non-traumatic amputation globally.[2, 6] These complications can be categorised into acute and chronic complications. Acute complications include hypoglycaemia, hyper-osmolar hyperglycaemic state and diabetic ketoacidosis.[15] Chronic complications of DM are associated with vascular pathology and plays a leading role in diabetic morbidity and mortality. On the one hand, macrovascular disease manifests as myocardial infarction, cerebrovascular accidents, and peripheral vascular disease.

On the other hand, microvascular disease (microangiopathy) is a frequent long-term sequel of DM that culminates in nephropathy, neuropathy and retinopathy, and the latter will be reviewed in more detail below.[16]

1.3 Pathogenesis of diabetic retinopathy

Diabetic retinopathy is a severe microvascular complication of poorly controlled DM and is reported to be the major cause of blindness.[17] It is characterised by vessel damage, capillary hyperpermeability, loss of pericytes, capillary occlusion, shedding of the endothelial glycocalyx layer and loss of astrocytes. DR is classified as either proliferative or non-proliferative, with proliferative being characterised by the growth of new blood vessels (retinal neovascularisation). Proliferative diabetic retinopathy (PDR) and diabetic maculopathy are the leading causes of severe visual loss.[18] Most patients with Type 1 diabetes and over 60% of patients with Type 2 diabetes are at risk of retinopathy within the first decade of developing diabetes.[19, 20] PDR occurs due to the formation of new vessels that is a sequel to severe retinal ischaemia.[21] Non-proliferative diabetic retinopathy (NPDR) is classified into mild, moderate, and severe forms, with or without the involvement of macular oedema development.[22] The mechanisms underlying NPDR are abnormal permeability of retinal capillaries and closure of capillaries leading to retinal oedema and retinal non-perfusion and ischemia respectively.[22] The significant reasons for visual loss in PDR are vessels haemorrhage and retinal detachment. In untreated patients, approximately 50% may proceed to blindness within five years.[22]

The underlying mechanism of how hyperglycaemia leads to retinal microvascular damage is still unclear. However, several interconnecting biochemical pathways that have been proposed and tested as major contributors in the development of diabetic retinopathy include increased polyol pathway, activation of protein kinase C and sorbitol pathways, accumulation of

advanced glycation end products (AGES), oxidative stress, activation of the renin-angiotensin-aldosterone system, inflammation, capillary occlusion and growth factors expression such as vascular endothelial growth factor (VEGF) and insulin-like growth factor-1(IGF-1), endothelial dysfunction and procoagulability state.[23, 24] In diabetes, the polyol pathway is activated and metabolises excess glucose through the action of the enzyme aldose reductase present in the various retinal cells into sorbitol. Sorbitol dehydrogenase then converts sorbitol into fructose. Since sorbitol does not penetrate cellular membranes, it accumulates within the cell, and eventually, sorbitol is metabolised to fructose.[25] The accumulation of sorbitol is believed to have osmotic damage to retinal cells.[26] Studies have reported high levels of aldolase reductase in several retinal cells such as pericytes[27], Müller cells[28], retinal endothelial cells,[28, 29] ganglion cells[28, 30] and neuronal cells.[30] These studies have reported that increased activity of aldolase reductase leads to damage of these retinal cells. The pathophysiological mechanisms involved in the development of diabetic retinopathy is summarised in Figure 1.1.

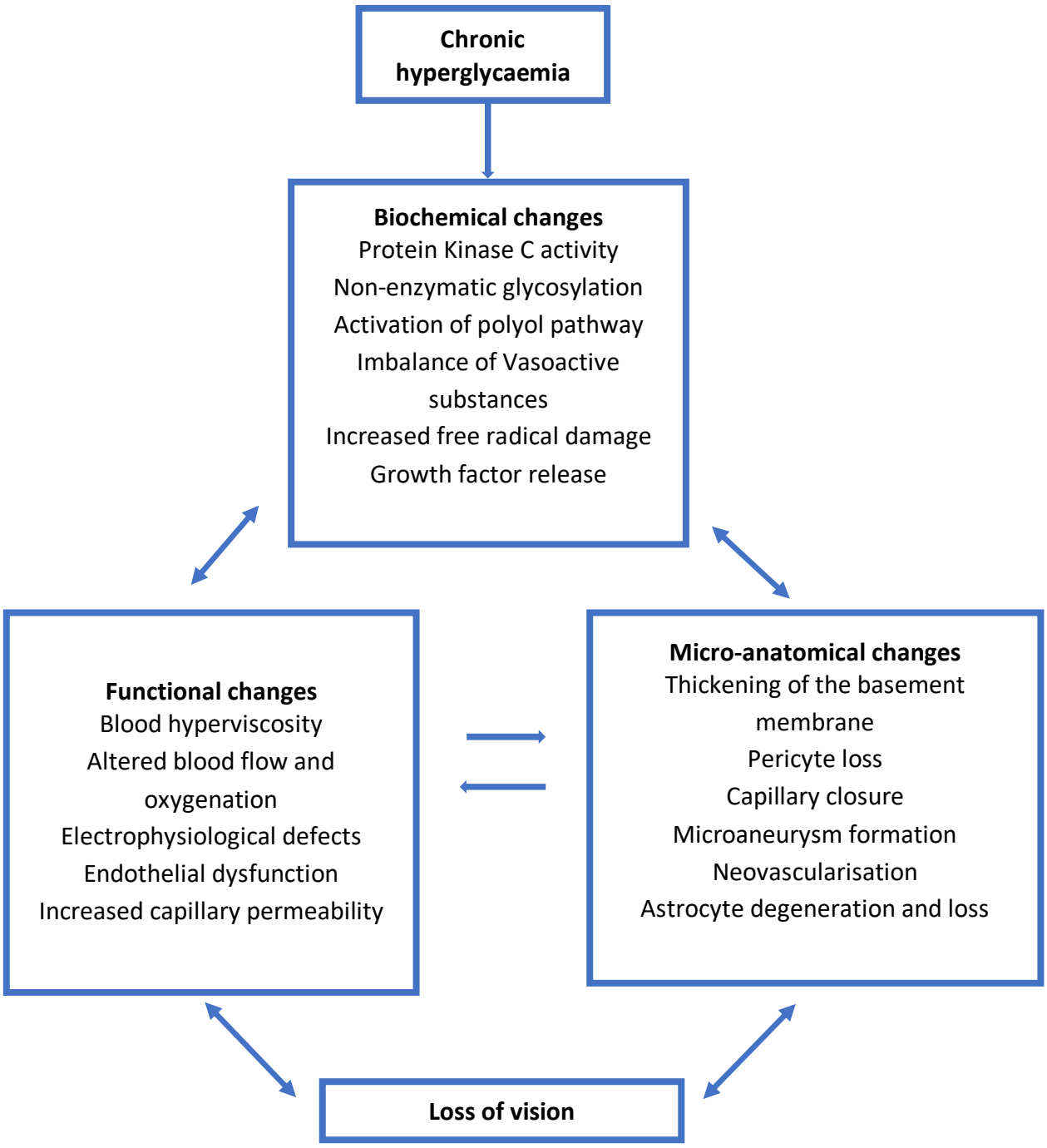

Figure 1.1. Pathogenic mechanisms involved in the development of diabetic retinopathy. *Adapted from Simo et al.*[31]

1.4 Blood retinal barrier and diabetic retinopathy

The BRB is a selective physical barrier that consists of tightly joined cells that regulate the movement of molecules and solutes across the retina.[13] The BRB comprises of two functional compartments, which includes the inner and outer BRB compartments that consist of adherence and tight junctions of the vascular endothelial cells and retinal pigment epithelium, respectively.[32, 33] The retinal endothelium of the inner BRB is covered by pericytes. Like the tightness of blood brain barrier (BBB), the BRB is being attributed to adherent and tight junctions located between endothelial cells.[14] The coverage of pericytes on the BRB is paramount in forming a structurally mature barrier and helps maintain the barrier function and tissue homeostasis. These pericytes, together with the endothelium, glial and neuronal cells, form the neurovascular unit.[34] The glial cells such as astrocytes are important in maintaining retinal neurons and blood vessel function. They also modulate the function of the BRB via the antioxidants and trophic factors released in the retinal microenvironment.[35] The BRB integrity is maintained by endothelial tight and adherence junctions that form a tight monolayer to prevent free penetration of macromolecules across the retinal unit.[36] The hallmark of diabetic retinopathy is blood retinal barrier breakdown, sequel to chronic hyperglycaemia and is associated with pericytes death and decline in endothelial function.[37] These cascade of events lead to visual loss as a result of macular oedema as well as vitreoretinal neovascularization.[38, 39]

1.5 Functions of the endothelial glycocalyx

The glycocalyx layer, a membrane-bound glycolipid, is an essential component of the vascular endothelial layer.[40] It is primarily made up of negatively charged proteins and lipid side-chains.[41] Syndecan-1 protein, encoded by the *SDC1* gene in humans, is a vital component of the vascular endothelial glycocalyx structure and has been demonstrated to mediate cellular

function by interacting with their receptors.[42-44] The endothelial glycocalyx provides a physical barrier between the vascular wall and blood, thereby regulating the transportation of cellular components and ions across the vascular endothelium.[40, 45, 46] It has been shown to promote vascular dilatation through shear stress-induced nitric oxide production.[47] In addition, the endothelial glycocalyx also modulates inflammation, which is one of the mechanisms mediating retinal vascular disease in diabetes,.[48, 49] The disruption of the endothelial glycocalyx results in vascular hyperpermeability, inflammatory responses and activation of the coagulation pathway.[45, 46] The endothelial glycocalyx is compromised in retinal blood vessels in DM where thinning of the glycocalyx, seen in retinal arteriole but not venules has been demonstrated, clearly indicating an alteration in the glycocalyx integrity in DM.[50] Furthermore, shedding of glycocalyx components, particularly syndecan-1 in many chronic inflammatory states such as cardiovascular disease and DM has been reported.[51-53] In diabetes, syndecan-1 is shed systemically, and increased levels are found in the blood of DM patients, but little is known about its expression in the retina of diabetic persons. Insights into the potential role of the endothelial glycocalyx in diabetic retinopathy may serve to provide evidence for the development of targeted therapeutic approaches for the treatment of diabetic retinopathy.

1.6 Role of pericytes in vascular endothelial function

Perivascular cells and endothelial cells are two critical vascular cellular components that interact to maintain vascular integrity, function and regeneration.[54] Pericytes are specialised perivascular cells that are also known as Rouget or mural cells which surround arterioles, venules and capillaries throughout the body where they modulate vascular tone and capillary bed integrity as well as regulating blood flow, vessel permeability, and stabilization.[55, 56] Also, pericytes by interacting with endothelial cells regulate neovascularisation via the regulation of vessels formation and stabilisation effect during wound healing as well as having a role in

inflammation by directly inducing inflammatory responses in endothelial cells and perivascular infiltration of macrophages.[57]

Pericytes were first reported over 100 years ago as perivascular cells surrounding capillaries.[58] They have a prominent nucleus and a small cytoplasm content with several long processes embracing the endothelium wall. They have been found to express alpha-smooth muscle actin (αSMA), a contractile filamentous component that mainly indicates vascular smooth muscle cells.[59] Pericytes are often found embedded within the basement membrane of small vessels,[60] and communicate with endothelial cells through paracrine signalling pathways and direct physical contact. Gap junctions are important mediators of the physical connection between pericytes and the endothelial cells and allow for ions and small molecules exchange.[61] Pericytes are anchored to the endothelial cells by adhesion plagues.[62] The ratio of pericytes to endothelial cells differ according to various vascular regions of the body, and varies from 1:1 in the retina and central nervous system, 1:10 in the skin and lungs, and 1:100 in striated muscle.[63] Degeneration of retinal pericytes has been reported at early stages of retinopathy in mouse models of diabetes.[64, 65] Pericyte loss is the earliest sign of diabetic retinopathy prior to vascular permeability and progressive vascular occlusion, but the cause remains unclear.[60] Understanding the role of these cells in early diabetes may aid in developing a future therapeutic intervention that targets the pericytes.

1.7 Astrocyte interaction within the retinal vasculature

Glial cells secrete cytokines by interacting with retinal vessels to modulate the BRB that are essential for maintaining the normal function of the retina.[66, 67] They are involved in neurotransmission, transport of energy metabolites from the vasculature to neurons and BRB integrity maintenance.[68] Microglial and macroglial cells are present in the retina. Microglial

cells are CNS inflammatory cells that play a significant role in the pathogenesis and progression of diabetic retinopathy, and its activation has also been reported as an early sign of diabetic retinopathy.[69, 70] In the retina, astrocytes and Müller cells are the two main types of macroglial cells.[67 71] Astrocytes are produced from different progenitor cells in the CNS neuroepithelium, and they are characteristically stellate in their morphology. Most astrocytes in the CNS cells express the glial fibrillary acidic protein (GFAP).[72, 73] In the retina, astrocyte cell bodies and processes are almost entirely restricted to the nerve fibre layer that overlies the ganglion cell layer. Both astrocytes and Müller cells have processes surrounding retinal blood vessels forming the glia limiting membrane where they regulate various endothelial cell functions.[67] Macroglial cells secrete neurotransmitters, eicosanoids, steroids, neuropeptides, and growth factors such as VEGF, as well as maintaining both the ion balance and pH of the retinal environment.[68] The specific role of astrocytes in retinal function is still not fully understood as their processes do not project into the synaptic layer of the retina. Therefore, they cannot similarly modulate neuronal function as the Müller cells involved in removing neurotransmitters through high affinity or potassium buffering.[67, 74] Astrocytes are reported to play a critical role in ion homeostasis neuronal signalling as well as the formation of retinal endothelial properties.[75] Overall, macroglial cells provide functional and structural support to the BRB through crosstalk between neural and vascular endothelial cells; and alteration of these critical functions may lead to adverse retinal damage.[67] Overall, in diabetic retinopathy, the breakdown of the BRB leads to vascular leakage (hyperpermeability).[76] Denuded capillaries and microglial cell proliferation and loss or death of astrocytes have been reported in rodent models of type 2 diabetes.[64]

1.8 Small heat shock proteins and DR

Oxidative stress is highly implicated in the pathogenesis of DR**.** The metabolic dysfunction seen in diabetes leads to the overproduction of mitochondrial superoxide in endothelial cells of macro and microvessels. This increased superoxide production results in the activation of major pathways involved in the pathogenesis of complications.[77] Expression of stress proteins is markedly elevated in numerous pathological and pathophysiological conditions such as hyperthermia, hypoxia, ischemia, endotoxins, and reactive oxygen species and are shown to proffer protection against tissue damage. These stress proteins are also called heat shock proteins (Hsps). Chronic hyperglycaemia found in diabetes may impose cellular stress on the retina. There is a group of low molecular weight Hsps ranging from 16 to 27 kDa in monomer size, called small Hsps (sHsps). These sHsps are heterogeneous with a characteristic feature of a conserved C-terminal region, called the α-crystallin domain. Ten Hsps exist in mammals and include HspB1, myotonic dystrophy protein kinase (MDPK) (HspB2), HspB3, α-crystallin A (HspB4), α-crystallin B (HspB5), HspB6, HspB7, HspB8, HspB9 and sperm outer dense fibre protein (HspB10). The Hsps were derived using the human Hsp27 protein sequence present in the human genome.[78, 79] Small Hsps function as molecular chaperones by inhibiting protein aggregation during stress; they also play a role in cellular processes such as maintaining cytoskeleton architecture, intracellular protein transport and antiapoptotic events.[80, 81] It has been reported that heat shock response is regulated by heat shock transcription factors, such as HSF1, HSF2 and HSF4. HSF1 mediates many heat shock genes and responds to external stressors such as hyperthermia. HSF2 is involved in cellular differentiation and development; the third, HSF4, regulates postnatal expression of Hsps expression.[82] In diabetes, studies have reported increased expression of MDPK, HspB3 and αBC in the retina.[83] In diabetic rat retina, increased αA-crystallin, αBC and Hsp22 expression but decreased Hsp20 expression was demonstrated.[84] Furthermore, increased Hsp27 mRNA levels and reduced protein expression

were reported. The study also showed that the expression of HSFs was reduced or remained unchanged in the diabetic rat retina. Also, Hsp27, αAC, αBC and pS59-aBC aggregation was induced in the retina. Strong Hsp27, αAC, αBC and phosphorylated αBC immunoreactivity was localised in different retinal layers of diabetic.[84]

1.9 Previous experimental approaches on rodents and relevance to this study

Different experimental approaches have been used to evaluate the presence of pericytes, astrocytes and the endothelial glycocalyx, which are implicated in the pathogenesis of diabetic retinopathy. Enzyme linked immunosorbent assay (ELISA) has been used to demonstrate the presence of soluble syndecan-1 in the ocular vitreous in non-diabetic individuals and those with diabetic retinopathy.[53] The study further found that mean levels of vitreous soluble syndecan-1 were higher in PDR patients compared to their non-diabetic counterparts.[53] ELISA has been used to investigate serum syndecan-1 levels where syndecan-1 concentrations were found to be higher in type 2 diabetic patients compared to controls.[44]

Toh et al. investigated the early vascular retinal changes in diabetic Nile rats by correlating increased acellular capillaries and pericyte loss with the duration of diabetes.[85] Here, they utilised retinal whole-mounts and transverse sections stained with isolectin GS-IB_4 conjugated to Alexa-647 to label retinal blood vessels and microglial cells following induction of diabetes. They found that diabetic rats exhibited a spectrum of retinal lesions mostly seen in humans, including vascular leakage, capillary non-perfusion and neovascularisation, and decreased pericyte-to-endothelial cell ratio and pericyte loss over time in early retinopathy.[85] Also, fundus fluorescein angiography, an essential and powerful technique, has been used for the measurement of retinal blood vessel diameter *in vivo.*[86, 87]

Furthermore, introducing confocal microscopy, which has not been largely used in previous rat eye studies, adds to the merits of this study. Briefly, confocal microscopy is largely used to resolve the detailed structure of specific objects within the cell. Various components of living and fixed cells or tissue sections can be specifically labelled using immunofluorescence and then visualized in high resolution. Confocal microscopy enables the creation of sharp images of the exact plane of focus with minimal background from autofluorescence or other regions of the specimen; this is a unique and distinctive feature.[88] Therefore, structures within thicker objects can be conveniently visualized using confocal microscopy. Furthermore, by stacking several images from different optical planes, 3D structures can be analysed. The sample penetration depth is limited, however, when using confocal microscopy.

1.10 *Ex vivo* experimental models

The BRB *ex vivo* model has been reported as a useful experimental technique for interrogating the mechanisms underpinning retinal diseases. The *ex vivo* technique generally includes superfusion and culture models.[89-92] Superfusion is a technique where tissue is bathed with a physiologically treated solution under standard conditions such as supplemental oxygen (O_2) and carbon dioxide (CO_2) to maintain tissue viability.[91] About a century ago, Finkleman suspended a portion of rabbit intestine in air and kept it in a physiological state by a running solution over the tissue to study the nature of inhibition of smooth muscle contraction.[89] More recently, Mishra et al. have used the superfusion model on male Long-Evans rat eyes perfused with HEPES buffer.[93] Retinal explant culture models have been well established in understanding the pathobiology of retinal disease. Similarly, while characterising insulin signalling in rat retina, Reiter et al. used an *ex vivo* tissue culture model where they demonstrated insulin signalling pathway activation following the addition of exogenous insulin similar to observations from *in vivo* technique.[94] Also, multiple cell co-culture of BRB has been

previously utilised for understanding the interaction between the cellular components of BRB.[91, 95, 96] For example, endothelial cells and pericytes were cultured in transwells with each seeded on either side of the membrane. Astrocytes were seeded at the bottom of the culture plate, which demonstrated similar histology and function of retina unit.[95, 96] In addition, Gaddum et al. added 40 mmol/L and 5 mmol/L of glucose to triple cultured retinal cells for 48 hours while studying the effect of hyperglycaemia BRB cellular components.[91] None of these studies have investigated this model of the intact retina *ex vivo* for examining the effect of hyperglycaemia on the BRB. Overall, there are merits to the use of the *ex vivo* approach such as bypassing any form of systemic physiological compensation that may occur *in vivo* in a diabetic rat, and ability to challenge the tissue with specific levels of hyperglycaemia while not harming the animals.

1.11 Summary

The above review has identified gaps in the knowledge of structural changes associated with retinal vessels, particularly in early DR. It has also discussed the functions and characteristics of the key cells that are implicated in the pathogenesis of DR. To the best of our knowledge, no previous studies have categorically assessed the retinal vasculature for syndecan-1 changes, pericytes and astrocyte loss altogether in a single study and at an early stage of the disease. The current study thus seeks to provide further insight into the potential functions and structural characteristics of the endothelial glycocalyx, pericytes and astrocytes in vascular remodelling in diabetic retinopathy. Furthermore, this study will provide a basis for further research that may lead to the development of targeted therapeutic approaches for the treatment of diabetic retinopathy.

CHAPTER HYPOTHESIS, AIM AND OBJECTIVES

2.1 Hypothesis

There is depletion of pericytes, astrocytes and endothelial glycocalyx in the rat retina of hyperglycaemic but not normoglycaemic *ex vivo* conditions over time.

2.2 Null hypothesis

There is no difference in the structural integrity of the retinal vasculature, pericytes and astrocytes and their vascular associations in hyperglycaemic and normoglycaemic *ex vivo* conditions over time. Furthermore, the endothelial glycocalyx is unchanged.

2.3 Aim

To establish and validate an *ex vivo* rat retinal model and use a multi-immunofluorescent approach on the retina to study the effects of hyperglycaemia on the vasculature and cellular components of the BRB, including effect of time and the type of retinal preparation.

2.4 Relevance of the study

This study aims to provide a better understanding of the structural changes that may impact the functional mechanisms implicated in the early stages of diabetic retinopathy, which may contribute towards the development of future targeted therapeutic approaches to ultimately decrease morbidity resulting from diabetes mellitus.

2.5 Specific objectives

1. To optimise retinal preparations for fixation, fixation period, antibody dilutions and antibody combinations/cocktails used for multiple immunolabelling.

2. To evaluate the presence of any morphological differences between the dissected-out retinae (explant) and the retinae in the intact eye globe (eyecup).

3. To investigate the structural changes of pericytes and astrocytes within the retinal vasculature in normo- and hyperglycaemic *ex vivo* conditions over time.

4. To determine whether the retinal vascular endothelial glycocalyx is affected by hyperglycaemia *in vitro*.

5. To determine the expression of potential signalling factors such as heat shock proteins that may be expressed in the retina in acute exposure to hyperglycaemia by multi-immunolabelling of retinal whole-mounts.

3.1 Ethical approval

Ethical approval for this study was obtained from the Animal Research Ethics Committee of the Faculty of Health Sciences, University of Cape Town, South Africa (UCT HSF AEC018-021 and C 019_021, Appendix 1). All animal procedures were authorised by the South African Veterinary Council (SAVC) (Number: AR20/17790).

3.2 Materials

The materials that were used for the experiments in this study were obtained from MERCK (PTY) LTD, Sigma-Aldrich and B&M Scientific. Those obtained from MERCK (PTY) LTD included bovine serum albumin (BSA) calcium chloride ($CaCl_2$), ethanol, magnesium sulphate (MgSO4), potassium chloride (KCl), sodium chloride (NaCl), glycerol/1, 4-diazabicyclo (2.2.2) octane (DABCO), disodium hydrogen phosphate (Na_2HPO4) and methanol. Others include, Triton-x, Tween-20, paraformaldehyde (PFA), potassium dihydrogen phosphate (KH_2PO4) and glucose, all from Sigma-Aldrich, and sodium bicarbonate (NaHCO3) from B&M Scientific. Other solutions used were phosphate buffered saline (PBS) and Krebs-Henseleit buffered solution pH 7.4 (hereon referred to as Krebs buffer), Dulbecco's Modified Eagle Medium (DMEM) and penicillin/streptomycin (1%). The details of primary and secondary antibodies used, and their concentrations are presented in Table 3.1. Note that the dilutions used for the secondary antibodies are from 1:1 antibody: glycerol stock solution.

Table. 3.1 Antibodies and vascular marker used for immunolabelling

Antibodies and Lectin	Dilution	Catalogue number	Source
Rabbit monoclonal Anti syndecan-1	1:500	Ab32337/56-2	Abcam
Rabbit Anti-Syndecan-1	1:2000	Ab128936	Abcam
Mouse monoclonal Anti-alpha smooth muscle actin (αSMA) [1A4]	1:50	Ab7817	Abcam
Chick Anti-GFAP	1:1000	Ab4674	Abcam
Mouse Anti-NG2 [132.38]	1:200	Ab50009	Abcam
Rabbit Anti-NG2 chondroitin sulphate proteoglycan	1:200	AB5320	Merck
Rabbit Anti-collagen IV	1:500	Ab19808	Abcam
Rabbit Anti-α-crystallin A	1:200	GTX65843	GeneTex Inc (North America)
DyLight TM 405 Affinipure Donkey Anti-Chicken IgY (IgG)(H+L)	1:50	703475155	Jackson Immuno Research Laboratories
Alexa Fluor® 647-AffiniPure F(ab')$_2$ Fragment Donkey Anti-Mouse IgG (H+L)	1:500	715606151	Jackson Immuno Research Laboratories
Cyanine Cy™3 AffiniPure F(ab')$_2$ Fragment Donkey Anti-Rabbit IgG (H+L)	1:1000	711166152	Jackson Immuno Research Laboratories
Alexa Fluor® 647 AffiniPure F(ab')$_2$ Fragment Donkey Anti-Chicken IgY (IgG) (H+L)	1:500	703606155	Jackson Immuno Research Laboratories
Fluorescein isothiocyanate- (FITC) Lycopersicon Esculentum (Tomato) Lectin	1:200	FL1171	Vector laboratories

3.3 Experimental design

A total of 68 rats were used in this study. Forty-eight rats were used for validation of the *ex vivo* retinal model, whereas twenty rats were used for the hyperglycaemic experiments on the retinae: 6 rats each were used for the control and hyperglycaemic superfused model, while another 6 rats were used for western blotting, the remaining rats were used for 48- hour culture model. The detail of the experimental design is seen in Figure 3.1.

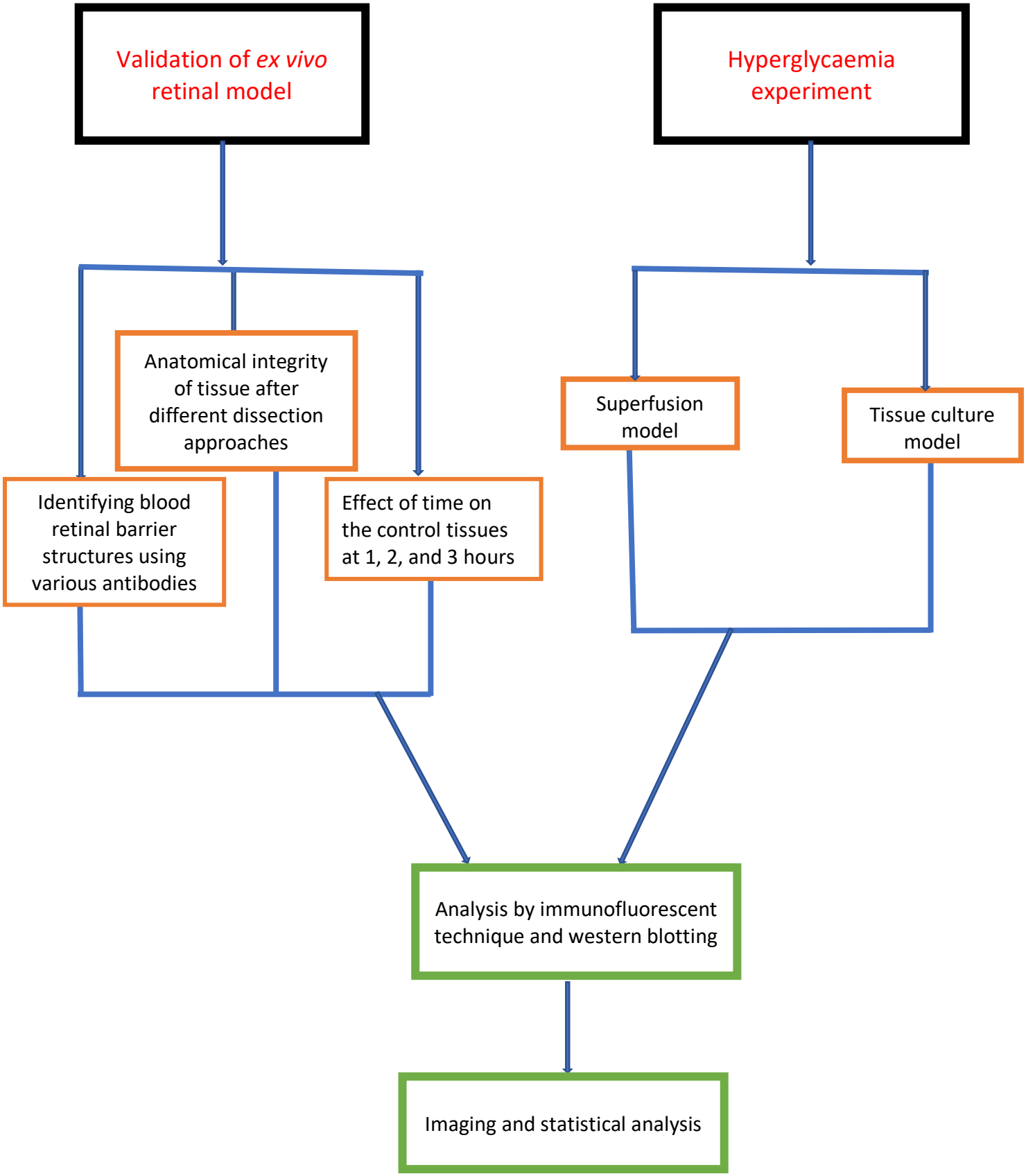

Figure 3.1. Flow chart showing the summary of experimental design.

3.3.1 Validation of the *ex vivo* retinal model: Three aspects were considered, viz:

1. Identifying the BRB structures using various antibodies.

2. Determining the anatomical integrity of retinal tissue after different dissection approaches (explant and eyecup).

3. The effect of time (1, 2 and 3 hours) on superfusion model using immunolabelling technique.

3.3.2 Hyperglycaemia experiments:

3.3.2.1 Superfusion model:

1. Hyperglycaemic group: Rat retinae (explant and eyecup) were superfused in Krebs buffer with a glucose concentration of 25mmol/l for 1 hour, 2 hours and 3 hours, respectively.

2. Control group (Normoglycaemia): Rat retinae (explant and eyecup) were superfused in Krebs buffer with a glucose concentration of 5.5mmol/l at 1 hour, 2 hours and 3 hours.

3.3.2.2 Tissue culture model:

1. Hyperglycaemia group: Rat retina (explant only) was incubated in Krebs buffer in a tissue culture chamber with a glucose concentration of 25mmol/l for 48 hours.

2. Control group (normoglycaemia): Rat retina (explant only) was incubated in Krebs buffer in a tissue culture chamber with a glucose concentration of 5.5mmol/l for 48 hours.

3.4 Animals

3.4.1 Animal welfare and housing

Two month-old male Wistar and Sprague-Dawley adult rats with an average body weight of 250-300g were obtained from the Faculty of Health Sciences Animal Facility, University of Cape Town (UCT HSF RAF). They were housed in groups of four per cage in a spacious euro standard type IV conventional cage and maintained at a temperature between 20-23^{o}C, with 12-

hourly on and off light autoregulation at an intensity of 150lux. Humidity was measured frequently using a manometer and was maintained between 40 -70%.[97] The rats had access to rat chow, and fresh drinking water *ad libitum*.

3.4.2 Anaesthesia, euthanasia and thoracotomy

Rats were deeply anaesthetized using either sodium pentobarbitone (Vertsev, Cape Town) administered intraperitoneally at a dose of 70mg/kg or lethal dose of isoflurane (3ml injected into a gauze in the euthanising chamber). The absence of pedal and corneal reflexes were checked intermittently to confirm deep anaesthesia, followed by thoracotomy for *in vivo* perfusion experiments by exsanguination or to remove the heart and induce euthanasia. A lateral incision of 5-6cm was made through the integument and abdominal wall under the rib cage, and the liver was carefully separated from the diaphragm, followed by another incision along with the diaphragm through the entire length of the rib cage to expose the pleural cavity using curved blunt scissors placed in one side of the ribs while carefully displacing the lungs and making a cut through the rib cage to expose the heart. The thymus was lifted away from the heart along with the sternum to provide a clear view of the major vessels (aorta and subclavian vessels). For rats from which eyes were to be harvested for immediate immersion-fixation and for glycaemic experiments, the heart was excised to confirm death.

3.4.3 Fixation of tissue by perfusion or immersion

For rats undergoing perfusion fixation, a small incision was made on the posterior end of the left ventricle using iris scissors. Then a 15-gauge blunt perfusion needle was passed through an incision on the left ventricle to cannulate the heart into the ascending aorta. Thereafter, the rat was exsanguinated with phosphate-buffered solution (PBS) at 37°C to washout out blood from the vasculature followed by fixation with 4% paraformaldehyde (PFA) for 15 – 20

minutes. An incision was then made at the right atrium to release the pressure of perfusion and the perfusate into a waste container during the perfusion process. Immersion-fixation in 4% PFA overnight was done for the aorta and retinae after tissue harvesting and dissection as described in section 3.4.4.

3.4.4 Tissue harvesting, eyes enucleation and retinal dissection

After thoracotomy, the aorta, eyes and occasionally the spleen were harvested. The aorta was removed first using a scalpel to carefully remove a segment just before the bifurcation and immediately placed into either 4% PFA or ice-cold Krebs buffer. Next, the spleen was removed, rinsed in PBS and placed into 4% PFA/PBS. Eyes were enucleated by using the scalpel to cut along both sides of the eye, thereby separating the eye muscles from the eye globe. A forceps was forced gently below the eye globe, and with a blade, the eyes were separated from the head around the optic nerve. This manoeuvre was done to prevent damage to the retina. Perfusion-fixed eyes were rinsed in 1 x PBS and then placed in 4% PFA/PBS for post-fixation, before being dissected under a stereomicroscope. Eyes dissected from non-perfused fixed rats were transported in ice-cold PBS. At the microscope, forceps were used to rotate the eye such that the posterior end with the optic nerve faces up. The eye was gripped with forceps the tissue and muscle surrounding the sides of the eye carefully cut away using micro dissection scissors, and the optic nerve cut off. The eye was gently rotated such that the cornea and lens points face the dissector lens. While still maintaining a grip on the eye a 30 G needle was used to puncture the eye at the iridocorneal angle. The one point of the dissection scissors was inserted into the puncture site and the cornea and iris were removed by cutting around the eye. The lens and most of the vitreous was gently removed with forceps while gripping the posterior end of the eyecup. The eyecup was placed on filter paper soaked with PBS which was laid on a wax platform, with the anterior end facing upwards. Four radial cuts

from the open anterior end towards approximately 2 mm away from the optic nerve head were made through the retina and underlying sclera of the eyecup using a no.11 scalpel blade, taking note not to completely severe each quadrant of the retina (see second image in Fig 3.2). The peripheral edges of the quadrants were trimmed using a blade to remove non-retinal tissue which allowed eye/retina to flatten out the and prevent each quadrant from folding back on itself when flat-mounted (see third and fourth images in Figure 3.2, and Figure 3.3). Retinae were either dissected out from the sclera (referred to hereon as explant) or remained *in situ* (hereon referred to as the eyecup), then superfused in Krebs buffer for 1, 2 and 3 hours or cultured for 48 hours before fixing in 4%PFA. The spleen was harvested as mentioned above, and used as positive tissue control for syndecan-1 immunolabelling. After 48 hours in 4% PFA at 4°C, the tissue was sliced into thick pieces, and sucrose-embedded for cryoprotection by placing the tissue sequentially in 10% 20% and 30% sucrose in PBS for 12 hours in each solution until the tissue had sunk to the bottom of the container. Thereafter, pieces of spleen were placed in OCT (optimal cutting temperature) tissue freezing medium and frozen. Cryosections (20µm thick) were produced on a Leica CM1850 cryostat.

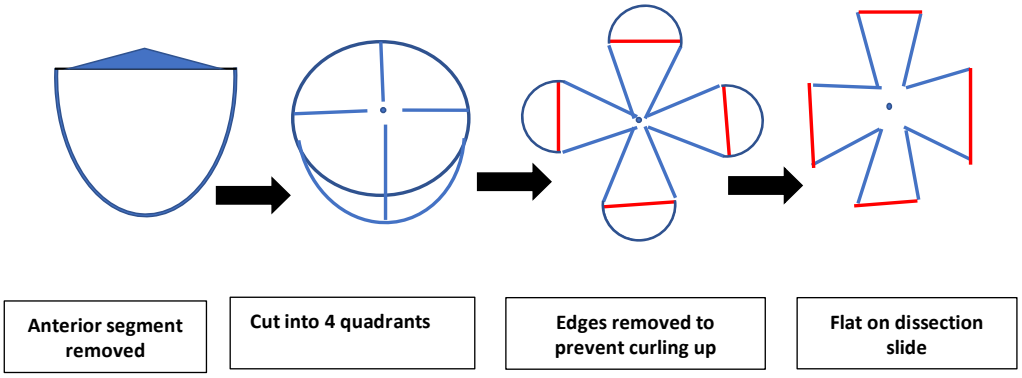

Figure 3.2. Schematic diagram illustrating a stepwise method for retinal dissection: from the eye globe to cutting into four quadrants, followed by cutting out the edges to allow the eyes flatten out.

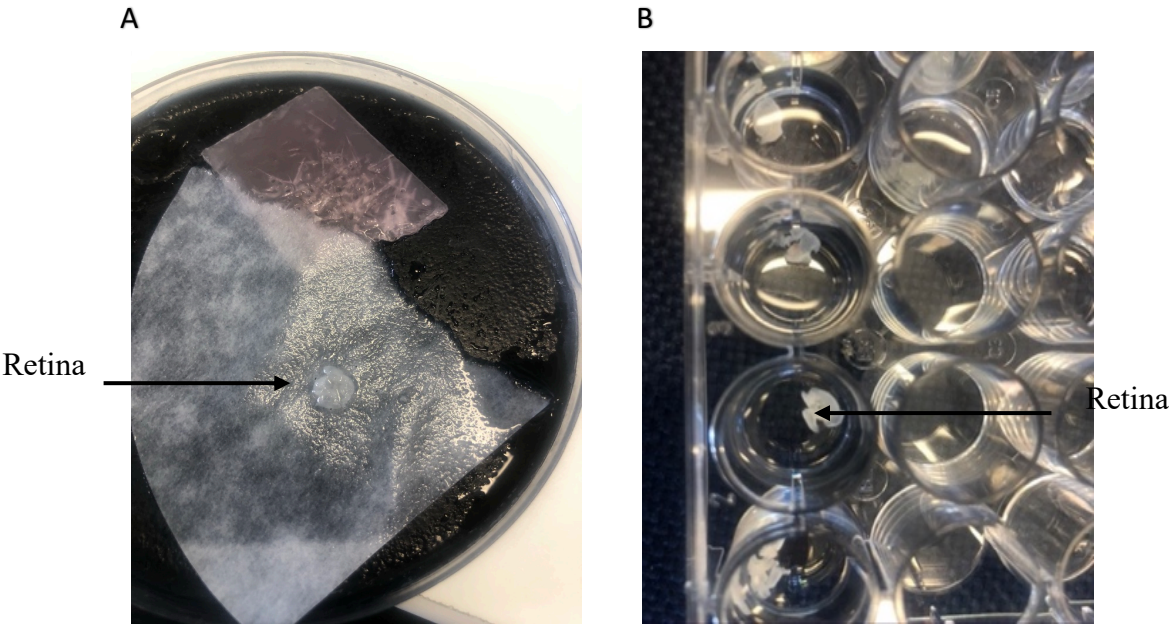

Figure 3.3. Picture showing freshly harvested retina. A. Dissected retinal flat-mount placed on a wet filter paper placed on solidified wax in a petri dish. B. Retinal flat-mount in a multi-well tissue culture plate used for the multi-immunolabelling process.

3.5 Hyperglycaemia experiments

3.5.1 *Ex vivo* superfusion

Enucleated eyes and pieces of the dissected aortas (see section 3.4.2) were placed into a pre oxygenated ice-cold (4°C) Krebs buffer solution containing NaCl 118.5, KCl 4.7, CaCl2 1.2, MgSO4 1.2, NaHCO3 25, KH2PO4 1.2 all in mmol/L. The harvested retinae (as described in section 3.5.4), either as explant or eyecup were flattened out onto a filter paper pre-wet with Krebs buffer and gently immersed into ice-cold Krebs buffer before mounting in the perfusion chamber. The retinae were superfused in a chamber simulating the Langendorff perfusion system. The Krebs buffer was continuously bubbled with 95% oxygen and 5% carbon dioxide (Air liquid, SA) and regulated to about 15-20 drops per minute to prevent damage to the retinal tissue due to high pressure flow, whilst being immersed in the buffer. The temperature of the buffer solution was maintained at 37°C by a heated water-jacketed system (Figure 3.4).

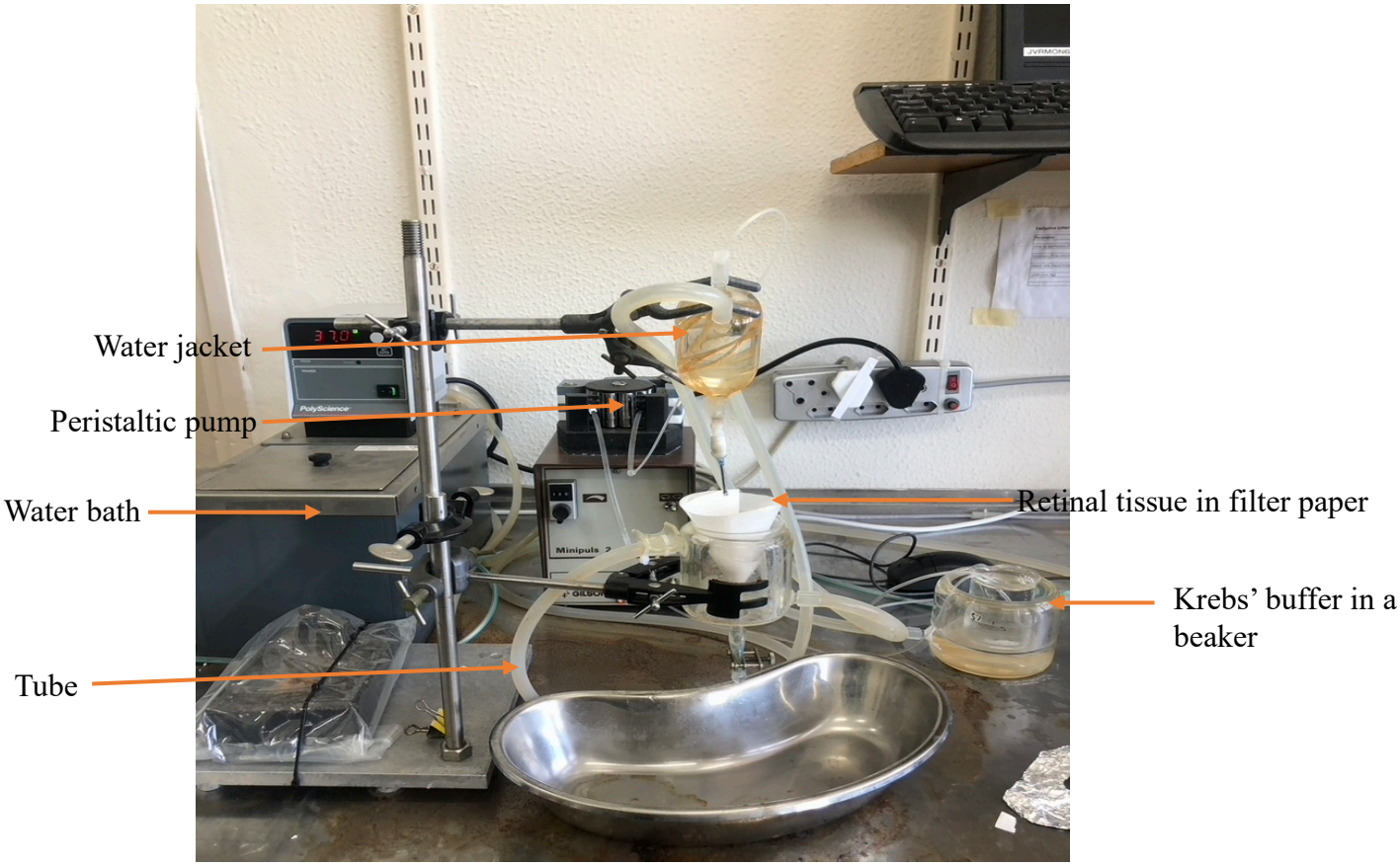

Figure 3.4. *Ex vivo* continuous oxygen superfusion system, used for the retinal tissue superfusion.

3.5.2 Retinal tissue culture

Extended time point experiments were not feasible on retinal tissue using the superfusion technique Therefore an exploratory investigation included culturing retinal explants for 48 hours to determine how well the structural integrity of the BRB was retained, and whether this timepoint could be suitable for *ex vivo* retinal studies. Tissue culture work was performed wearing clean laboratory coats and sterile gloves, and all procedures done using aseptic techniques. Retinal tissue cultures were handled under laminar flow in a Bio-Flow Biological Safety Cabinet. All bottles, pipette tips and centrifuge tubes were autoclaved and sprayed with 70% ethanol before use. Retinal tissue was cultured in 95% humidity and 5% CO_2 at 37ºC in

a water-jacketed incubator (Thermo Scientific, USA). After tissue harvesting under sterile conditions, the retinal tissue (explants only) were cultured in a sterile culture dish using culture media containing Dulbecco's Modified Eagle Medium (DMEM) 4.5 1 g/L (25mMglucose), or 1 g/L (5.5mM glucose), supplemented with foetal bovine serum (FBS) (10%), glutamax (1%), penicillin/ streptomycin (1%), and B-mercaptoethanol (0.1%). The culture medium was filtered through a 0.22 μm filter after preparation and stored at 4ºC. The retinae were cultured for 48 hours. Culture media and all components were purchased from Thermo Scientific, USA.

3.6 Laboratory procedures

3.6.1 Immunolabelling

3.6.1.1 Immunofluorescent labelling protocol

Retinal whole-mounts were fixed in 4% PFA overnight, washed three times (20 min each in 1x PBS), and thereafter permeabilised with 0.5%Tween 20 in PBS or in absolute methanol for 2 hours. After rinsing in 1 x PBS, retinae were blocked in 3% bovine serum albumin (BSA) in PBS, followed by incubation in different primary antibody combinations overnight to detect the retinal vascular bed, pericytes, endothelial syndecan-1 and astrocytes. This was followed by another washing step in 1x PBS (3 times for 20min each), then incubation overnight in species-specific secondary antibodies conjugated to fluorophores with excitation spectra of 488nm, 561, 647nm and 405nm to detect the bound primary antibodies raised in different species to achieve multi-immunolabelling. After the washing step in 1x PBS (3 times 20 minutes each), retinae were cleared in a DABCO-glycerol solution overnight or longer. Prior to microscopic imaging, retinae were mounted between two coverslips (Appendix 2). After microscopy, retinae were removed from the mounting coverslips and stored in DABCO/glycerol at 4ºC.

Importantly, various combinations of antibodies raised in different species, were used to find the optimal cocktail for detecting all the structures in one sample for multi-immunofluorescent labelling. In most cases, all primary antibodies were initially detected using a CY3 secondary antibody as this fluorophore has a strong emission. After that, secondary antibodies conjugated to other fluorophores were used to detect pericytes, astrocytes and syndecan-1 in multi-immunolabelling procedures. All primary antibodies used for the experiment were diluted in 0.1% Tween 20 in 3% BSA while all secondary antibodies were diluted in 0.1% Tween 20 in 0.1% BSA (see table 3.1 for details of antibodies). Methanol was found to be suitable for permeabilization and was used to permeabilise the retinae from the superfusion and culture experiments.

3.6.1.1.1 Immunofluorescent labelling of the BRB

3.6.1.1.1.1 Detection of retinal blood vessels: Fluorescein-labelled lycopersicon esculentum lectin (also referred to as tomato lectin -FITC) was used to detect vascular endothelium. Several dilutions were tested with a 1:200 dilution giving the best signal to background. To determine whether lectin stained up all retinal vessels, immunolabelling of the basement membrane with rabbit anti-Collagen IV antibody (1:500 dilution) was used as a proxy for blood vessels architecture. Note in all immunolabelling procedures below, lectin was included with the secondary antibodies to identify blood vessels.

3.6.1.1.1.2 Detection of pericytes: To identify pericytes**,** dual-immunolabelling was carried out with a pericyte marker and one of the blood vessel markers above (mainly lectins) on rat retinas using a mouse anti- alpha-smooth muscle actin (αSMA) at a1:50 dilution. This dilution was previously validated in our laboratory. Initially, a rabbit anti-NG2 chondroitin sulphate proteoglycan antibody was used at 1:200 dilution alone and in dual immunolabelling with the

αSMA antibody. Thereafter, the mouse anti-NG2 antibody was used at a 1:200 dilution in multi-immunolabelling protocols. The bound anti-NG2 antibody was detected initially with anti-mouse Cy3 (1:1000 dilution) and thereafter with anti-mouse Alexa 647 secondary antibody (1:500 dilution).

3.6.1.1.1.3 Detection of the endothelial glycocalyx: From previous studies in our laboratory, Araibi et al. established a syndecan-1 immunohistochemistry protocol on heart tissues using chromogenic detection.[98] The antibody used in this previous study was used to detect syndecan-1 protein in the retinas with some modifications. Monoclonal rabbit anti-syndecan-1 antibody at 1:200, 1:500 or 1:600 dilutions was used to determine the best signal to background labelling with 1:500 dilution giving the best signal. The antibody was detected with anti-rabbit Cy3 secondary antibody (1:1000). An additional syndecan-1 antibody suitable for WB was also attempted on whole-mounts as an alternative for labelling.

3.6.1.1.1.4 Detection of astrocytes: To detect astrocytes initially, rabbit anti-glial fibrillary acidic protein (GFAP – kindly gifted from Prof Lang and which was known to detect astrocytes in previous studies) was used to determine if the anti- GFAP antibody raised in chick (intended for the present study) was equally suitable. Rabbit anti-GFAP antibody was used in different dilutions viz- 1:1000, 1:500 and detected with anti-rabbit Alexa 647 1:500. Anti-chick Cy3 antibody at a 1:1000 dilution was initially used to detect the primary antibody, before using anti-chick 405 antibody at a 1:50 dilution. Chick anti-GFAP antibody (1:1000 dilution) was used for the rest of the immunolabelling procedures.

3.6.1.1.1.5 Detection of heat shock proteins: HSPs were detected using rabbit anti-α-crystallin A antibody and anti-rabbit Cy3 secondary antibody (1:1000 dilution)**.** Several dilutions were optimised and 1:200 dilution for the primary antibody gave the best signal.

3.6.1.2 Immunolabelling controls

To verify the specificity of the primary antibodies, the immunolabelling procedure excluded the primary antibodies and tissues were stained with only secondary antibodies and the blood vessel marker (lectin).

3.7 Western blotting

The purpose of western blotting was to confirm the specificity of syndecan antibody as it was unexpectedly immunolocalised to the ganglionic fibres in retinal whole-mounts. It was also used to determine if hyperglycaemia influenced syndecan levels and heat shock protein. The other organs (heart and kidney) previously known to express syndecan-1, were used as positive controls. After retinal tissues were superfused in a continuous oxygen bath chamber for 3 hours, tissues were homogenised by sonication (Soniprep 150, UK) for 20 seconds in Radioimmunoprecipitation assay (RIPA) lysis buffer containing 50 mM Tris-HCl (pH 8), 1% Triton x-100, 150 mM NaCl, 0.1% sodium dodecyl sulphate (SDS), 0.5% sodium deoxycholate with a protease and phosphatase cocktail inhibitor (Halt protease and phosphatase inhibitor, ThermoScientific, USA). Centrifugation of the lysates was done at 12000 relative centrifugal force for 20 minutes at a temperature of 4°C (Labnet International, NJ07095, USA). The supernatant was then collected, and the protein concentration of the supernatant was measured using the Pierce protein assay kit (Thermo Scientific, Rockford, USA). RIPA buffer is used to prepare the Bicinchoninic Acid (BCA) working reagent, a 96 well plate is used for the standards and samples, the absorbance is measured using a microplate reader, then finally a

standard curve was created, and the volume of protein required was calculated. For more details on the western blot protocol, see Appendix 3. The loading samples were prepared with equal amounts of the protein content of the lysate with Laemmli dye (Bio-Rad, SA), RIPA buffer and dithiothreitol. Samples were then boiled for 5 minutes at 95° before use. The samples were then loaded and electrophoresed on 12% SDS-polyacrylamide gel using Mini-PROTEAN Tetra Cell System (Bio-Rad, SA) at 150 voltage for 90 minutes. The protein was transferred from the gel to Polyvinylidene fluoride (PVDF) transfer membrane (Immuno-Blot PVDF Membrane for Protein Blotting, Bio-Rad, South Africa), using a semi-dry transfer unit (Trans-Blot Turbo Transfer System, Bio-Rad, South Africa). The transfer process was confirmed by staining the PVDF membrane with a ponceau stain. The membranes were then de-stained by washing with distilled water and blocked with 5% non-fat milk in phosphate-buffered saline with 0.1% Tween-20 (PBST) for 1 hour at room temperature. The membranes were incubated with primary antibodies (rabbit monoclonal anti-syndecan-1 antibody [EPR6454], # AB128936 Abcam) against the protein of interest at 1:1000, 1:2000 and 1:4000. 1 in 2000 dilutions was used in 5% non-fat milk in PBST rocking overnight at 4°C. Similar was done for sHsps (α-crystallin A) at 1:1000 dilution. The membranes were then washed with PBST 3 times for 10 minutes each and then incubated with horseradish peroxidase (HRP) conjugated secondary antibody 1:5000 for 2 hours, then washed using PBST 3 times for 10 minutes each. After draining excess PBST, detection solution was applied on the membrane, then covered with transparent plastic and into a film jacket for detections in the darkroom. The film was exposed for 30 seconds, 1 minute and 2 minutes respectively, to get the best signal. β-actin was used for the loading control at a 1:5000 dilution after stripping the membrane. Syndecan-1, heat shock protein and β-actin densitometry was analysed using GelQuantNET software version 1.8.2.

3.8 Imaging

Three-dimensional imaging was done on the Zeiss LSM 880 Airyscan and LSM 510 Confocal microscopes (Zeiss.com) fitted with an Argon laser (488nm), Diode laser (405 nm), diode-pumped solid-state laser (564 nm) and Helium-Neon laser (647). Lectin-labelled blood vessels were detected in the green channel (488nm). Astrocytes were detected in the blue channel (405 nm), syndecan-1 was detected in the red channel (564 nm), pericytes in the far red (yellow) channel (647nm) and HSPs were detected in the red channel on the confocal microscope. The choice of secondary antibodies couple to these fluorophores was based on the relative brightness of the signals for each of the structures, as determined by the optimization steps. The pinhole was set to 189 nm and 20x objective used, and optical sections were for most part 6-8µm apart. A minimum of six regions of interest (ROI) selected from the mid-peripheral retina, covering all quadrants were selected for detailed image analysis. Additional images were also taken from regions near the optic disc.

3.9 Analysis

3.9.1 Image analysis:

The morphological assessment was done by examining the images for general morphology, blood vessel architecture, location of syndecan-1 positive signals and associated pericytes and astrocytes.

3.9.2 Qualitative analysis

The retinal blood vessels were analysed for lectin signal intensity as well as their architectural patterns- large, primary and secondary branched vessels and capillaries. The astrocytes and pericytes were examined for the degrees of their signal intensities cellular coverage, which included the presence of nuclear bulge of pericytes, preservation, and presence of any

morphological changes. Furthermore, syndecan-1 immunolabelling and distribution in different blood vessel type were assessed.

3.9.3 Semiquantitative/quantitative analysis using image J

Image J software (National Institute of Health, USA)[99] with plug-in macros specifically designed for astrocytes for this study was used to analyse the proportional area coverage of astrocytes overall and the proportional area covered by astrocyte processes interfacing with the blood vessels. Pixel intensity was used to analyse syndecan-1 signal intensity in blood vessels and ganglionic fibres. Maximum pixel intensity was determined from lines drawn across the blood vessels (5 lines per image) and across ganglionic fibres (5 lines per image) as well as randomly across the background. The background values were subtracted from the lower pixel intensity values. For detailed instructions for Image J used for the images analysis, (see Appendix 4).

3.10 Statistical analysis

All data were analysed using GraphPad Prism version 8 for windows (San Diego California, USA). Descriptive analyses were conducted, and normally distributed quantitative variables were presented as means and standard error of mean. Non-parametric quantitative variables were presented as median and interquartile range. Shapiro-Wilk test was used to determine data normality distribution. The Students' t-test and Mann Whitney U test were used to determine the difference between two normal and not normally distributed data groups, respectively. P-values of < 0.05 was considered statistically significant.

4.1 Validation of antibodies and identification of BRB components

4.1.1 Identification of the retinal vasculature

Two vascular markers, collagen IV and Fluorescein labelled Lycopersicon Esculentum Lectin (lectin), previously used in other studies on whole-mount tissues in our laboratory, were tested to determine suitability for the planned multi-immunolabelling protocol on retinae in the current study. In the perfusion-fixed and immersion-fixed retinae labelled with lectin (Figure 4.1 A) and anti-collagen IV antibody (Figure 4.1B), a typical branching pattern of blood vessels was observed. Both signals were colocalised on all blood vessels (Figure 4.1C) with a high signal intensity to background fluorescence, thus validating that lectin was a suitable immunolabelling vascular marker. Lectin-labelling revealed different patterns of blood vessels in relation to the different parts of the retina with a radiating pattern emerging from the central retinal artery in the optic nerve, a prominent branching pattern towards the peripheral region, and the presence of a capillary plexus in the lowermost layer of the retinal vasculature (Figures 4.2 and 4.3). Lectin also labelled other non-vascular cellular structures thought to be glial or microglial cells based on their morphology (Figure 4.3). The lectin fluorescence signal quality was similar for perfusion and immersion-fixed retinae. Lectin was used in all the subsequent experiments presented below in this study to label blood vessels due to its allowance for multi-channel labelling.

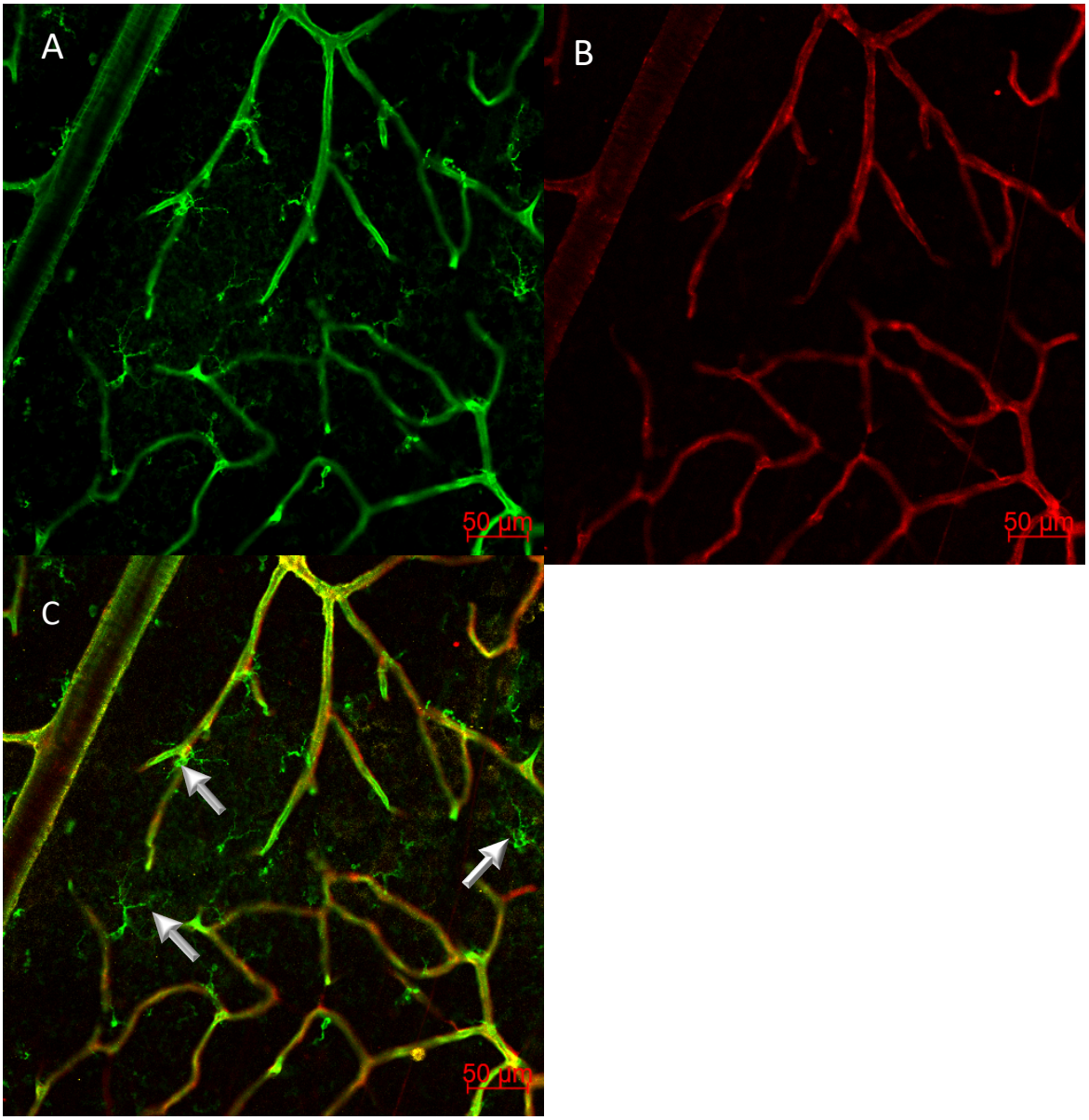

Figure 4.1 Single plane images of the superficial retinal vascular layer showing lectin and collagen IV colocalization (immersion-fixed). A. Lectin-labelled blood vessels shown in the green channel. B. Collagen IV-labelled blood vessels shown in the red channel. C. Merged channel showing lectin and collagen IV colocalization. White arrows indicate possible microglial cells.

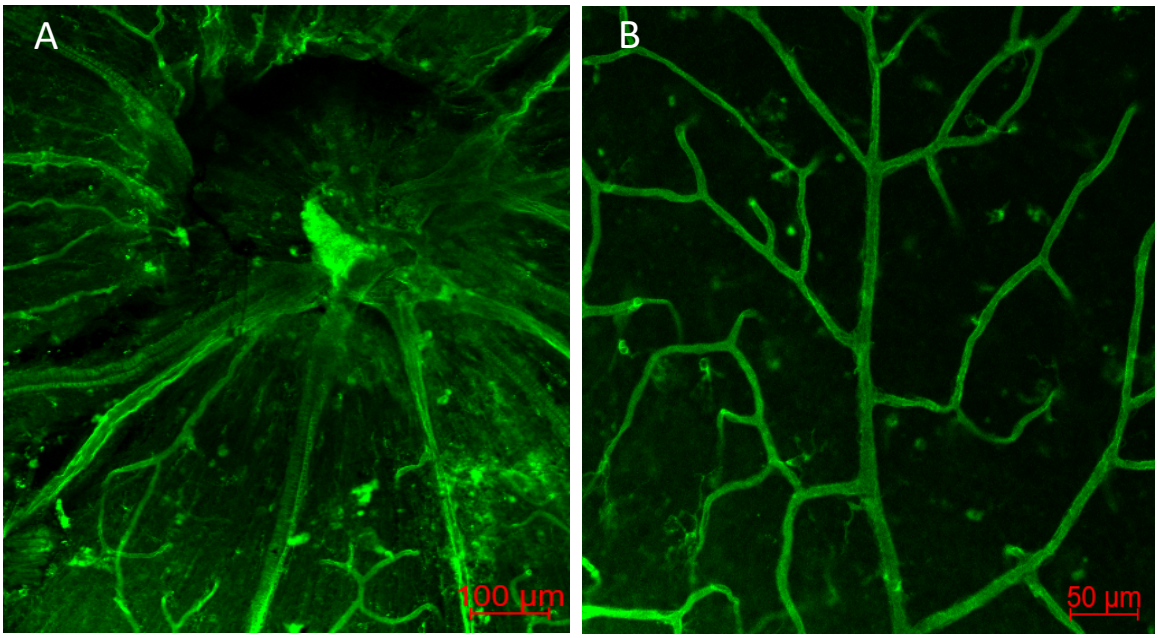

Figure 4.2. Single plane image of lectin-labelled blood vessels showing different patterns in different regions of the retina. Superficial image planes showing: A. Radiating pattern of blood vessels from the central retinal artery (arrow) at the optic nerve head in the central retinal region (perfusion-fixed). B. The peripheral region of the retina shows a branching pattern of blood vessels (immersion-fixed). Note the similarity in lectin fluorescence signal quality in both perfusion-fixed and immersion-fixed retinae.

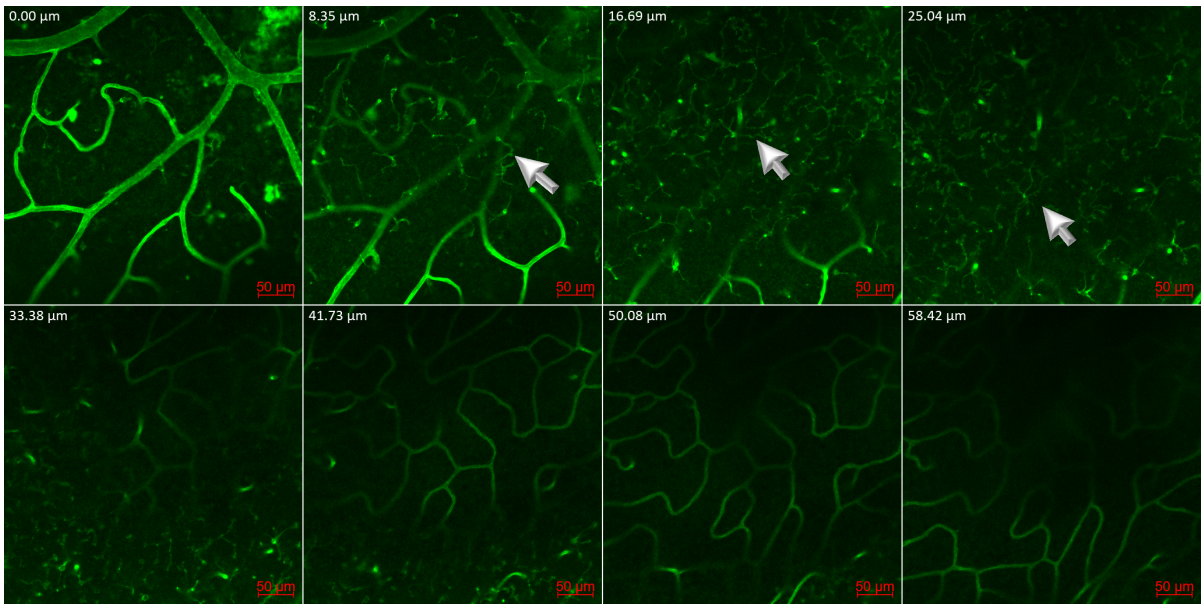

Figure 4.3. Gallery showing Z-stack images of lectin-labelled retinal blood vessels. The superficial plane shows a branching pattern of retinal blood vessels and the deepest vascular bed appears as a capillary plexus. Sections were taken at Z planes of 00.00 – 58.2µm, respectively. Note the vasculature is clearly seen in all Z planes with a slight reduction in lectin signal intensity in the lower planes. Non-vascular cells (white arrowheads) are detected in layers 8.35 to 25.04µm which are likely microglial /glial cells. Note that these predominate just below the superficial vessel layer.

4.1.2 Identification of pericytes

The alpha smooth muscle actin antibody (αSMA) was initially used to determine its suitability for detecting vascular mural cells, including pericytes, but as shown in Figure 4.4, αSMA-positive signals were only detected in mural cells (based on the location of the signal which appeared more peripheral to the lectin signals) associated with the radial retinal arteries and precapillary arterioles (primary branches), while pericytes associated with the retinal capillaries were not detected. By contrast, the NG2 antibody used at 1:200 dilution was optimal and showed up all retinal vessels (Figure 4.5 B). Interestingly, NG2 was also detected in mural

cells (smooth muscle cells) lining the radiating retinal arteries, the latter vessel type which was also αSMA-positive. Pericytes were identified by their nuclei bulges observed around the periphery of the blood vessels and which are more obvious when pseudocoloured in red (Figure 4.5B, C and D). A gallery image that shows bright NG2 fluorescence intensity on pericytes from the superficial to the deep layer of the retina is shown in Figure 4.6. Note that the signal intensity is still bright at the deepest layer compared with the image on lectin labelling shown in Figure 4.3 above.

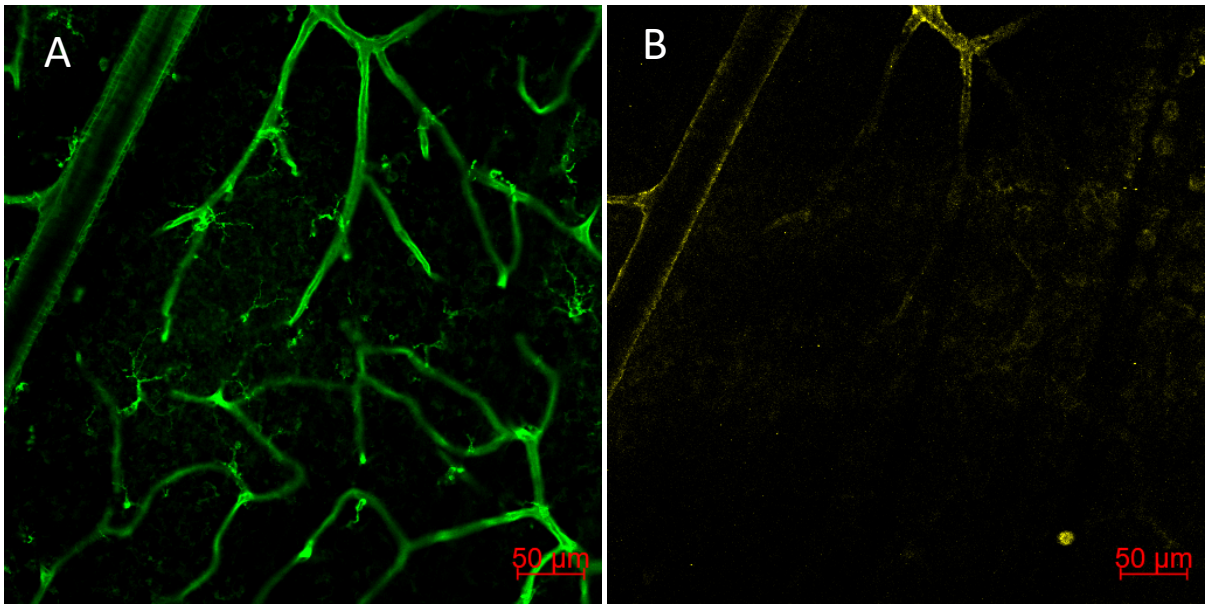

Figure 4.4. Single plane images of lectin and αSMA-labelled retinal blood vessels to detect pericytes. Superficial image planes of the perfusion-fixed retina showing: A. Lectin-labelled radial artery, its branches and capillaries. B. Perfusion-fixed retinae showing that αSMA is detected only in the radial artery (on the left) and its primary branch, where capillaries are undetected (right).

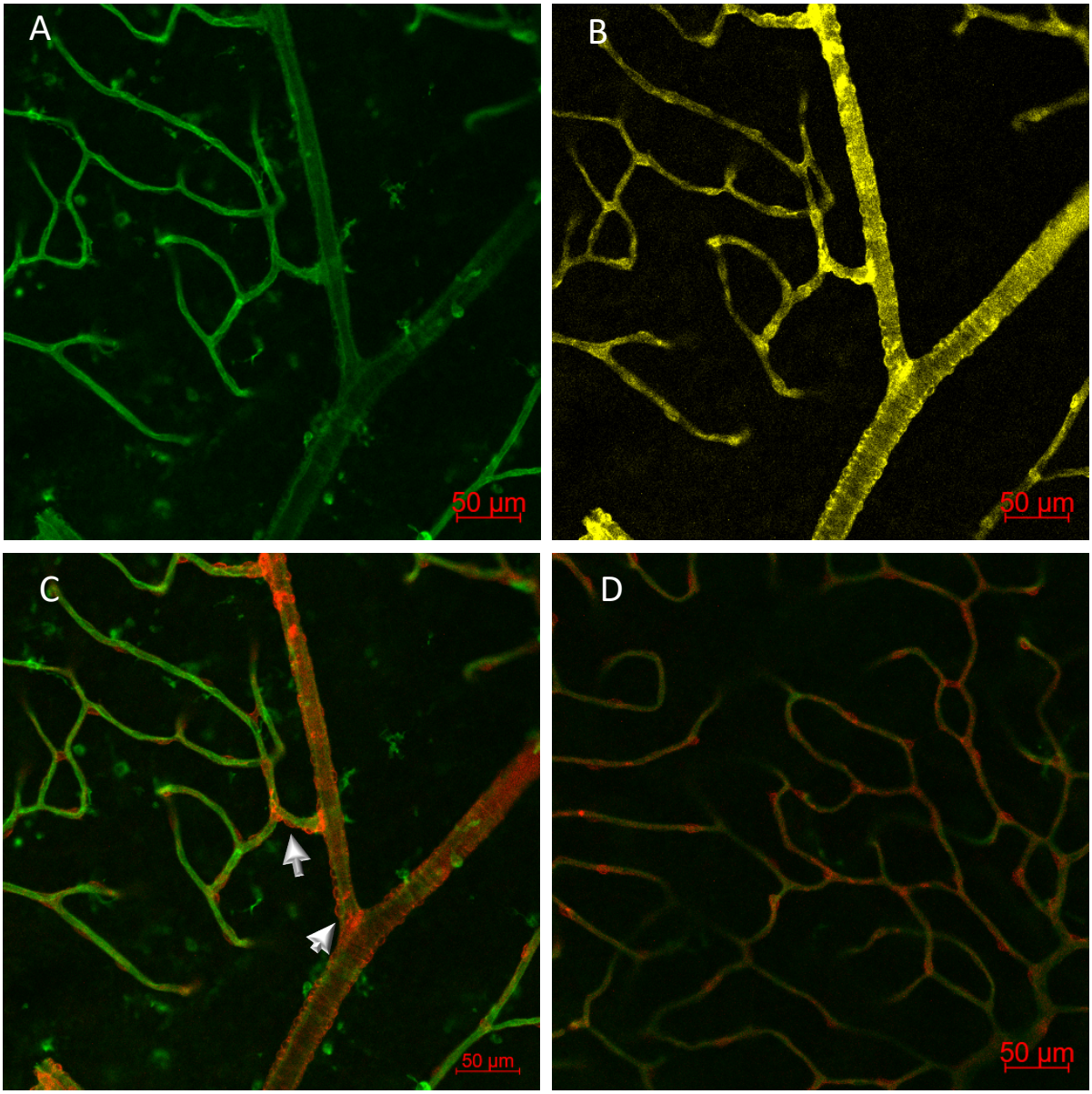

Figure 4.5. Single plane images of lectin and NG2-immunolabelled retinal blood vessels to detect pericytes. Superficial planes showing: A. Lectin-labelled radial arteries, primary and secondary branches and the capillary bed. B. NG2 is detected in pericytes covering the radial arteries and capillaries which are also stained by αSMA C. Showing perivascular pericytes nuclei bulge (white arrowheads). D. Pericyte nuclei bulges at the deep layer. Note that the NG2 signal in C and D are pseudocoloured (red) to show the nuclear bulge more clearly.

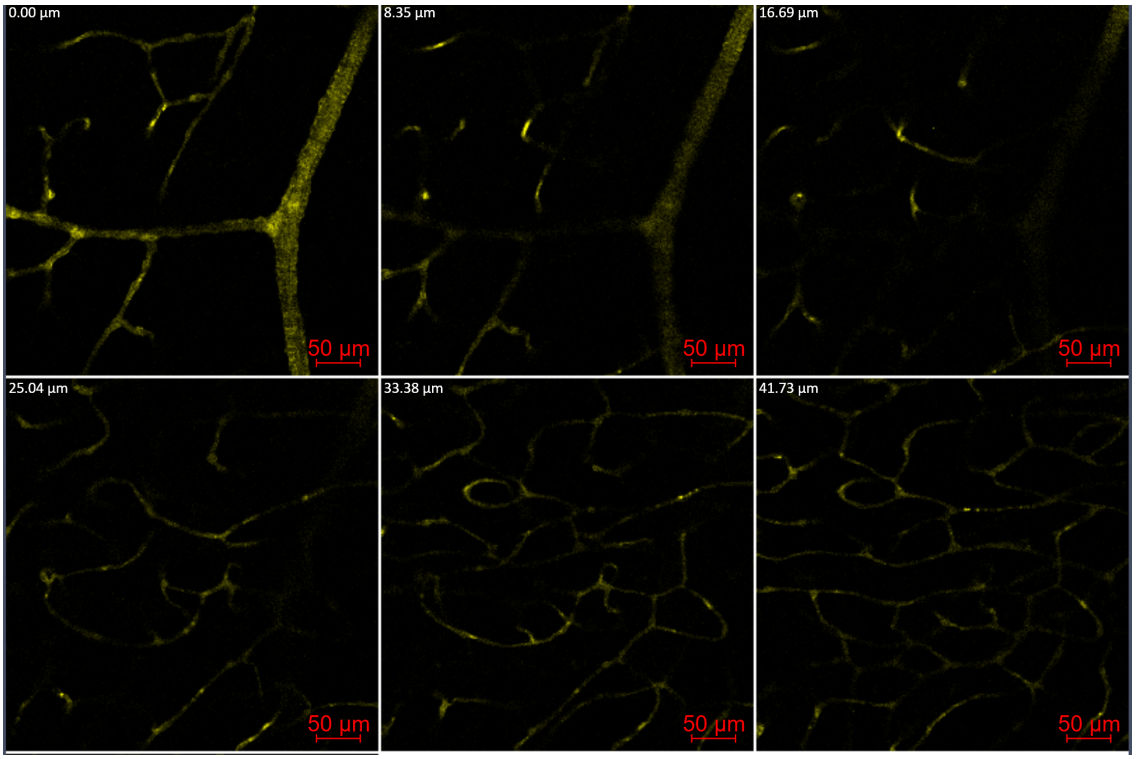

Figure 4.6. Gallery showing Z-stack images of NG2-immunolabelled retinal blood vessels to detect pericytes. Note the signal clarity of NG2 positive signals from the superficial layer (0.00um) to the deepest capillary plexus.

4.1.3. Identification of astrocytes

Anti-glial fibrillary acid protein (GFAP) antibody was used to detect astrocytes. Several dilutions were used, with a 1:1000 dilution providing the best signal to background fluorescence. Astrocytes were seen as stellate-shaped cells with processes forming a network around the blood vessels (Figure 4.7). Microglial-like cells were detected with lectin and these cells also associated with astrocytes in the superficial planes, as seen in Figures 4.7 and 4.8.

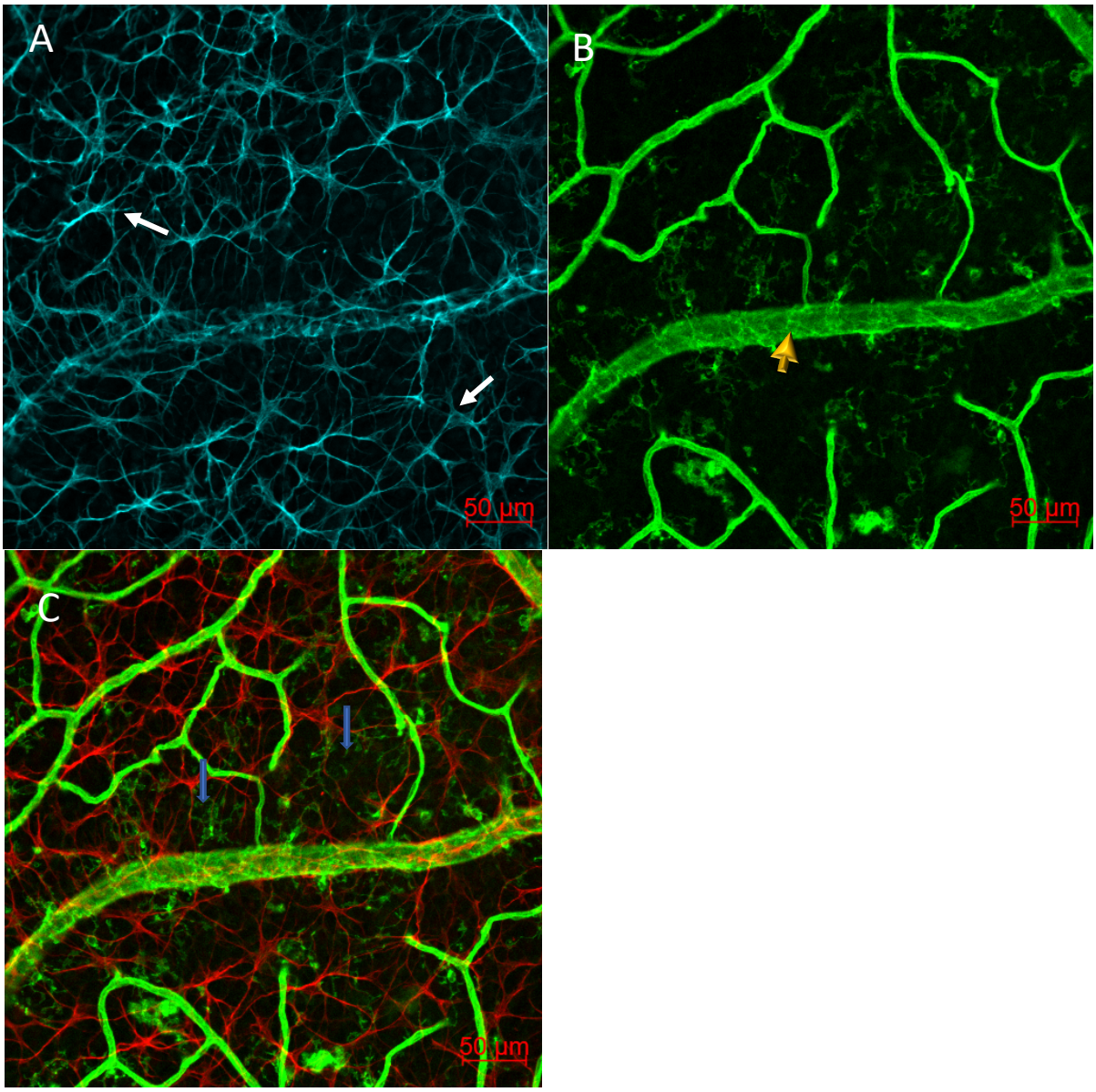

Figure 4.7. Single plane images showing GFAP immunolocalisation in astrocytes in the rat retina. A. GFAP-positive astrocytes in the blue channel. Note the stellate shape of astrocytes and their processes (white arrows). B. Lectin-labelled blood vessels in the green channel. Note the associated outline of the blood vessel (yellow arrowhead) with astrocytes in Figure 4.7A. C. Merged channel shows colocalisation of GFAP-positive signals with lectin-labelled microglial cells (blue arrows). Astrocytes are represented in pseudocolour red for better clarity.

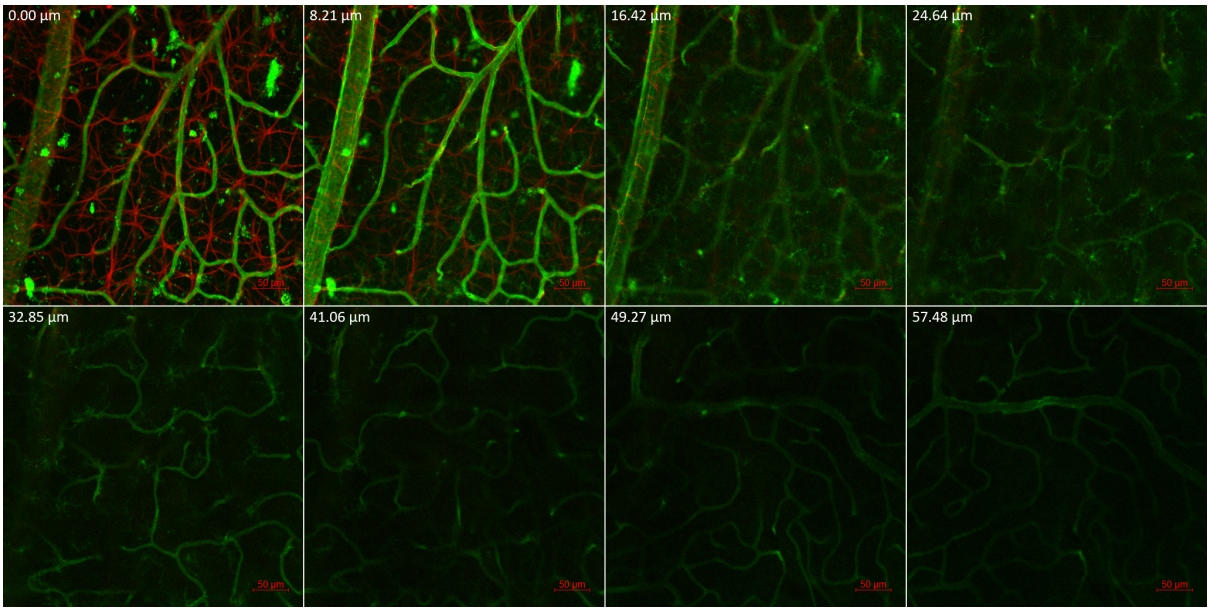

Figure 4.8. Gallery of Z-stack images showing the location of astrocytes (in pseudocolour red) and microglial cells in the retina. Astrocytes are located in the most superficial plane. Lectin-labelled microglia are present in the superficial retinal vascular layer through to approximately halfway down to the deepest layer (0.00µm – 32.85µm).

4.1.4 Identification of the endothelial glycocalyx and syndecan-1 immunolocalisation

Syndecan-1 monoclonal rabbit antibody had previously been used to detect rat coronary blood vessels in our laboratory.[98] Other tissue types, including rat aorta and spleen, were used as positive tissue controls to optimise for syndecan-1. Syndecan-1 positive signals were detected in the vasa vasorum and capillaries in the adventitia of the aorta (Figure 4.9) as well as on the luminal endothelium of the aorta (Figure 4.10) with a high signal to background intensity. Syndecan-1-positive signals were detected in the retinal blood vessels with the best signal to background intensity at a 1:500 dilution of this antibody. However, signal intensity varied in different regions of the retina, with some areas showing higher signal intensity of syndecan-1 compared to other regions (Figure 4.11). Nerve fibre-like structures located in the plane just beneath the superficial retinal vessels and which were seen to converge on the optic disc, were

incidentally found to have a consistently high signal intensity, mainly at the central region compared to the peripheral region but still more intense than that seen in the blood vessel with this antibody (Figure 4.11 A). Based on the morphology and z-plane location of these fibres, they were identified as the nerve fibres arising from neurons in the ganglionic cell layer (hereafter referred to as the ganglionic fibres). Retinal tissues were stored in either ethanol or methanol, and it was observed that tissues stored in ethanol yielded a slightly brighter signal to background fluorescence. Also, retinae that were perfusion-fixed with PFA showed a brighter signal compared to retinae that were not perfusion-fixed (Figure 4.12 C, D).

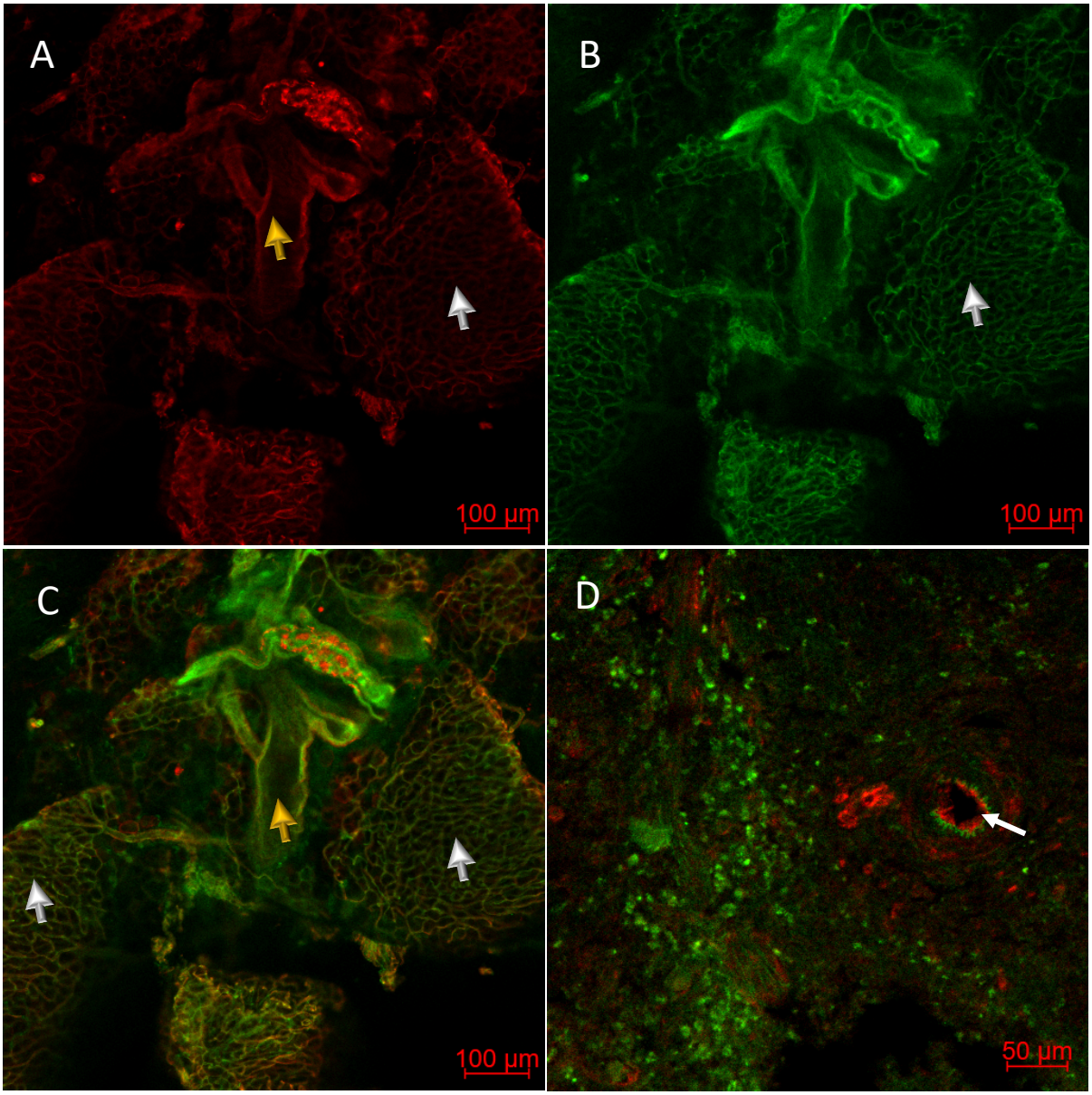

Figure 4.9. Single plane images of syndecan-1 localisation in the rat aorta and spleen. A. Syndecan-1 is present in the vasa vasorum (yellow arrowhead) and capillary bed (white arrowhead) in the adventitia of the aorta. B. Lectin-labelled counterpart and C. Merged channel showing syndecan-1 and lectin are colocalised. D. Syndecan expression in the rat splenic vessel (white arrow).

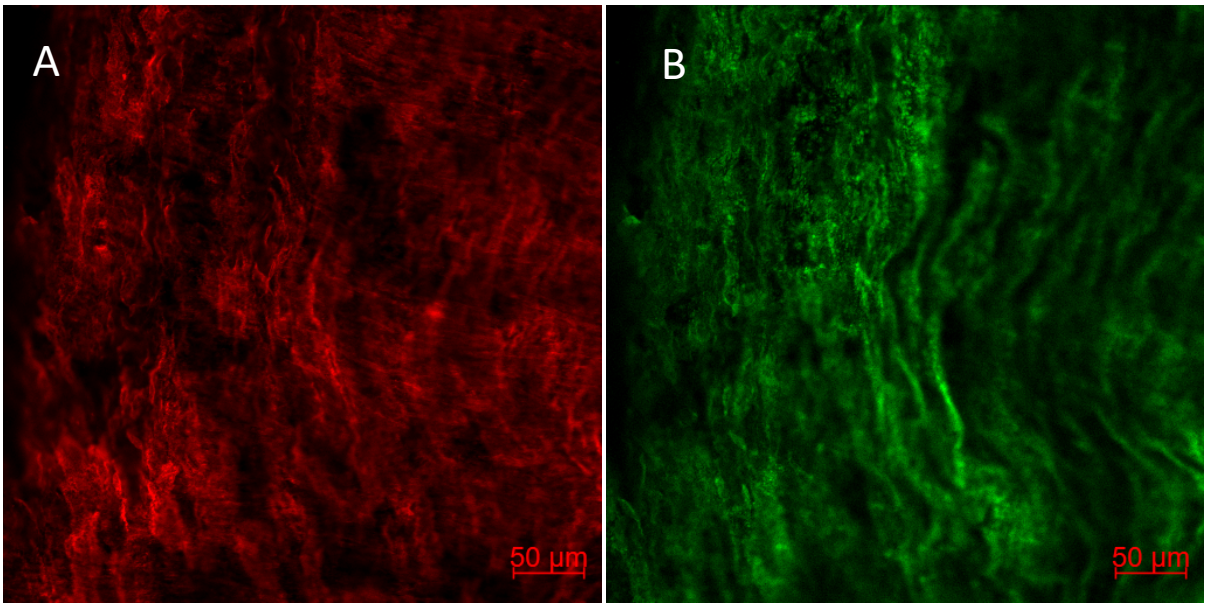

Figure 4.10. Extended focus image covering the endothelial surface of syndecan-1 and lectin-labelled rat aorta. A. Syndecan-1 is immunolocalised on the endothelial surface of the aorta. B. Corresponding lectin-labelled channel.

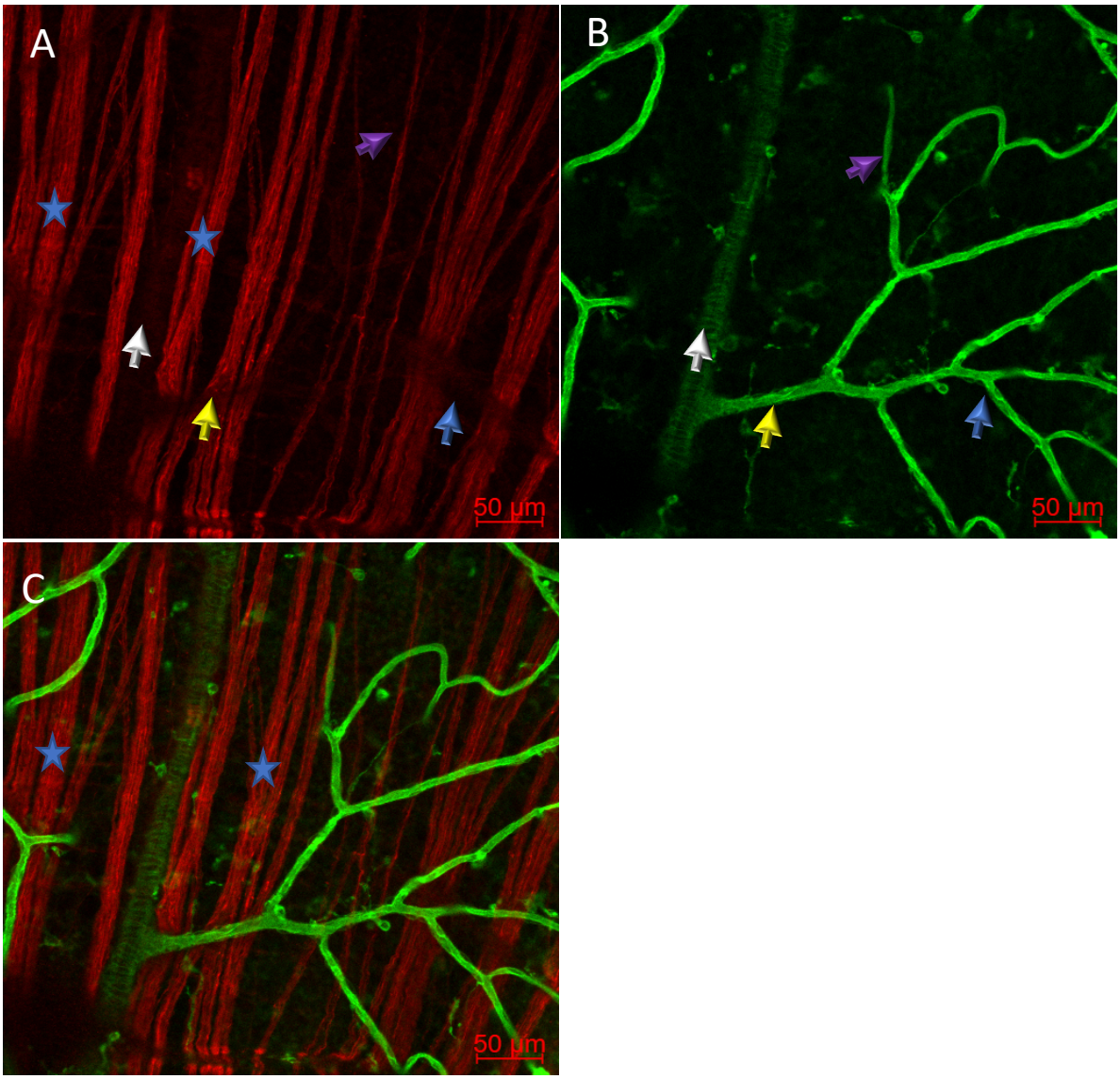

Figure 4.11. Single plane image of syndecan-1 and lectin labelling of the central rat retina. A. Syndecan-1 positive fluorescence signals were more intense in the ganglionic fibres (blue star) compared to that seen in the blood vessels. Large retinal radial artery (white arrowhead), primary branch (yellow arrowhead), secondary branch (blue arrowhead) and location of capillaries (purple arrowhead). Note the absence of syndecan-1 in the capillaries. B. lectin-labelled showing the corresponding vessels in A. C. Merged channel for syndecan-1 (red) and lectin (green).

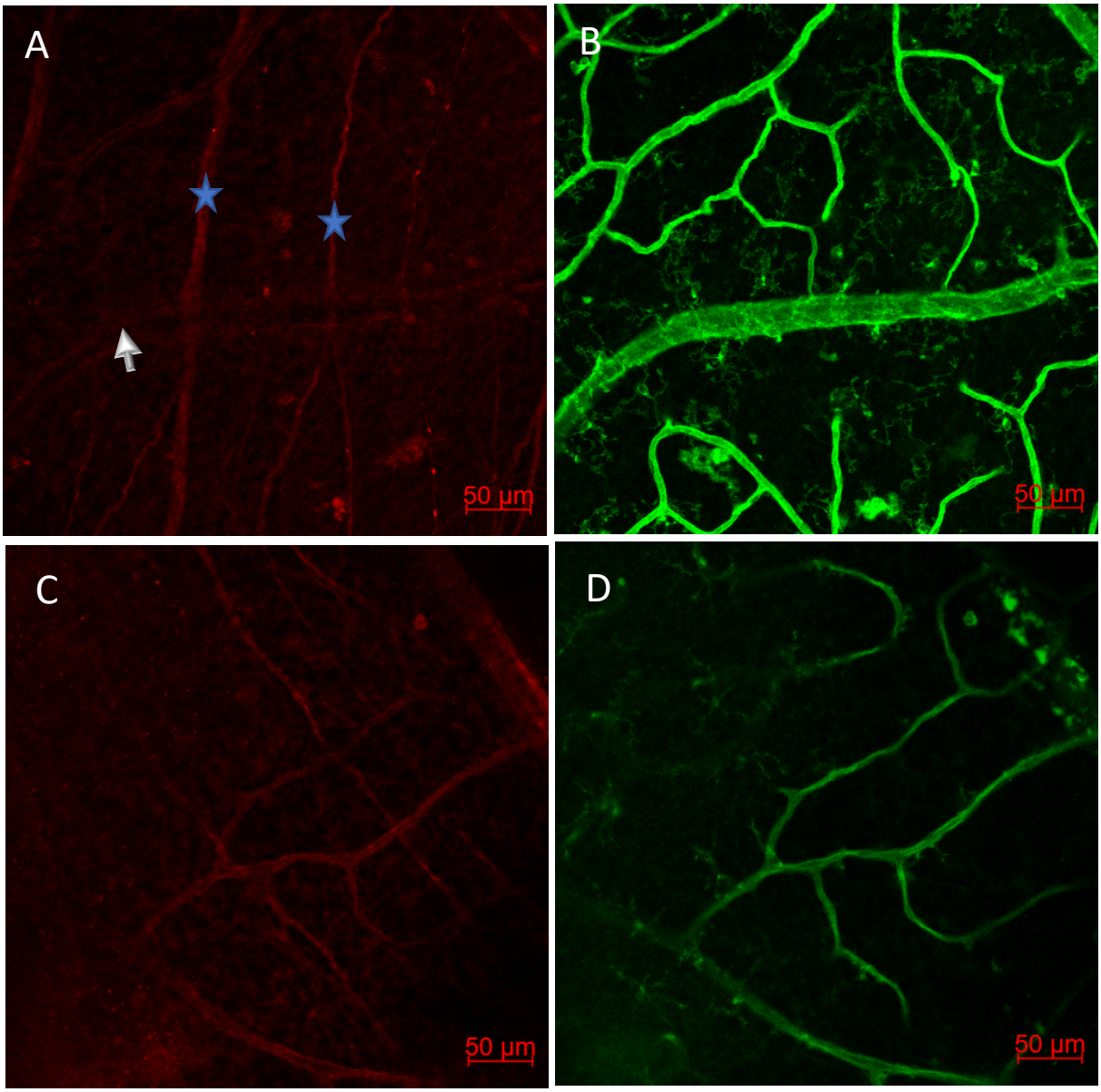

Figure 4.12. Single plane images of syndecan-1 and lectin labelling of the peripheral rat retina. A. Syndecan-1 expression is stronger in the peripheral region of the retina in the blood vessel (white arrowhead), blue star indicates ganglionic fibres. Note that ganglionic fibres in the peripheral region have thinner fibres and paler syndecan-1 staining B. Corresponding lectin labelling in the vessels (immersion-fixed) Syndecan-1 labelling in the peripheral region shows brighter signal intensity compared to A. D. Corresponding lectin labelling in the vessels (perfusion-fixed).

4.1.5 Identification of all BRB structures by multi-immunolabelling

Multi-immunolabelling with the final selection of antibodies (rabbit anti syndecan-1, mouse anti-NG2, and chick anti-GFAP, detected with anti-rabbit Cy3, anti- mouse Alexa 647 and DL 405) of the rat retina revealed intact structures of all the BRB components. These antibody combinations were then used for the rest of the study (Figure 4.13).

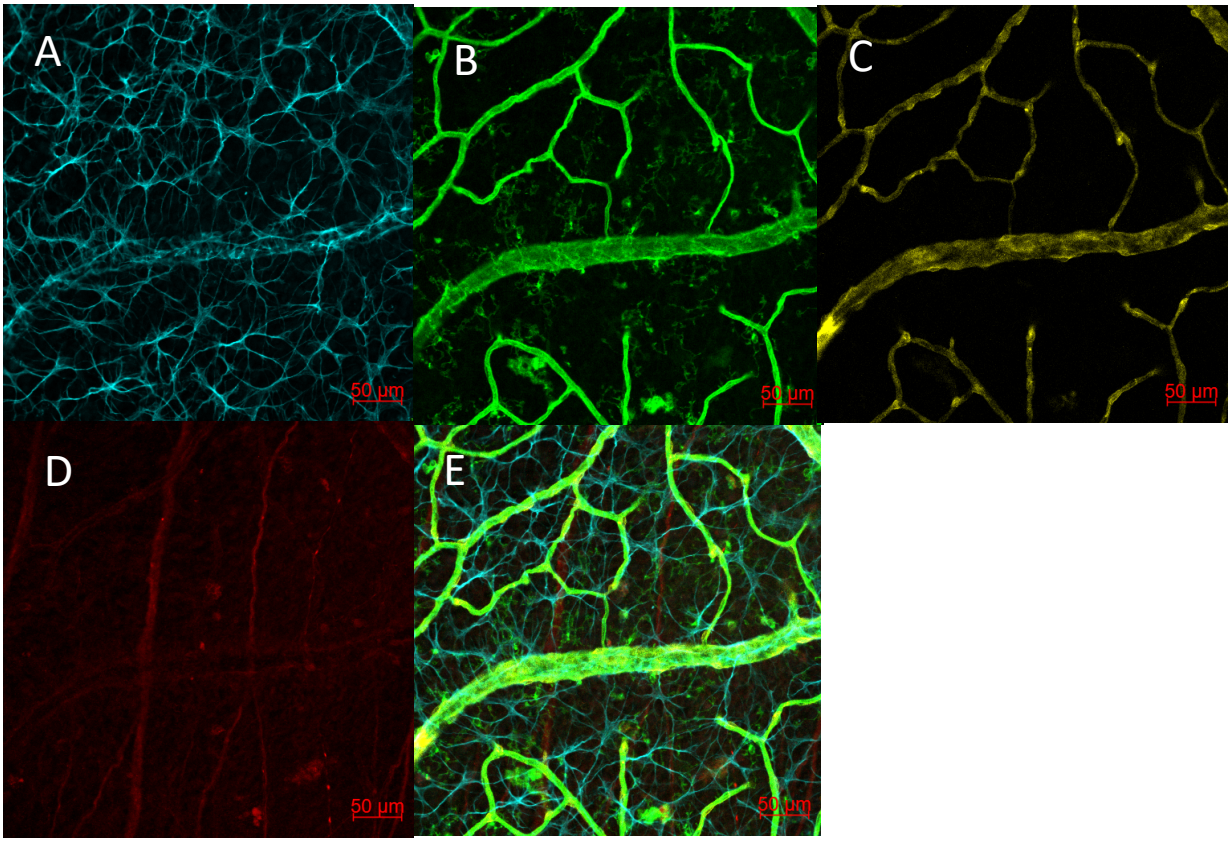

Figure 4.13. Single plane images showing multi-immunolabelled rat retina identifying all the BRB components. A. GFAP-positive astrocytes in the blue channel. B. Lectin labelling blood vessels in the green channel. C. NG2-labelled pericytes in the yellow/far red channel D. Syndecan -1 in blood vessels in the red channel. E. Merged channel image. All structures are clearly identified showing the multi-immunolabelling of all antibodies.

4.1.6 Identification of Heat shock protein (α -Crystallin A)

Different dilutions of α-Crystallin A antibody were used to identify Hsp, and a 1:200 dilution gave the best signal intensity. The Hsp was expressed in the superficial layers with intense fluorescence on ganglionic fibres similar to that seen for syndecan-1 (Figure 4.14). Some cellular like structures between the ganglionic fibres are being detected with Hsp antibody but with a lower signal intensity.

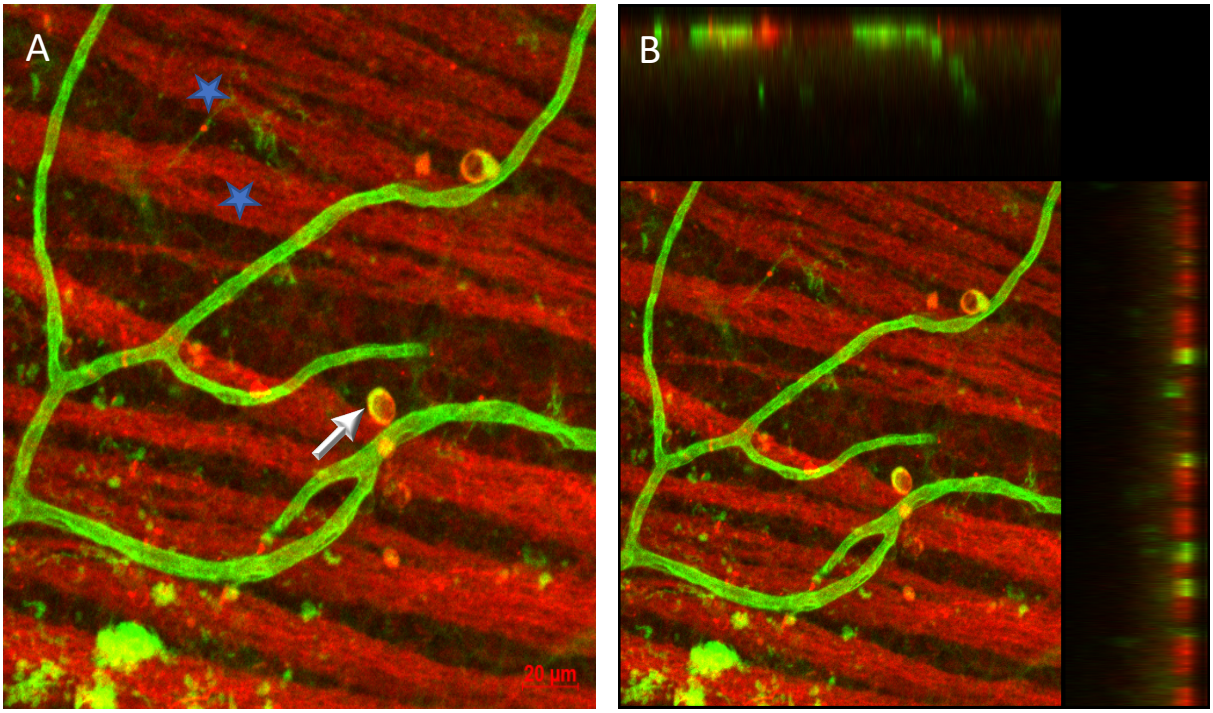

Figure 4.14. Single plane images showing multi-immunolabelling of the rat retina identifying Heat shock proteins (α-Crystallin A). A. Merged channel of lectin (green) and α-Crystallin A (red) showing ganglionic fibres (blue star) with some cellular-like structures showing positive signal (white arrow). B. An orthogonal image showing Hsp at the superficial level.

4.1.7 Negative immunolabelling controls

To verify the specificity of the primary antibodies, the immunolabelling procedure excluded the primary antibodies, with only secondary antibodies and lectin used in the secondary antibody solution. Only lectin signals are present with no detection of primary antibodies seen in the other channels (Figure 4.15).

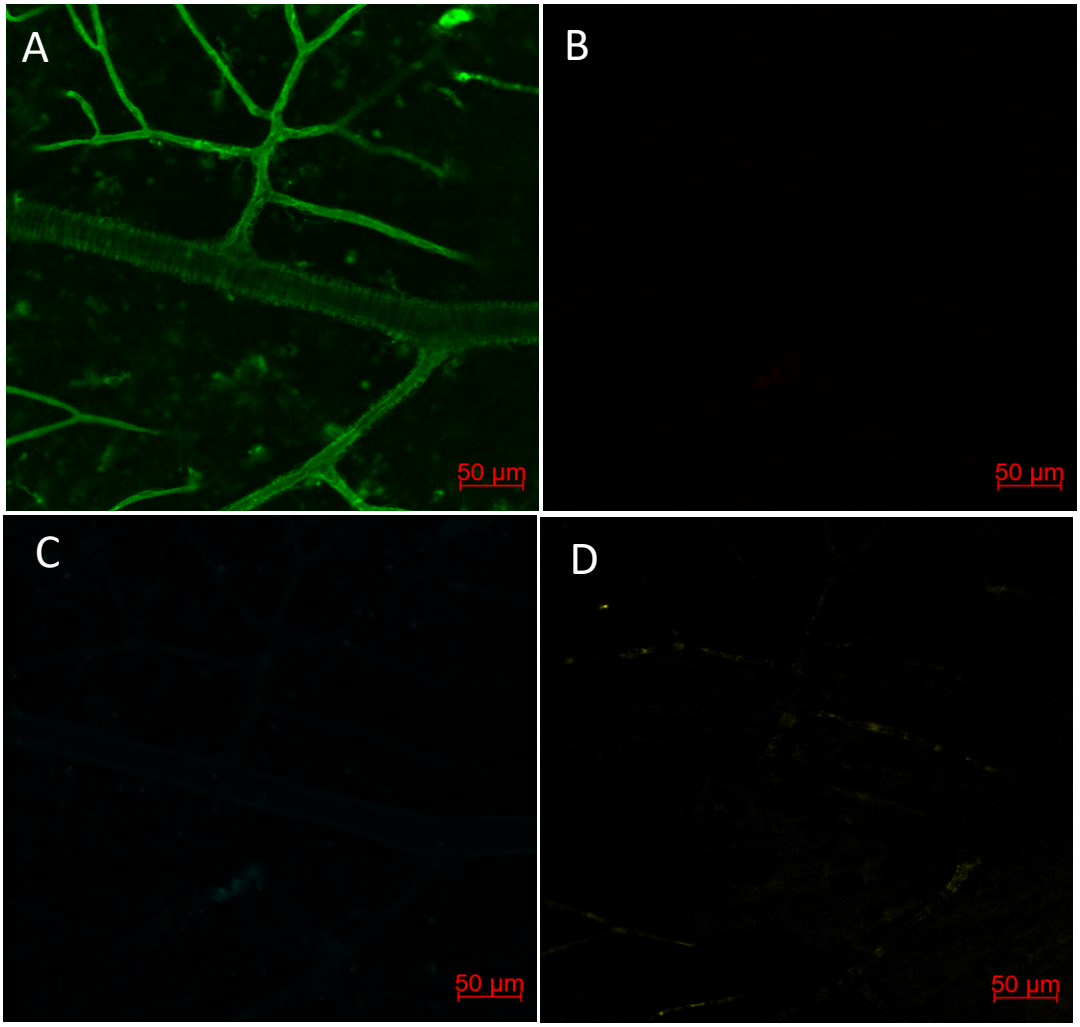

Figure 4.15. Single plane image of rat retina immunolabelled with only secondary antibodies. A. Lectin-positive signals delineating the blood vessels. B. Anti-rabbit Cy3 used for detecting rabbit anti-syndecan-1 or anti-α-crystallin A antibodies. C. Anti-ChickDL405 antibody used for detection of Chick anti-GFAP D. Anti-mouse Alexa 647 used for detection of for mouse anti-NG2.

4.2 The effect of time and retinal preparation on the integrity of the BRB in normoglycaemic superfused or cultured retinae

4.2.1 The effect of time and retinal preparation on the vascular cellular components of the BRB in normoglycaemic superfused or cultured retinae

All structures that make up the blood retinal barrier (BRB, i.e., the vascular endothelium, pericytes and astrocytes), were well preserved after 3 hours of normoglycaemic oxygen superfusion in both retinal explants and eyecups. The only noticeable difference between the superfused versus freshly harvested retinae was a slight reduction in signal intensity of the pericytes and astrocytes (Figure 4.16). In general, there were no significant morphological differences in the vasculature, pericytes and astrocytes between explant and eyecup preparation types after 3 hours of superfusion. However, a slight reduction in GFAP signal intensity and occasional possible clumping of astrocyte processes was observed at the 3-hour time point in explants (Figure 4.17). Similarly, there was no morphological evidence of significant differences in astrocyte area coverage between 1 and 3 hours of normoglycaemic superfusion (Figure 4.17). Quantitative analysis showed no significant differences between time points for either explant or eyecup preparations but statistically significant higher astrocyte area coverage in the eyecup compared to explant retinae at the 1-hour superfusion time-point (Figure 4.18). In retinal explants cultured for 48 hours, GFAP-positive astrocytes were still present with a moderate signal intensity. However, on morphological examination, astrocyte processes appeared to be thickened or clumped and astrocytes showed moderate to severe apoptotic-like changes with a punctate pattern which appeared to be associated with possible degenerating astrocytes processes along vessels (Figure 4.19).

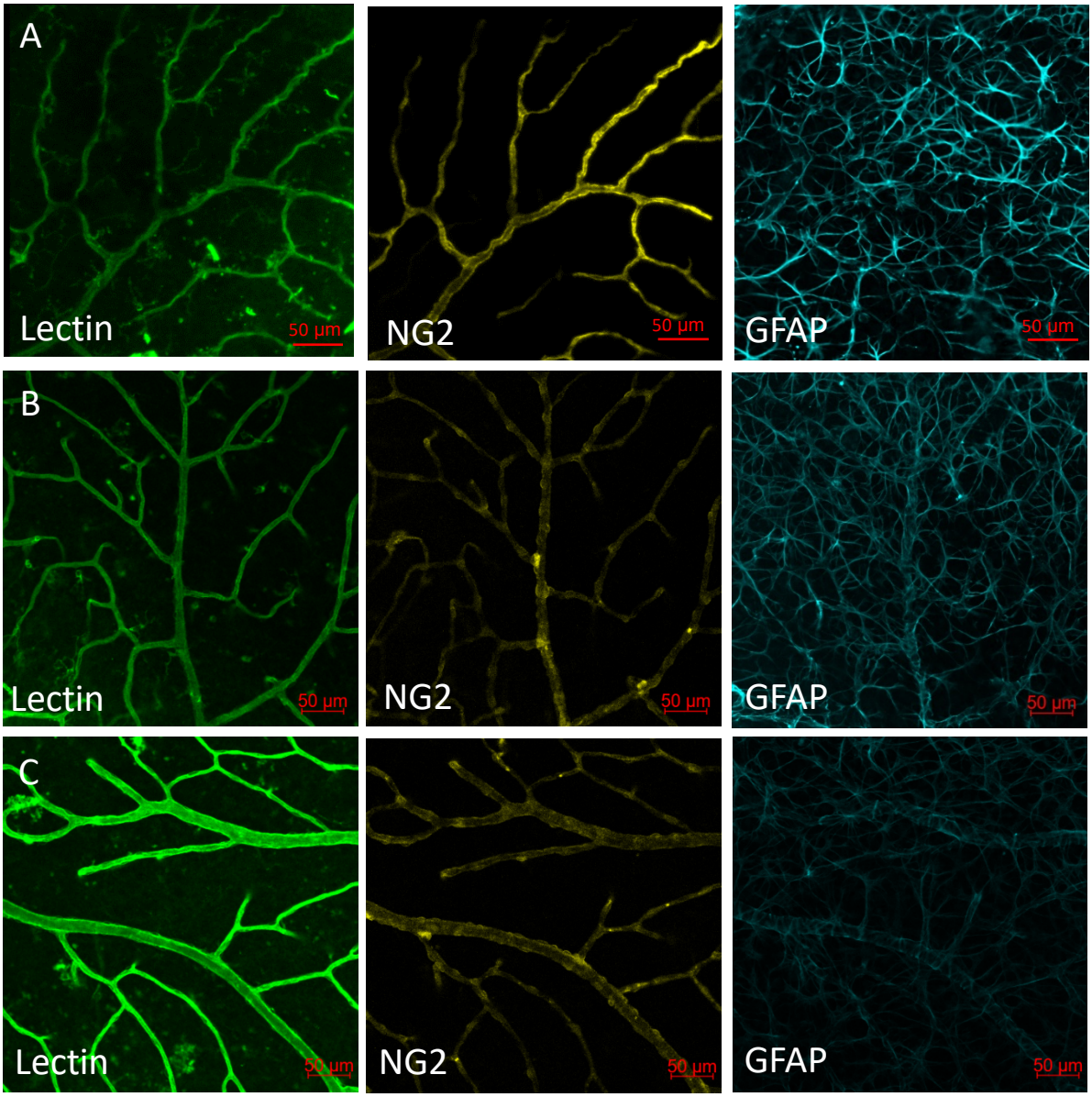

Figure 4.16. Single plane images showing evidence of intact structures and preservation of the blood retinal barrier for up to 3 hours: Superficial retinal planes showing lectin-labelled blood vessels, NG2-immunolabelled pericytes and GFAP-immunolabelled astrocytes. A. Freshly harvested (time zero) retina B. Retinal explant after 3 hours of superfusion. C. Retinal eyecup after 3 hours of superfusion.

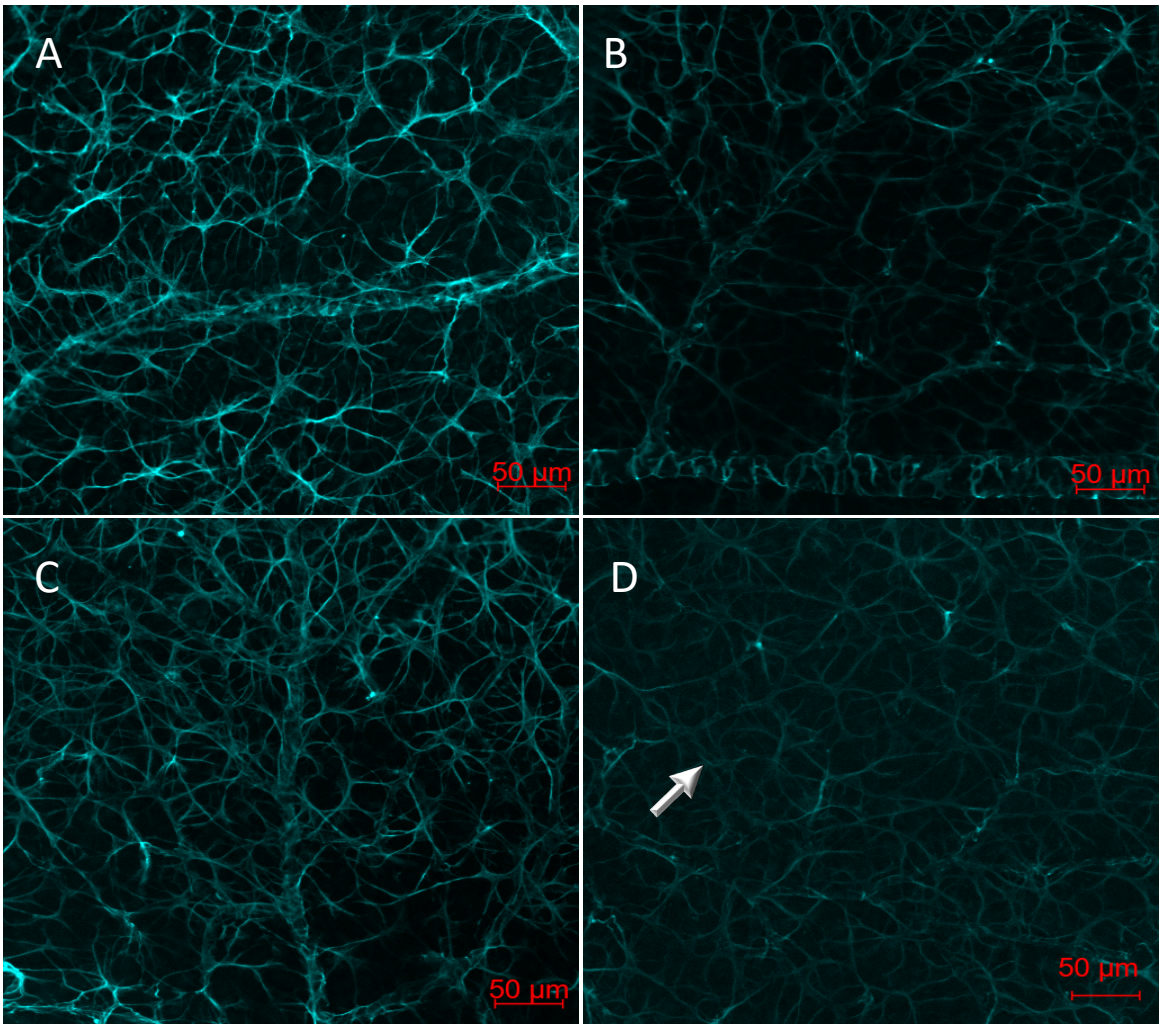

Figure 4.17 Effect of time in normoglycaemic superfusion on astrocyte coverage. A. Retinal eyecup preparation after 1 hour of superfusion. B. Retinal explant preparation after 1 hour of superfusion. C. Retinal eyecup preparation after 3 hours of superfusion. D. Retinal explant preparation after 3 hours of superfusion. Slight clumping of astrocyte processes (white arrow).

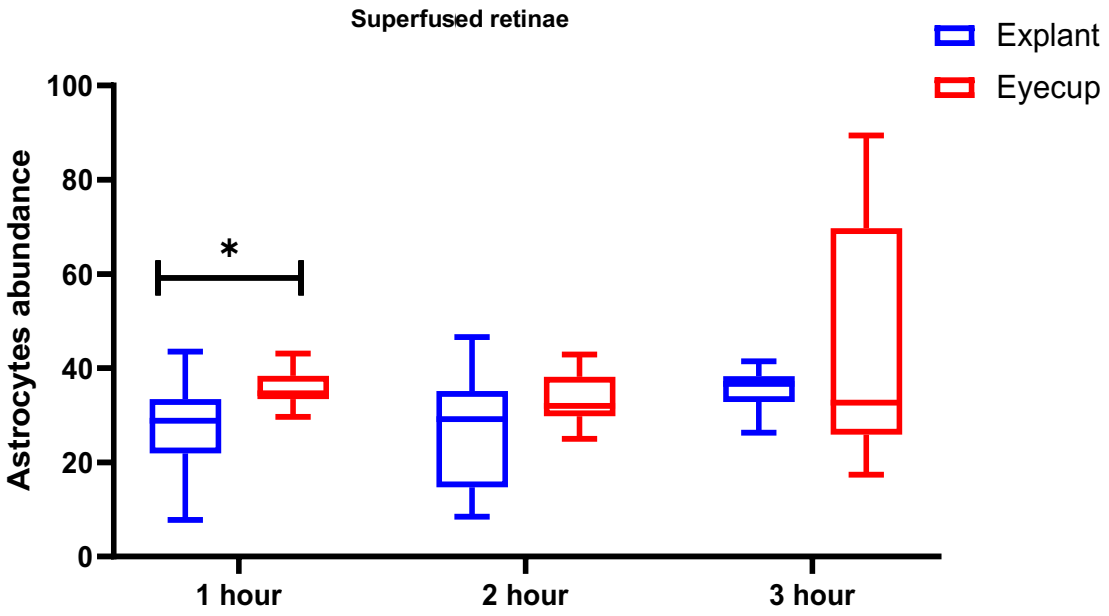

Figure 4.18 Box and whisker plots of astrocyte abundance (area coverage) in retinal explant and eyecup preparations superfused under normoglycaemic conditions for 1, 2 and 3 hours. P <0.0108 (n = 2 retinae per group).

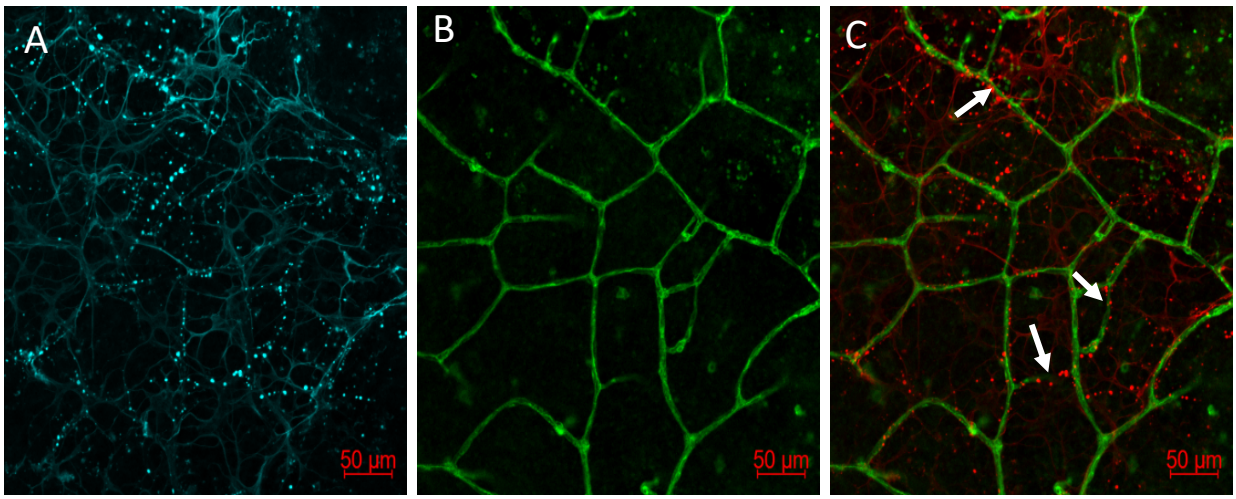

Figure 4.19. Single plane images of astrocyte morphology after 48 hours in normoglycaemic culture conditions. A: GFAP-positive astrocytes with punctate pattern suggestive of apoptotic-like features. B: Lectin-labelled blood vessels in corresponding green channel. C: Merged pseudocoloured GFAP signal (red) showing a punctate pattern concentrated along blood vessels (arrows).

4.2.2 The effect of time and retinal preparation type on Syndecan-1 in retinal blood vessels of normoglycaemic superfused or cultured retinae.

This section describes the effect of time and retinal preparation type on Syndecan-1 in retinal blood vessels of normoglycaemic superfused or cultured retinae on the expression of syndecan-1. Morphological assessment of the blood vessels of explant and eyecup retinal preparations superfused under normoglycaemic conditions for up to 3 hours, showed the presence of syndecan-1-positive signals in the larger blood vessels, with lower fluorescence intensity in the primary and secondary branches and lastly, the capillaries, which had the lowest fluorescence intensity (Figure 4.20). Semiquantitative analysis of syndecan-1 fluorescence intensity in retinal blood vessels showed no significant difference in Syndecan-1 fluorescence intensities between time points for explant and eyecup preparations, but showed a significantly higher syndecan-1 signal intensity in the retinal explants compared to the eyecup preparations after 1 hour of normoglycaemic superfusion ($p = 0.0034$) (Figure 4.21). After 48 hours in culture under normoglycaemic conditions, retinal explants showed bright syndecan-1 signal intensity in all blood vessels which was higher than that seen in the superfusion groups (Figures 4.22 and 4.23).

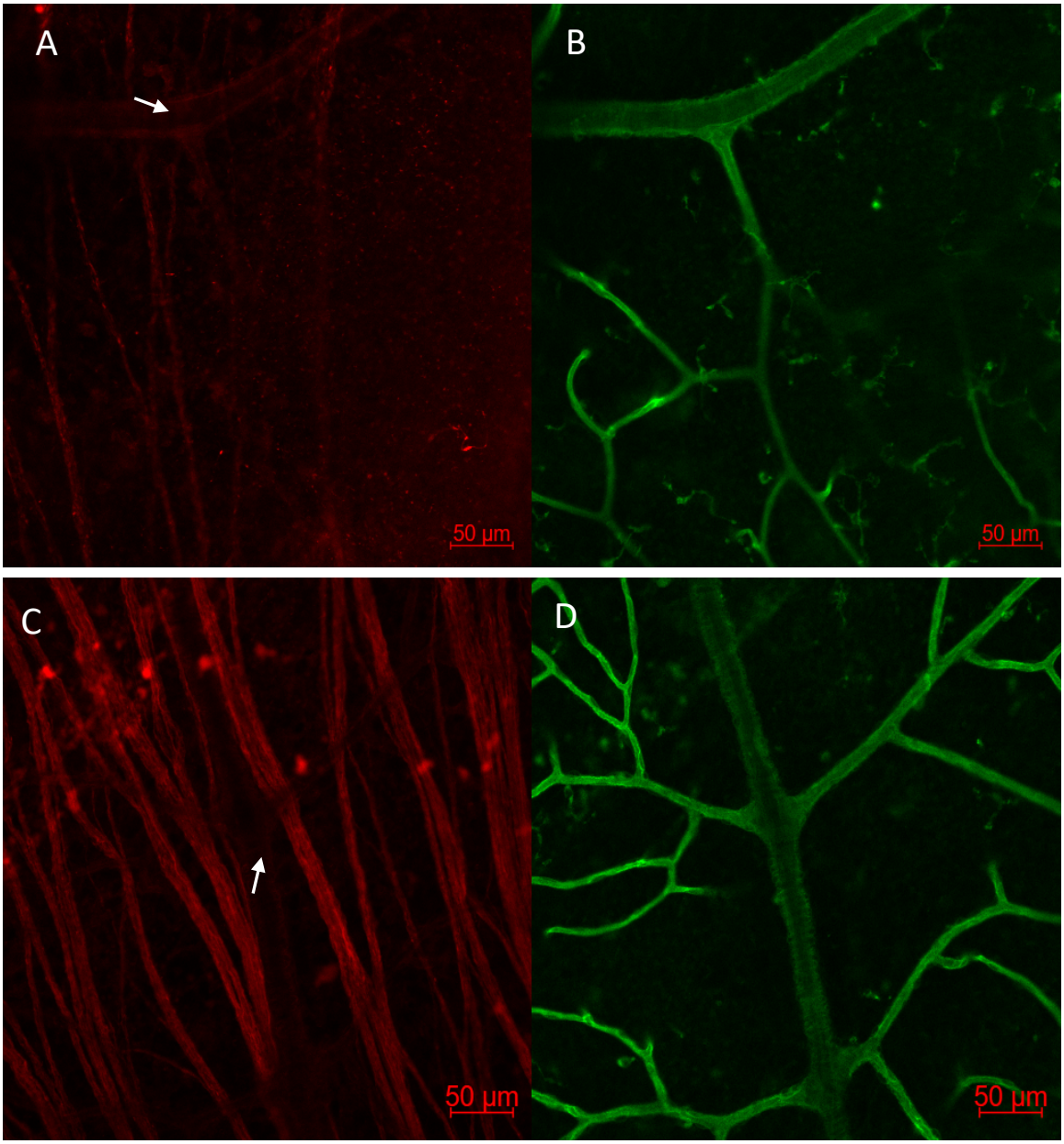

Figure 4.20. Single plane images of astrocyte morphology after 48 hours in normoglycaemic culture conditions. A. Syndecan-1 immunolocalisation in blood vessels in a retinal eyecup preparation after 1-hour normoglycaemic superfusion (white arrow indicates retinal radial artery) B. Lectin-labelled blood vessels in the corresponding green channel. C. Slightly reduced syndecan-1 signal intensity is seen in the blood vessel in a retinal explant preparation after 1-hour normoglycaemic superfusion (white arrow indicates retinal radial artery). D. Lectin-labelled blood vessels in corresponding green channel**.** Note: although 1-hour image is shown above, findings were similar at 3 hours.

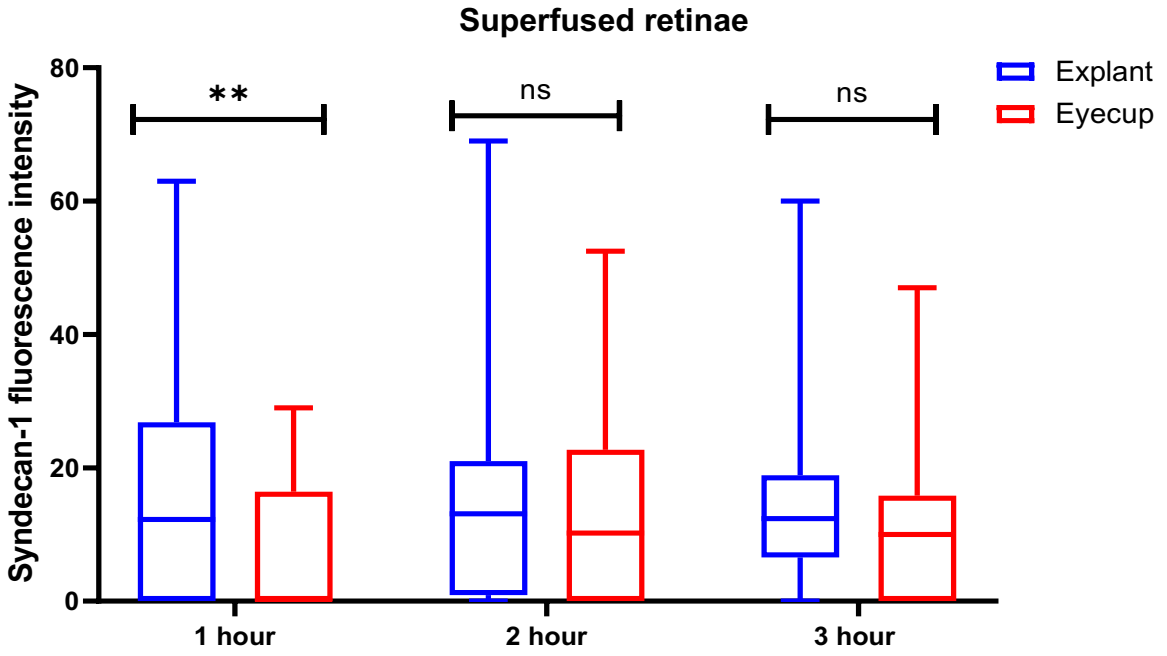

Figure 4.21. Box and whisker plot of Syndecan-1 fluorescence intensity in explant and eyecup preparation types after 1, 2 and 3 hours of normoglycaemic superfused retinae. P = 0.0034. (n = 2 retinae per group).

.

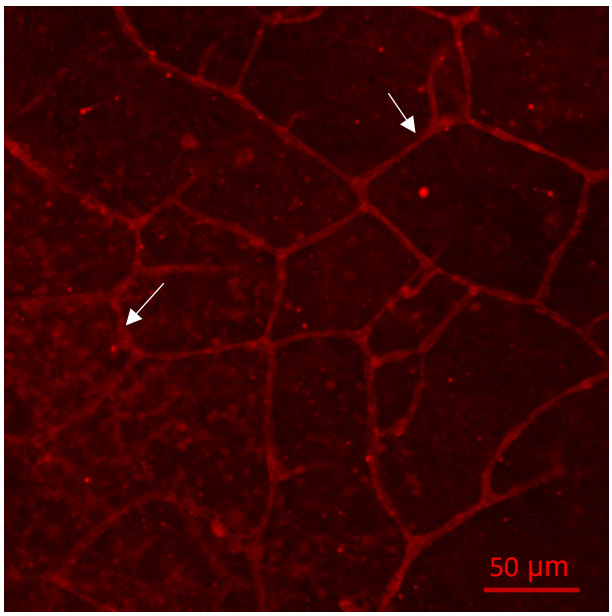

Figure 4.22. Single plane image of syndecan-1 in the capillaries of a retinal explant after 48 hours in culture under normoglycaemic conditions. White arrows indicate syndecan-1 in the capillaries.

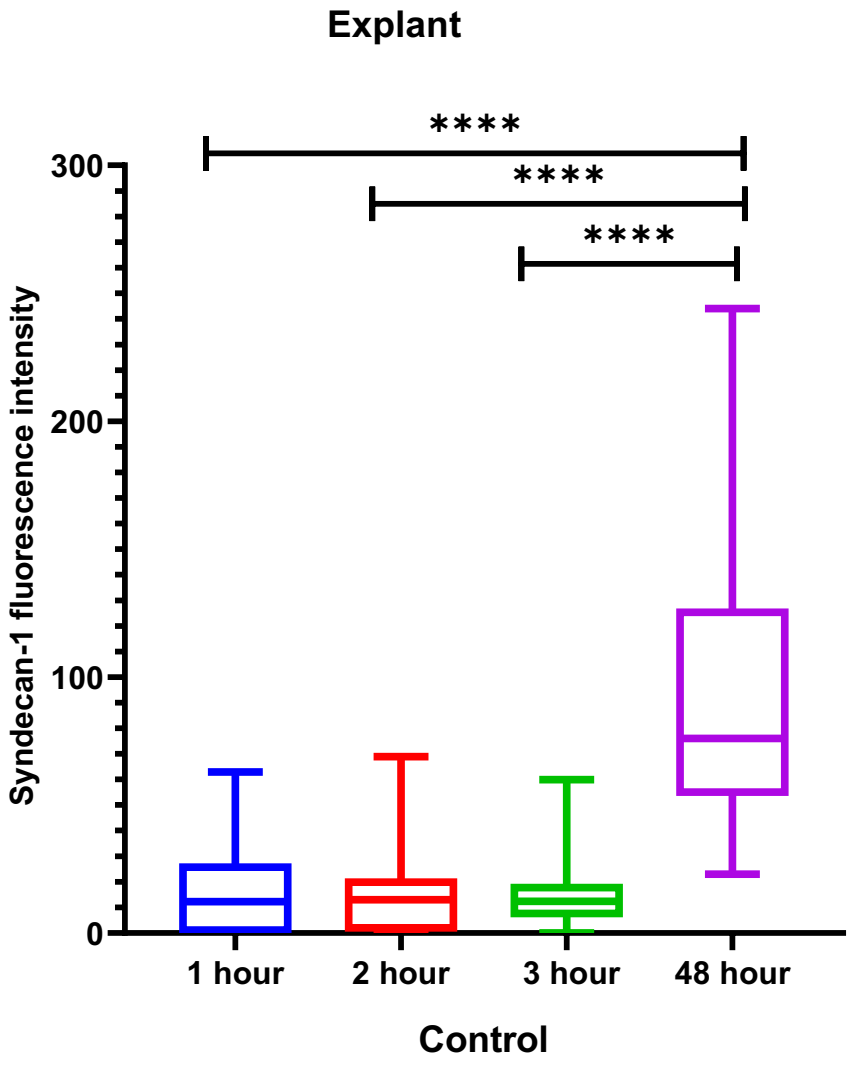

Figure 4.23. Box and whisker plots of syndecan-1 fluorescence intensity in control superfused retinal explants over time. **** = $p<0.0001$. (n = 4 retinae per group and n=1 for 48-hour group)

4.3 Effect of hyperglycaemia on the integrity of the BRB and other retinal structures

4.3.1 Effect of hyperglycaemia on retinal blood vessels

4.3.1.1 Effect of hyperglycaemia on blood vessel morphology

In the rat retinal superfused model, the lectin-labelled blood vessels were intact across all time points in the control and hyperglycaemic groups for both retinal explants and eyecup preparations. A slight difference was noted in the blood vessel width in randomly selected images between the control and hyperglycaemic group in the deep layers of the 3 hours superfusion eyecup group (Figure 4.24) with the lowest width = 4.09μm and highest width = 6.18μm in the control group, and lowest width = 3.57μm and highest width = 4.84μm in the hyperglycaemia group. Other representative images of the superficial and deepest vascular planes of explant and eyecup groups at the 1 and 3 hours superfusion time points are in Appendix 5. After 48 hours in culture, lectin-labelled blood vessels were relatively intact and signal intensity was bright in control and hyperglycaemic groups. The width of the capillaries was reduced in the hyperglycaemic group compared to the control counterpart both in the superficial and deep vascular layers (Fig 4.25).

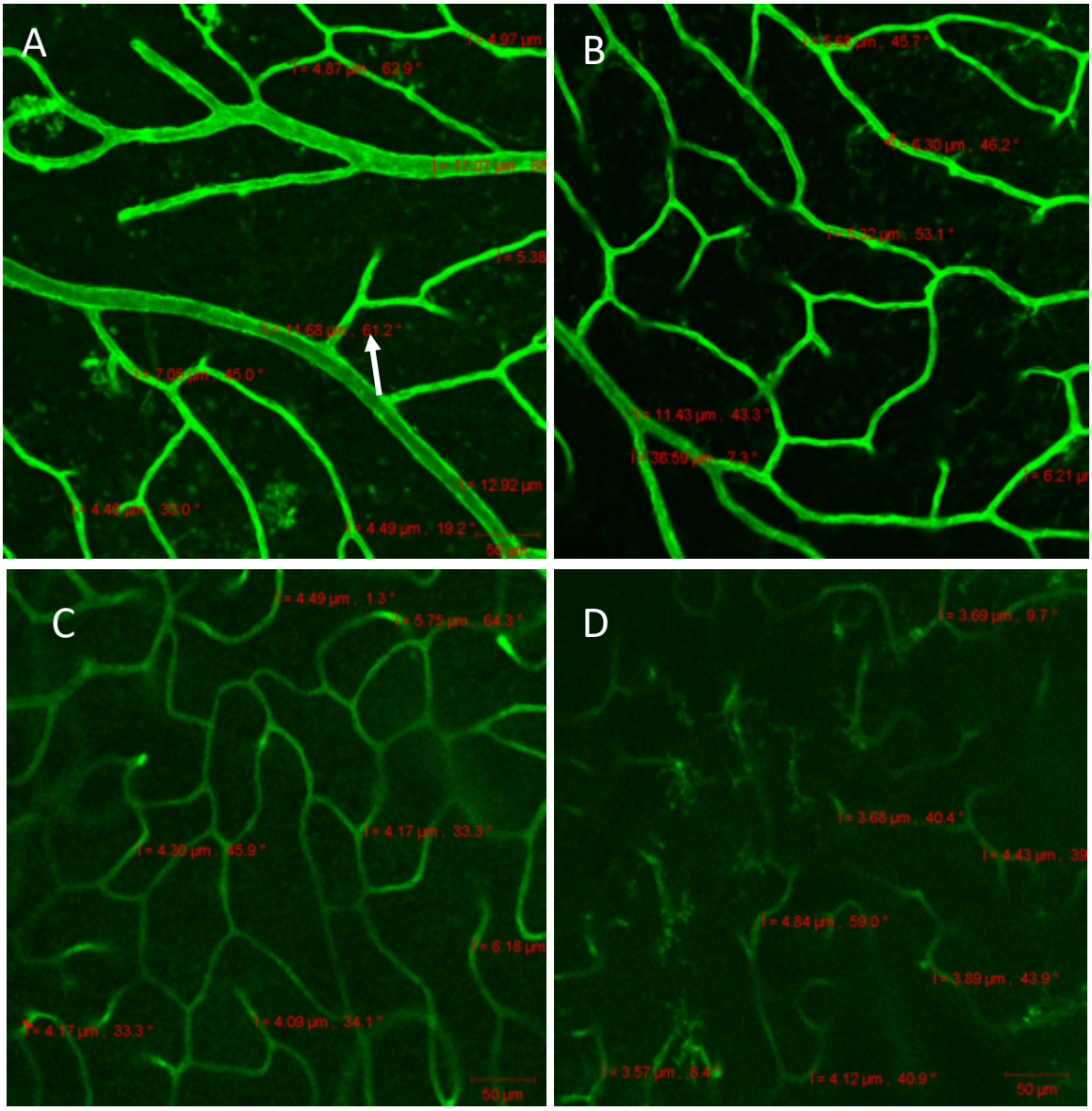

Figure 4.24. Superficial and deep optical planes showing the effect of hyperglycaemia on rat retinal blood vessels in 3 hour superfused rat retina. A. Control eyecup after 3 hours of superfusion – superficial layer. B. Hyperglycaemia eyecup after 3 hours of superfusion – superficial layer. C. Control eyecup after 3 hours of superfusion – deep layer. D. Hyperglycaemia eyecup after 3 of hours superfusion – deep layer. Note the narrowing of the blood vessels seen in the hyperglycaemic groups compared to the control. The values in red on the images represent retinal blood vessel width (white arrow).

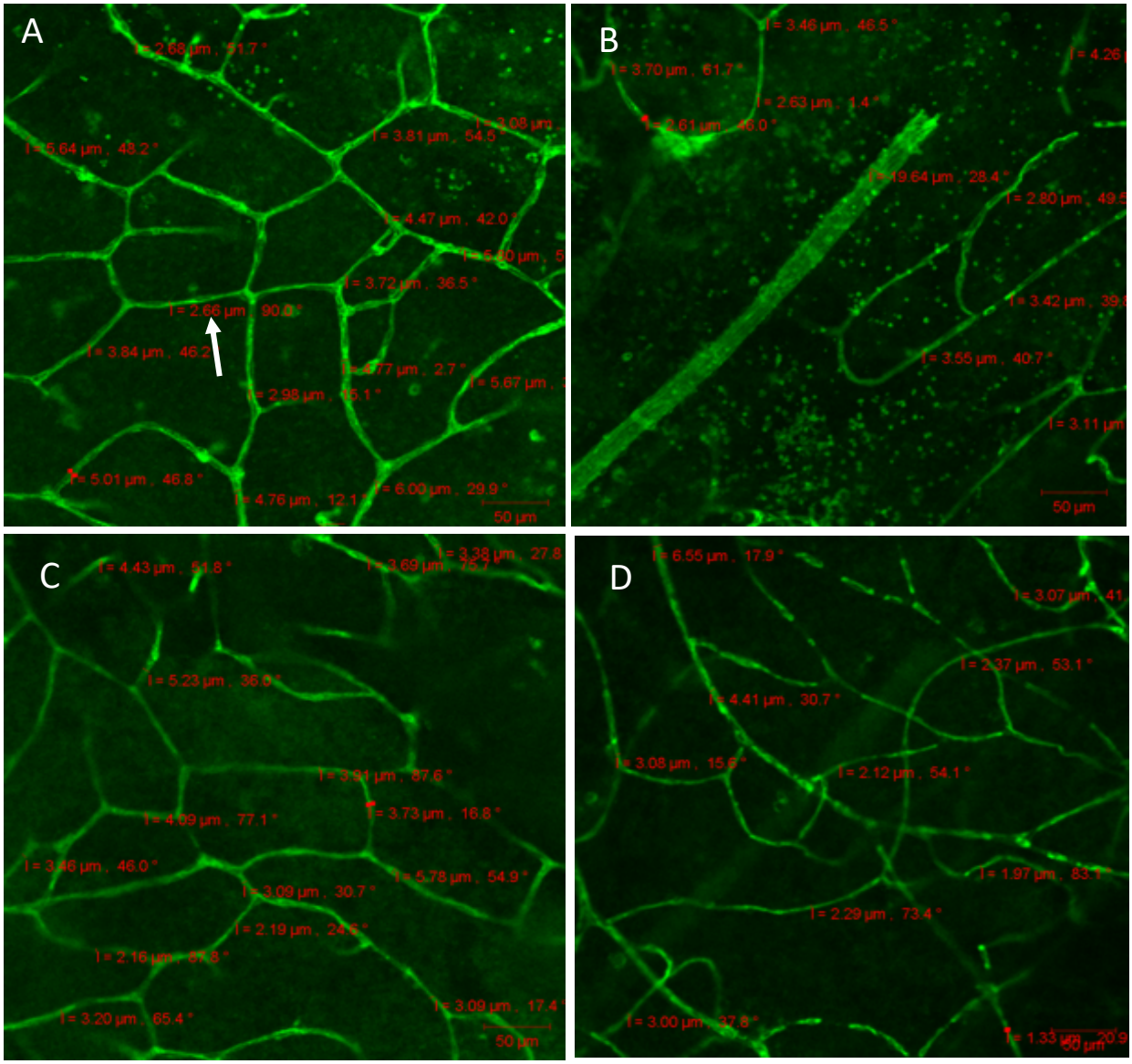

Figure 4.25. Superficial and deep optical planes showing the effect of hyperglycaemia on rat retinal blood vessels after 48 hours in culture. A Control – superficial layer B. Hyperglycaemia - superficial layer. C. Control – deep layer. D. Hyperglycaemia – deep layer. Note the narrowing of the blood vessels seen in the hyperglycaemic groups compared to the control. The values in red on the images represent retinal blood vessel diameter (white arrow).

4.3.1.2 Effect of hyperglycaemia on syndecan-1 fluorescence intensity in blood vessels

Analysis of immunolabelled retinae revealed that syndecan-1 fluorescence intensity was significantly higher in the 1-hour hyperglycaemic superfused retinae compared to the controls (p = <0.0001). A similar trend was observed at 2 and 3 hours, but these did not reach statistical significance (p = 0.7734, p = 0.7965, respectively). Although the statistical power is very low (n=1), syndecan-1 fluorescence intensity was lower in the hyperglycaemic group compared to the control after 48 hours in culture (Figure 4.26). Syndecan-1 fluorescence intensity was also statistically analysed at individual time points for explants and eyecups. Eyecups showed a statistically significant increase in signal intensity at 1 hour and 3 hours in the hyperglycaemic groups. Explants from 1 to 3 hours showed no significant difference between control and hyperglycaemic groups across the time points (Figure 4.27).

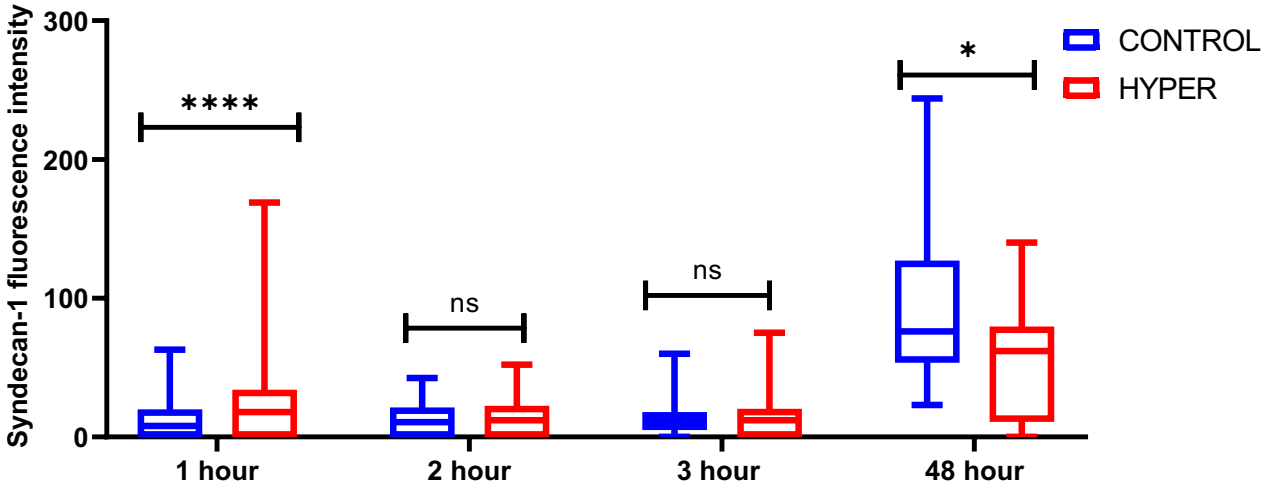

Figure 4.26: Box and whisker plots of syndecan-1 fluorescent intensity in hyperglycaemic and control groups of rat retina at different time points (1, 2, 3 and 48 hours). P value <0.05 = statistically significant, **** = p value <0.0001, * = p value <0.0083. (n = 4 retinae per group and n = 1 for the 48-hour group). Note: HYPER= hyperglycaemia.

Table 4.1. Syndecan-1 protein expression in hyperglycaemic and control combined explant and eyecup at 1, 2 and 3-hour time points

	Syndecan-1 CONTROL	**Syndecan-1 HYPERGLYCAEMIA**	**P value**
	Median (25% -75% IR)	Median (25% -75% IR)	
1-hour	7.95 (0.00-19.33)	18.05 (0.00-33.50)	**<0.0001**
2-hour	11.00 (0.00- 21.00)	12.00 (0.00- 22.40)	0.7734
3-hour	11.65 (5.60- 17.38)	12.15 (0.00- 19.83)	0.7965

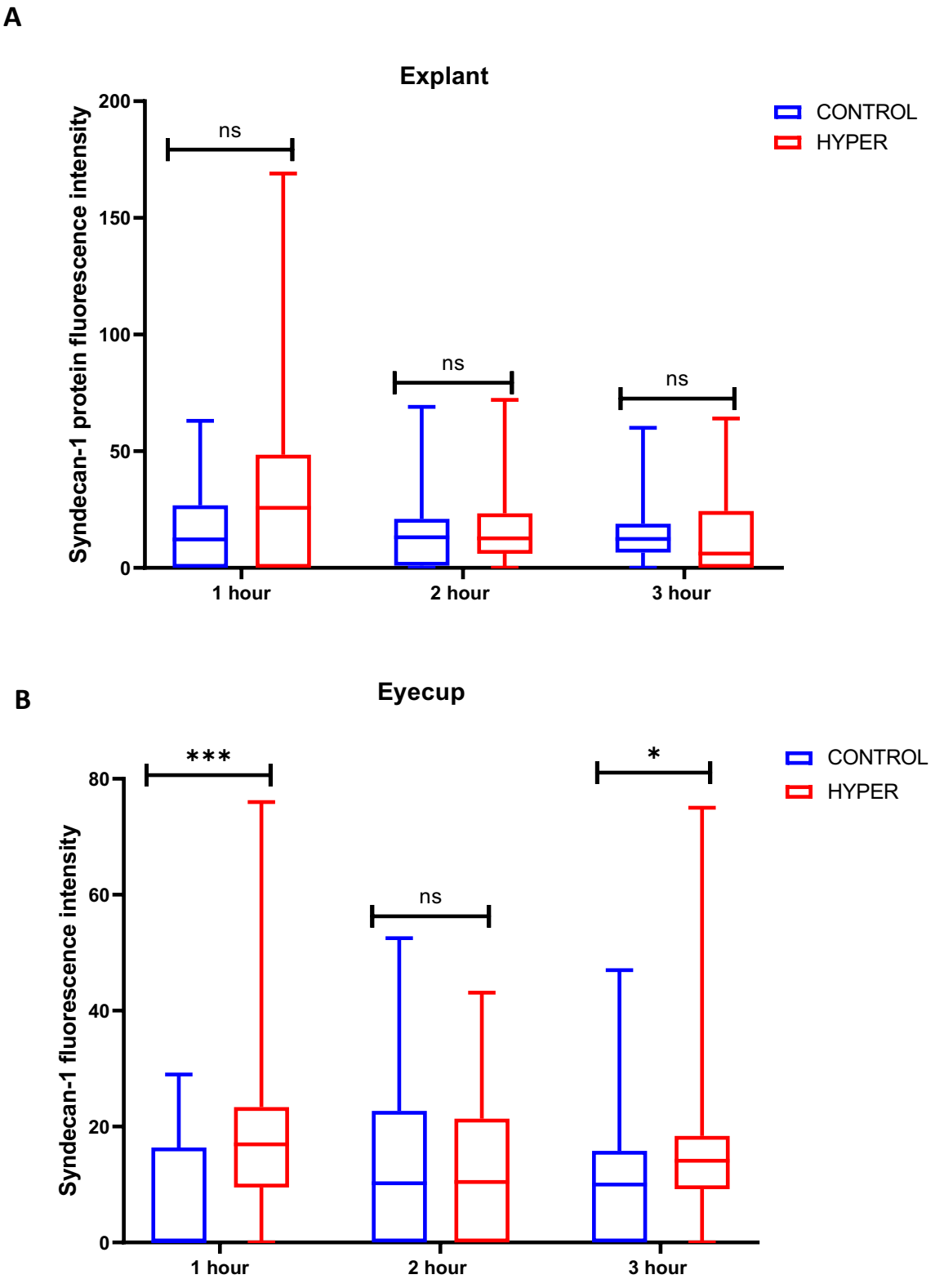

Figure 4.27 Box and whisker plots of showing the effect of hyperglycaemia on Syndecan-1 fluorescence intensity. A. eyecup hyperglycaemic and control groups of rat retina 1, 2 and 3 hours. B explants hyperglycaemic and control groups of rat retina at 1, 2 and 3 hours. P value <0.05 = statistically significant. **** = <0.0001 * = <0.0199, (n = 2 retinae/group). Note: HYPER = hyperglycaemia.

4.3.1.3 Effect of hyperglycaemia on pericyte morphology

After superfusion and immunolabelling of rat retinae, morphological assessment showed no difference in NG2 signal intensity in both the control and hyperglycaemic explant and eyecup preparations across the time points (Figure 4.28). However, the hyperglycaemic group showed a reduced number of "nuclear bulges" of the pericytes in the deep layers of the retina (both eyecup and explant). This was objectively scored based on the number of nuclei in the capillaries per field. All control superficial layers had a semiquantitative score of 3, while the deep layers had a score of 1. Additional images are attached in Appendix 6, (where there is a clear difference between the control and hyperglycaemia at 3 hours). After 48 hours in culture, there was no reduction in the fluorescence intensity of pericytes compared to the superfused retinae. However, there was a marked reduction in the number of pericyte nuclei bulges after 48 hours in culture with slightly greater loss in the hyperglycaemic group compared to the control group which was more evident in the deep layer of the hyperglycaemic group having a score of 0 with complete loss of pericytes. (Figure 4.29).

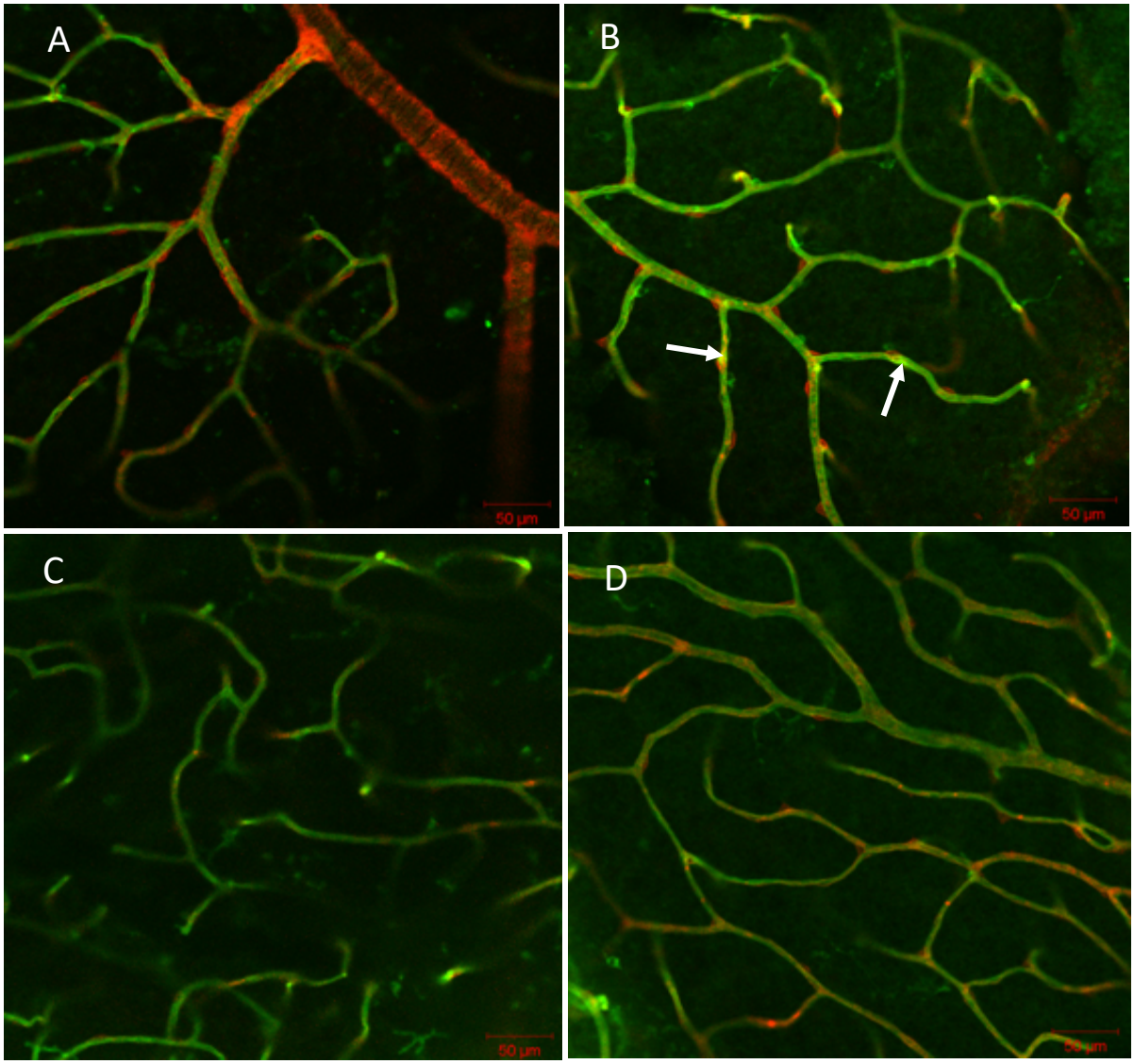

Figure 4.28. Single image planes of the superficial and deep layers of the retinal vessels showing the effect of hyperglycaemia on pericytes. A. Control explant: after 1-hour superfusion – superficial layer. B. Hyperglycaemia explant: after 1-hour superfusion – superficial layer. C. Control explant: after 1-hour superfusion – Deep layer. D. Hyperglycaemia explant: after 1-hour superfusion – Deep layer. Note: Pericytes and their nuclei around lectin-labelled blood vessels (white arrow).

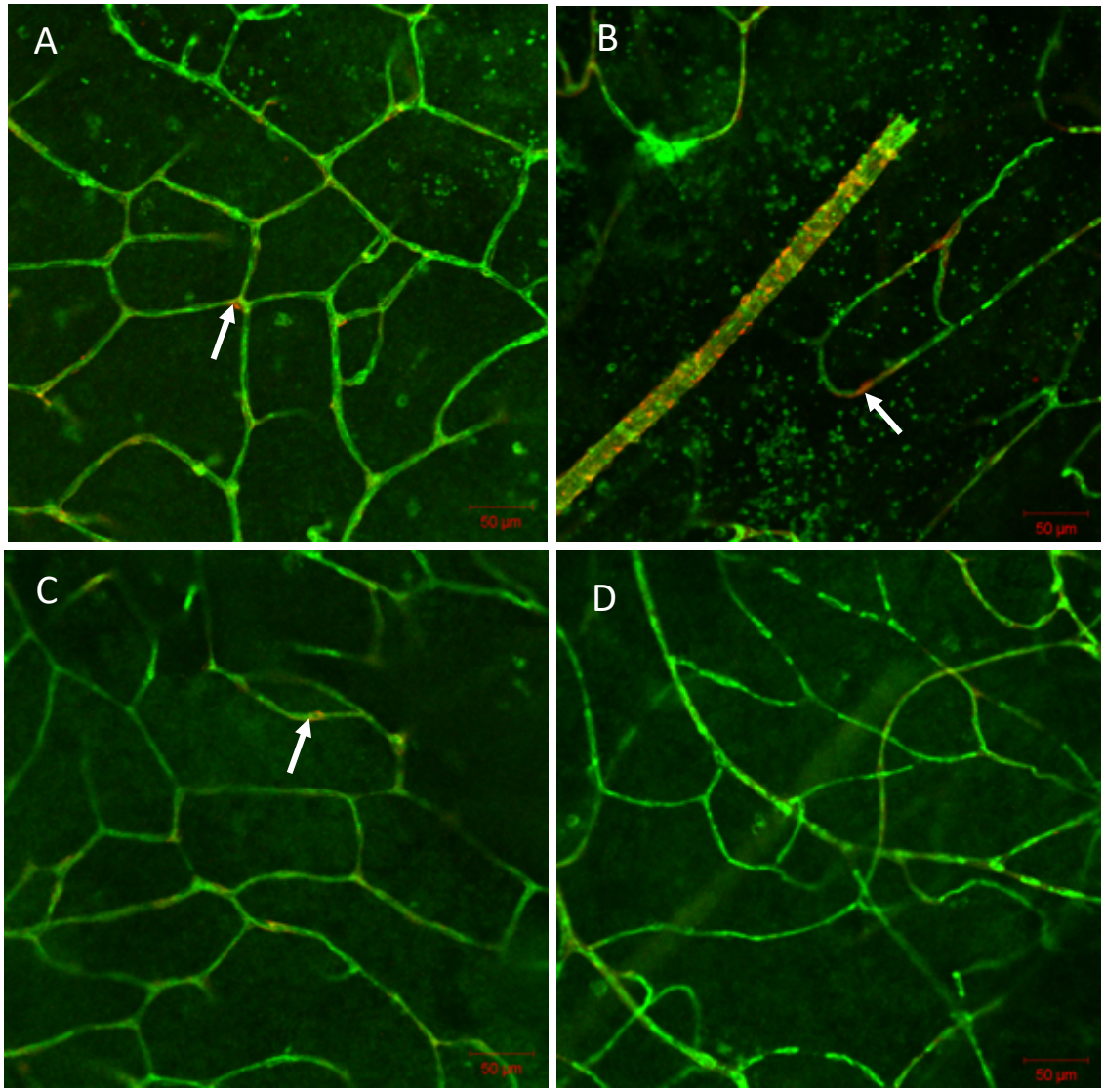

Figure 4.29. Single image planes of the superficial and deep layers of NG2 labelling on pericytes after 48 hours in culture. Combined channel images of lectin and NG2- labelled pericytes. A. Control – superficial layer. B. Hyperglycaemia– superficial layer. C. Control – Deep layer. D. Hyperglycaemia– Deep layer. Note: White arrows showing pericyte nuclei bulge.

4.3.2 Effect of hyperglycaemia on neural tissues

4.3.2.1 Effect of hyperglycaemia on astrocyte morphology and area coverage

Astrocytes area coverage in the hyperglycaemic and control groups of the superfused model were assessed in different retinal preparation types, i.e. explant and eyecup and at different time points 1, 2 and 3 hours. Morphologically, astrocytes were observed in all fields of the retinal explant, and there was no significant difference in signal intensity in both the hyperglycaemic and control groups across the time points. At 3 hours post-superfusion, there was some evidence of astrocytes appearing fragmented with features of apoptosis (Figure 4.30). Similarly, quantitative analysis showed no statistical difference between astrocyte area coverage in control and hyperglycaemia groups across the time-points in the superfused model (Figure 4.31). In the 48-hour cultures, astrocytes were substantially reduced in number with a higher degree of cell loss in the hyperglycaemic group compared to the control. Also, there was severe astrocytes damage in the hyperglycaemic group compared to the control group (Figure 4.32).

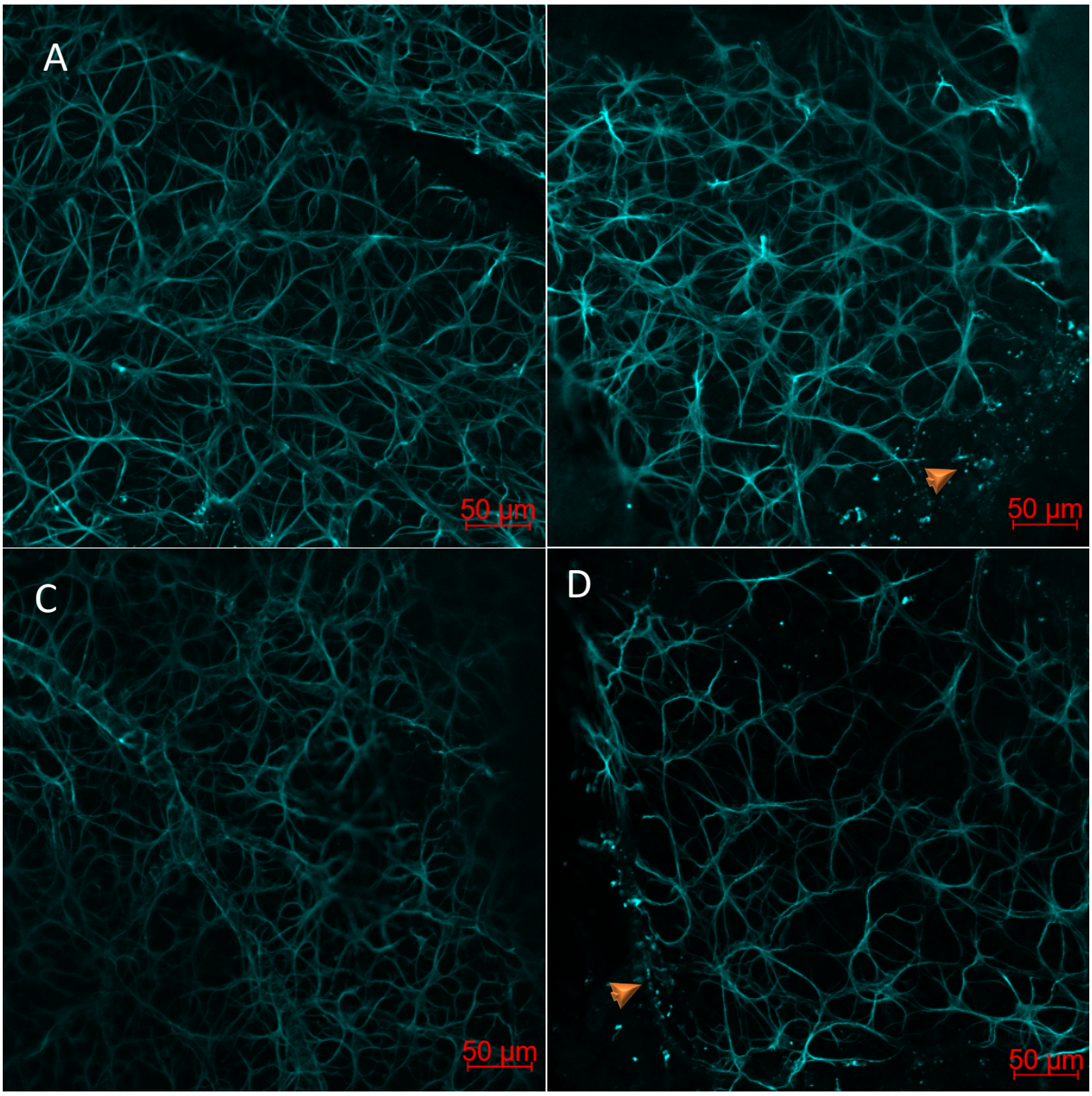

Figure 4.30. Single plane images of GFAP immunolabelling showing astrocytes in the superfused control and hyperglycaemic explant and eyecup rat retina at 1 and 3 hours. A. Eyecup from 1 hour hyperglycaemia group. B. Explant from 1-hour hyperglycaemia group showing punctate labelling (orange arrowhead) in the superficial layer of the image reflecting cell fragmentation. C. Eyecup from 3-hour hyperglycaemia group. D. Explant from 3-hour hyperglycaemia group showing punctate labelling (orange arrowhead).

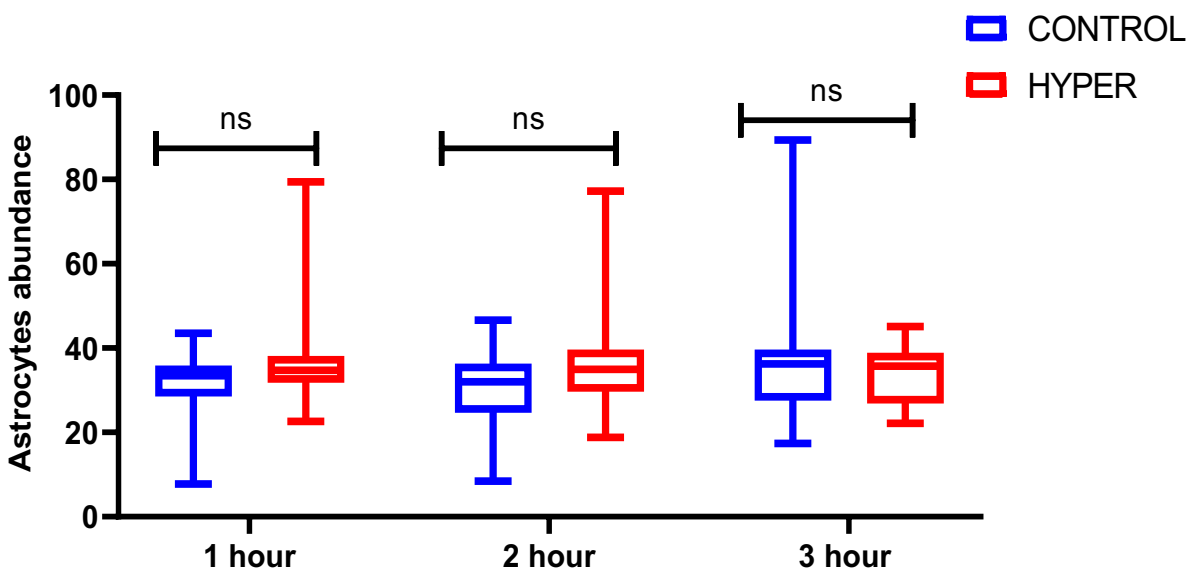

Figure 4.31. Box and whisker plots of Astrocyte area coverage in control and hyperglycaemic groups of rat retina at different time points (1, 2, and 3 hours). (n = 4 retinae/group) Note: HYPER = hyperglycaemia.

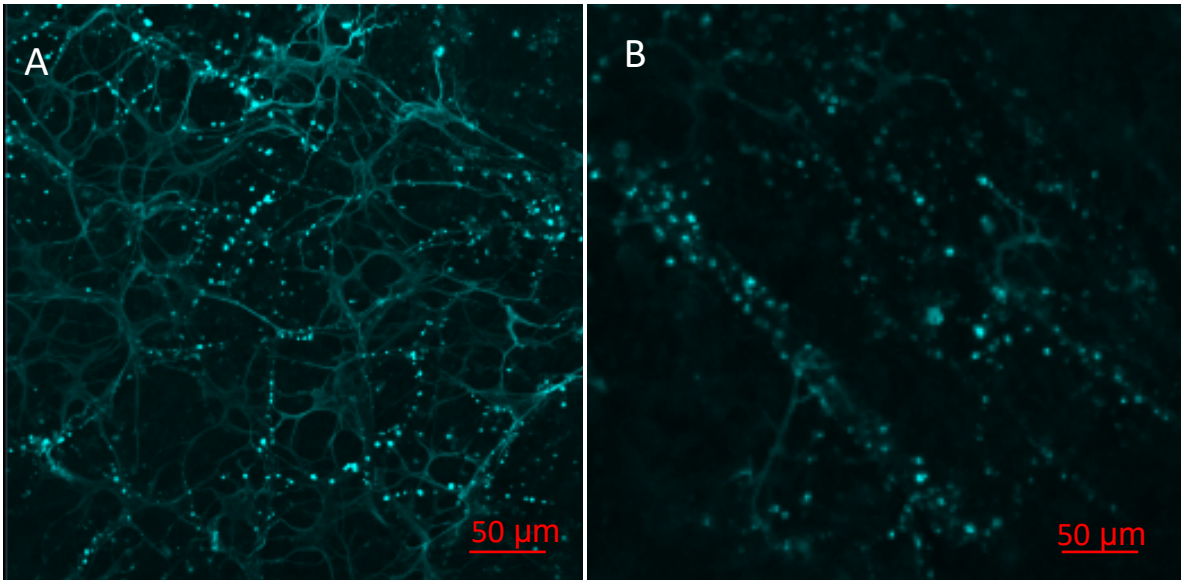

Figure 4.32. Single plane images of GFAP immunolabelled astrocytes in the 48-hour cultured retina. A. GFAP-positive astrocytes showing punctate signals along the processes suggesting disintegration (Control). B. Astrocytes in hyperglycaemic medium show weak GFAP signal intensity and show severe apoptotic-like changes associated with the areas where processes attach to the blood vessels.

4.3.2.2 Effect of hyperglycaemia on ganglionic fibres

Morphologically, ganglionic fibres, which were incidentally observed with syndecan-1 positive signals in the retina, were present in both retinal explants and eyecups but with decreasing signal intensity with increasing superfusion time (Figure 4.33). There was no difference seen in retinal ganglionic fibres of the hyperglycaemic and control groups in the superfused retina throughout the time points. (Figure 4.36). Ganglionic fibres were markedly absent in the 48- hour retinal cultures in both control and hyperglycaemic groups. (Figure 4.37).

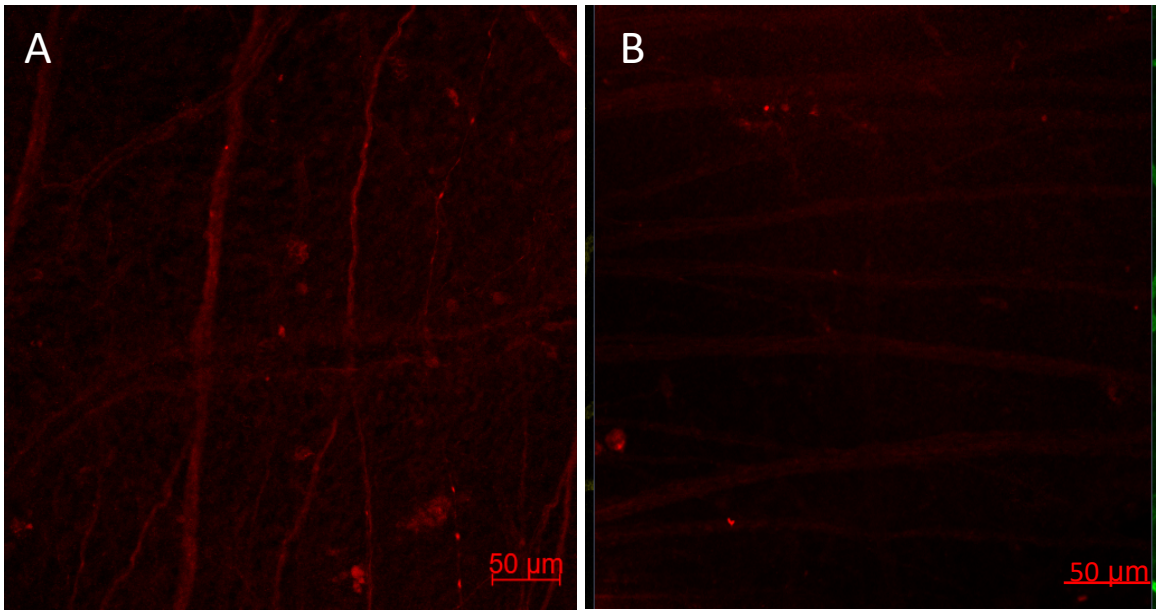

Figure 4.33. Single plane images showing syndecan-1 immunolabelled ganglionic fibres of the rat retina. A. Syndecan-1 positive signal in ganglionic fibres of the freshly harvested retina. B. Syndecan-1 positive signal in ganglionic fibres of 3-hour superfused control retina. Note the decline in signal intensity by the 3-hour time point.

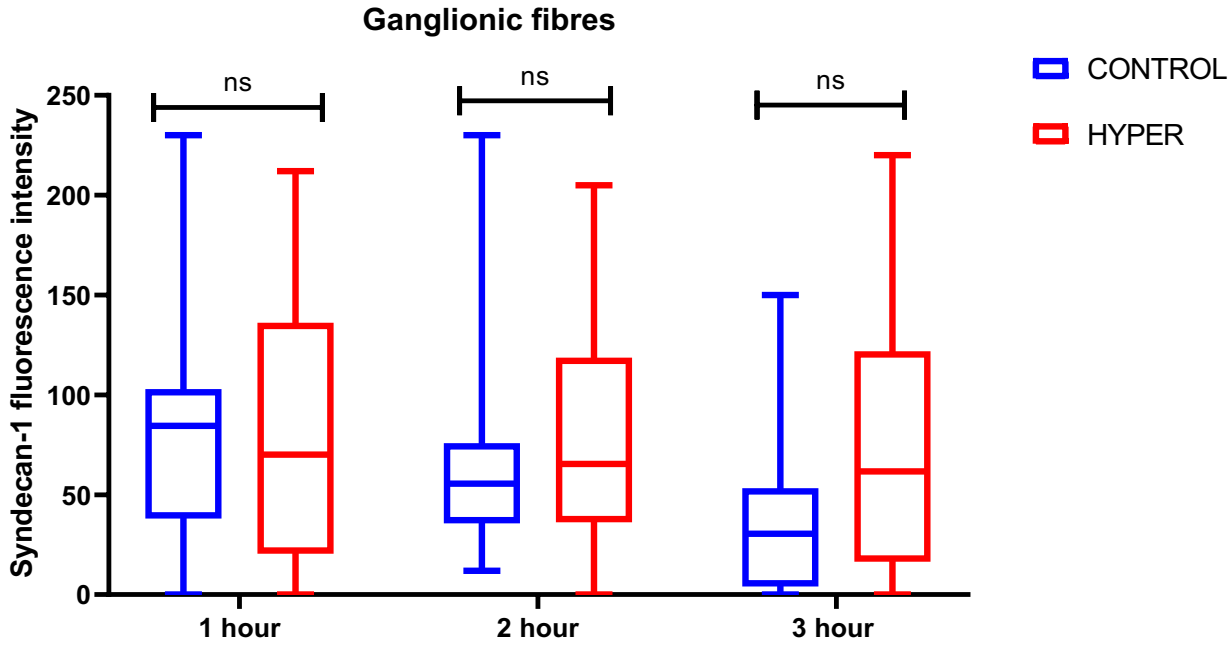

Figure 4.34. Box and whisker plots of syndecan-1 fluorescence intensity in ganglionic fibres of the superfused rat retinal model. There was no statistically significant difference between the hyperglycaemic and control groups across the time points 1, 2 and 3 hours of combined retinal explant and eyecup data. (n = 4 retinae/group) Note: HYPER = hyperglycaemia.

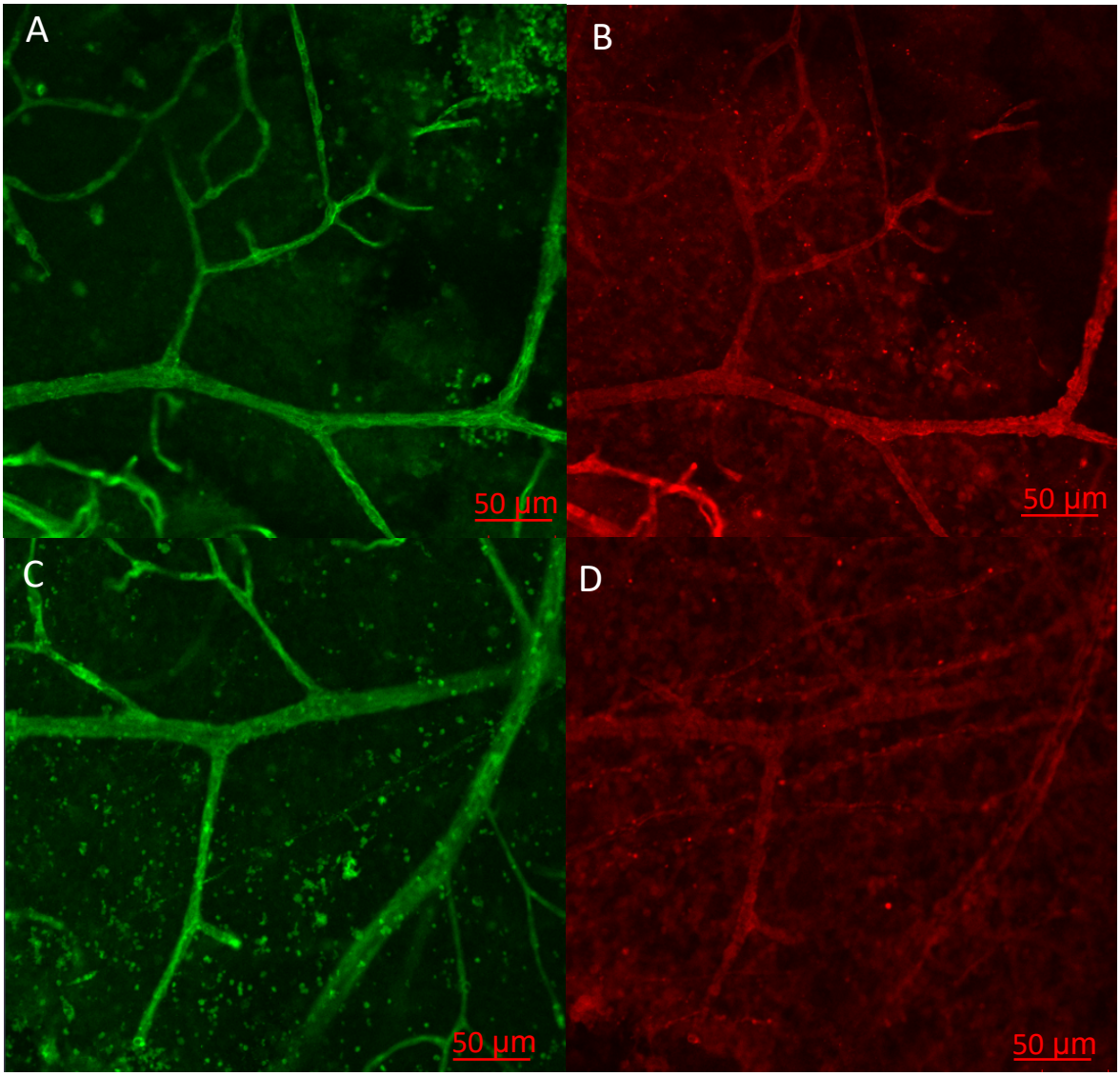

Figure 4.35. Syndecan-1 labelling on ganglionic fibres from hyperglycaemic and control retinae cultured for 48 hours. A. Control: Lectin-labelled blood vessels. B. Control: syndecan-1 positive signals in blood vessels, no ganglionic fibres seen. C. Hyperglycaemia: lectin-labelled blood vessel. D. Hyperglycaemia syndecan-1 positive signal in in blood vessels, no ganglionic fibres seen.

4.3.2.3 Effect of hyperglycaemia on microglial-like cells

Microglial cells were detected with the blood vessel marker (lectin) on the freshly harvested (time zero) rat retina (see Figure 4.1 C above). They were also present in all retinae after 3 hours superfusion of the rat retina (Figure 4.36 A and B). However, they were not present in the retina cultured for 48 hours. (Figure 4.36 C).

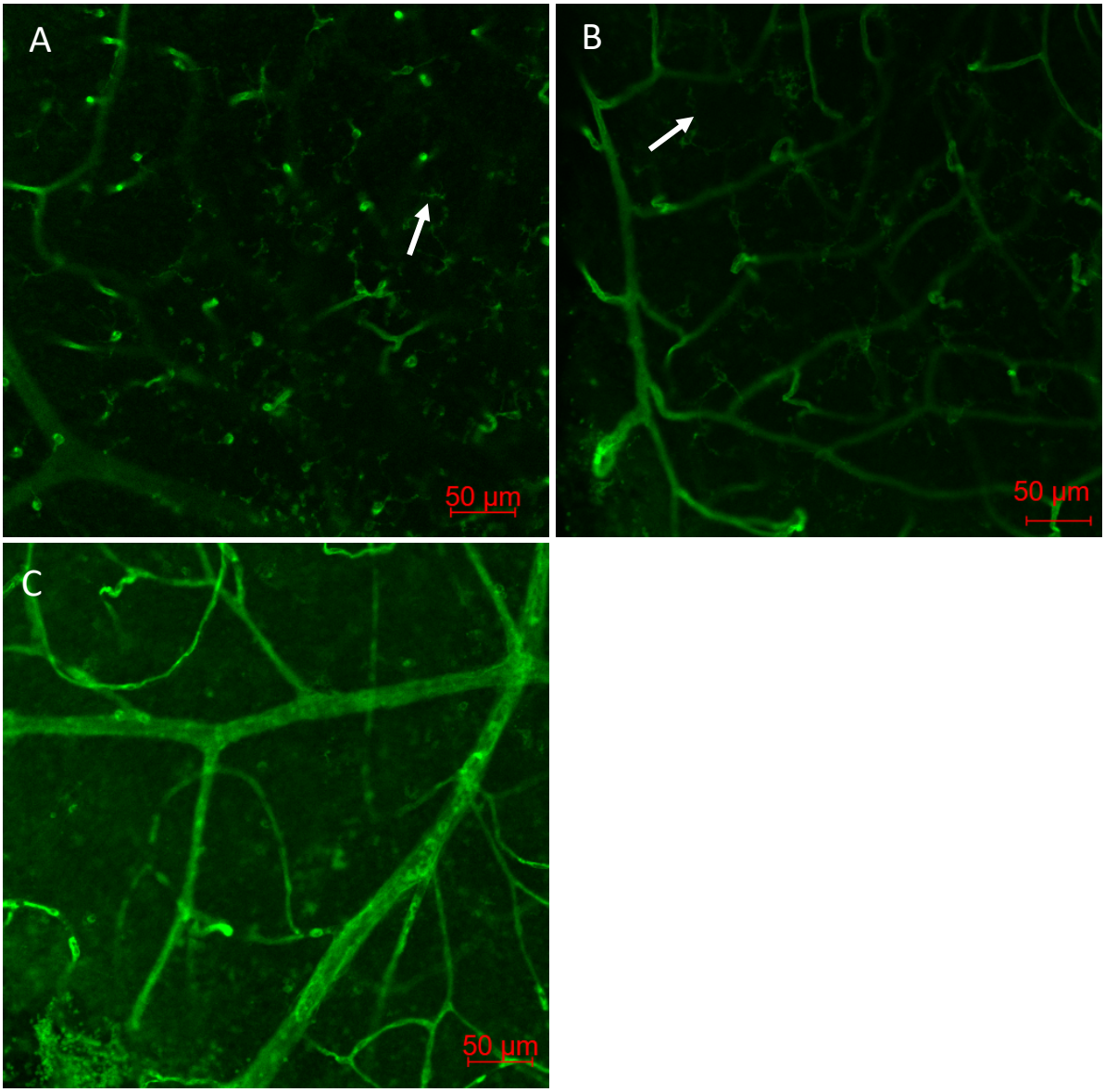

Figure 4.36. Single plane image showing microglial cells in the lectin labelled freshly harvested, superfused and cultured rat retina. A. Control explant after 3 hours superfusion showing microglial cells. B. Hyperglycaemia explant after 3 hours superfusion of the retina still showing microglial cells. C. Hyperglycaemia after 48 hours showing the absence of microglial cells.

4.3.3 Effect of hyperglycaemia on heat shock proteins

The α-Crystallin A antibody was used to detect heat shock protein in the retina in the 48-hour retinal cultures. Positive signals of α-Crystallin A were seen on ganglionic fibres like that seen with syndecan-1 with additional low signal intensity on cellular-like elements. This was also present at the 3-hour time point. However, at 48 hours, there were no positive signals noticed on ganglionic fibres (also like that shown in syndecan-1), which suggests that ganglionic fibres may have disintegrated (Figure 4.37).

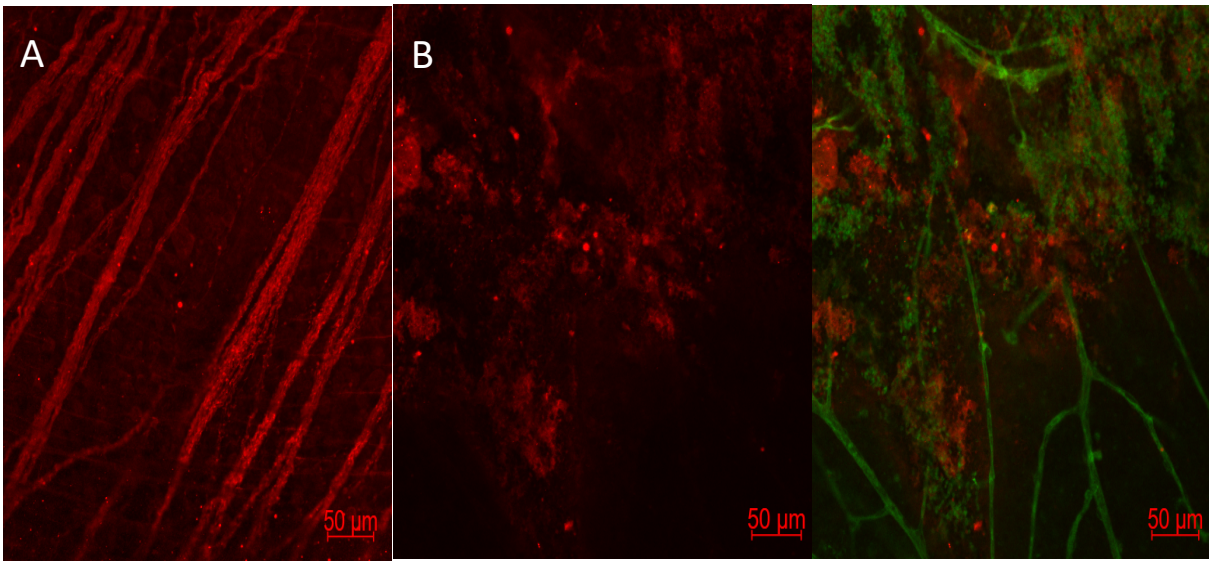

Figure 4.37. Single plane image of Hsp in the immunolabelling on superfused and cultured rat retina. A. Hyperglycaemia after 3 hours of superfusion showing Hsp in ganglionic fibres. B. Hyperglycaemia after 48 hours of culture showing Hsp positive signals (red channel) and the lectin-labelled blood vessel (green channel). Note the disintegration of ganglionic fibres in the retinae cultured for 48 hours.

4.4 Associations between retinal blood vessels, astrocytes and pericytes in the control and hyperglycaemic rat retinal model

This section describes the relationship observed between the blood vessels with the pericytes and astrocytes. The results of the experiment showed that blood vessels remained intact in the superfused retina both in the control and hyperglycaemic groups. Blood vessel narrowing was observed in the 48 hour culture model in the hyperglycaemic group. Pericytes that were present in the superfused control group were slightly reduced in number and signal intensity in the deeper layer of the retina. Astrocytes processes which were widely spread around blood vessels were seen retracting away from the blood vessels with signs of disintegration.

4.5 The expression of syndecan-1 protein in rat retina using western blotting

To confirm the specificity of syndecan-1 antibody on retinal proteins as retinal ganglionic fibres were unexpectedly labelled on retinal whole-mounts immunolabelling, western blotting was performed. The western blot of the 3-hour superfused rat retinal explants showed higher syndecan-1 protein expression in the hyperglycaemic group compared to the control with normalised syndecan-1 protein densitometric values of 43.26 and 22.59, respectively. Syndecan-1 protein was also expressed in the kidney tissue, which served as a positive control, while there was no demonstrable expression of syndecan-1 in the RIPA lane (negative control) (Figure 4.38).

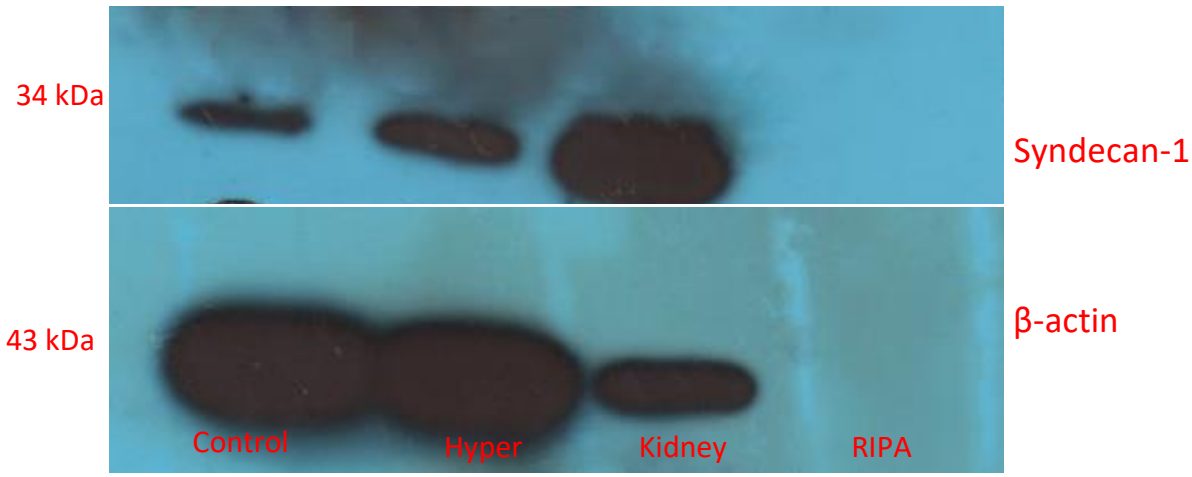

Figure 4.38. Representative immunoblot images showing syndecan-1 expression and β-actin protein expression in control and hyperglycaemic rat retina at 3 hour time point. Kidney (positive control). RIPA was used as a negative control. **Abbreviation:** Hyper = hyperglycaemia.

4.6 The expression of heat shock protein in rat retina using western blotting

Western blotting was performed to determine the expression of heat shock protein (using α-crystallin A antibody for detection) in control and hyperglycaemic superfused rat retina. The representative immunoblots images in Figure 4.39 show higher expression of heat shock protein in hyperglycaemic superfused rat retina compared to the control with normalised α-crystallin A densitometric values of 0.10 and 0.57 for control and hyperglycaemic groups, respectively. However, there was no demonstrable expression of heat shock protein in the RIPA lane (negative control).

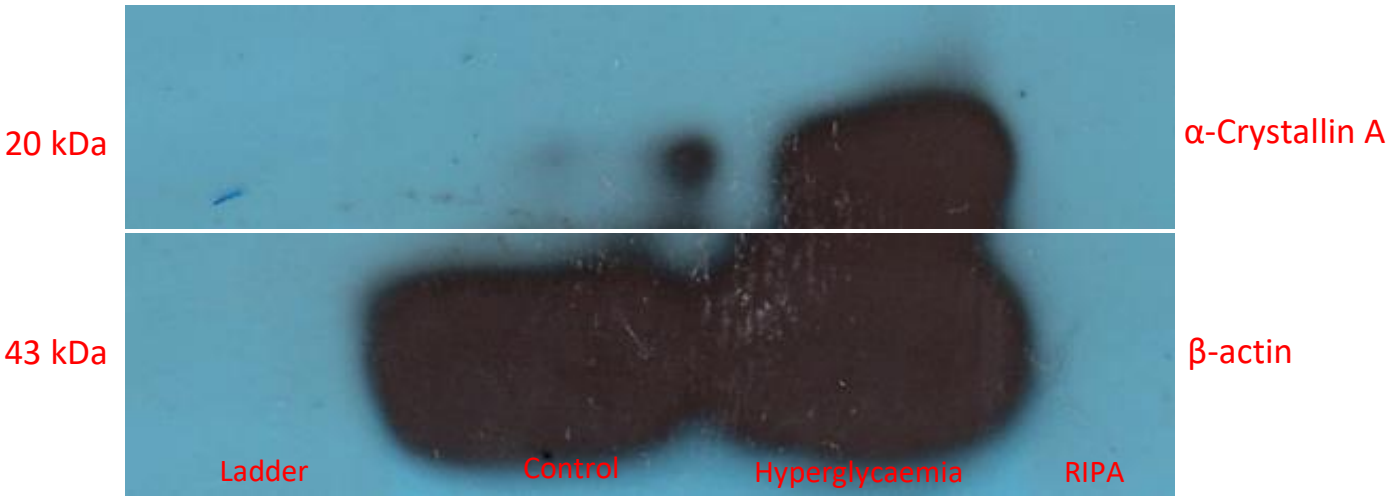

Figure 4.39. Western blot showing heat shock protein (α-Crystallin A) and β-actin protein expression in control and hyperglycaemic rat retina at 3-hour time point. RIPA was used as a negative control.

The BRB, a selective physical barrier within the eye, is made up of vascular and cellular components, namely endothelial cells, pericytes and astrocytes, which regulates molecules and solutes transportation across the retina.[32, 33] Disruption in the architecture in BRB may lead to increased vascular permeability, acellularity and angiogenesis heralding the early changes in DM retinopathy.[76, 100] Previous studies have reported that hyperglycaemia is associated with capillary hyperpermeability, neovascularisation and damage or loss of key components of the BRB namely endothelial glycocalyx layer, pericyte and astrocytes.[51, 64, 101] The structural changes that mediate functional mechanisms involved in the early stages of diabetic retinopathy is unknown. Animal and human diabetic models have been utilised to study the effect of hyperglycaemia on retinal structure and function. This study investigated the effect of retinal preparation type, superfusion time and hyperglycaemia on the vasculature and cellular components of the blood retinal barrier (BRB) utilising a multi-immunolabelling approach to study the early stages of diabetic retinopathy using *ex vivo* superfusion and culture models. The *ex vivo* diabetic rat model was used in this study as it might offer more flexibility in conditions that will not be affected by systemic physiology, and insights into early pathogenesis may not be possible with *in vivo* models. Additionally, optimisation on perfusion-fixed versus immersion-fixed retinae showed that all BRB structures were well preserved in both fixation methods. This is a key study that investigates the effect of rat retinal preparation types on the vascular and cellular components of BRB.

5.1 Optimisation of fixation and immunolabelling

Perfusion-fixed rats were initially used during optimisation to validate the *ex vivo* model as perfusion fixing is regarded as the gold standard for optimal morphological preservation of organs and particularly the retina. In the immersion-fixed freshly harvested retina, the lectin-

labelled retinal vasculature (*ex vivo* model) showed similar findings to the *in vivo* model i.e., a radiating pattern around the optic nerve, a branching pattern at the peripheral region and the presence of a capillary plexus in the lowermost vascular layer in the retina. Furthermore, the lowermost retinal vascular layer showed slightly reduced signal intensity and may be explained by the fact that markers and antibodies with lower wavelength may show higher tissue internal absorption leading to reduced signal intensity in the deeper layers (lowermost) as previously shown by Naidoo et al. in whole-mount imaging on another organ.[102] In a previous study that used lectin to label freshly harvested whole-mount retina, the authors showed a retinal vascular branching pattern in non-diabetic rats.[64] Perfusion-fixed retina had a higher syndecan-1 signal intensity compared to that seen in the immersion-fixed model in this study. Despite this, retinal vessels were clearly visible in immersion-fixed tissues and thus adequate to study the vessels in the *ex vivo* experiments. As far as we are aware, there is no study that has compared perfusion-fixed and immersion-fixed retinal whole-mounts to detect syndecan-1 using immunohistochemistry (IHC). The optimisation findings suggest that immersion-fixed retina show comparable results with the perfusion-fixation gold standard.

5.2 The effect of superfusion or culture time and retinal preparation types on the blood retinal barrier under normoglycaemia

Whole-mount immunolabelling provides better clarity with respect to target protein expression within a tissue compared to tissue sectioning and is therefore suitable for studying BRB components.[103] This study demonstrated normal morphology of blood vessels, pericytes and astrocytes, which make up the blood retinal barrier in both explant and eyecup of superfused retinae throughout 1- 3-hour time points. Furthermore, although there was some reduction in signal intensity at 1 hour there was no real significant difference in the signal intensities at the different time points in both explants and eyecups. With regards to the effect of time on

astrocyte morphology on the BRB integrity in superfused retinae, this study showed normal astrocytes coverage and morphology in both control explants and eyecups at 1 and 2 hours but with some retraction of astrocytes processes at 3 hours in the superfused model. However, in the 48-hour culture model, abundant apoptotic-like changes and retraction of astrocyte processes were markedly prevalent in the retinal explant. These findings imply that a time point earlier than 48 hours may be more suitable to study morphological and pathological changes of astrocytes in control and disease states.

This study showed patchy syndecan-1 immunolocalisation in the retinal vasculature of both explant and eyecup (central and peripheral regions) with similar signal intensity in both preparation types, implying that superfusion of explant and eyecup has no effect on the syndecan-1 pattern of distribution. The gradient in brightness of syndecan-1 signal intensity in rat retinal blood vessels from the larger arteries to the capillaries with least intensity in the latter, suggests that functional disruption of the endothelium in small vessels may be the earliest pathology to occur when the retina is exposed to toxic or metabolic insults such as hyperglycaemia, hypoxia, and hypertension. Interestingly, this is the first study to identify syndecan-1 expression in either animal or human retinal vessels in superfused or culture models. In this study, the expression of syndecan-1 protein was demonstrated in both normoglycaemic superfused retinal explant and eyecup at three different time points (1, 2, and 3 hours). Additionally, both retinal explants and eyecups had comparable syndecan-1 signal intensity and astrocytes abundance (area coverage) over time.

Overall, under normoglycaemic conditions, there is no difference between explant and eyecup retinal preparations with regards to all parameters investigated in this study. Hence, this study shows that eyecup preparations will be very suitable to study the BRB cellular and

physiological components in future studies. The eyecup retinal preparation protocol may show some benefit in terms of reproducibility, error minimisation, easy handling, shorter experimental duration and cost-effectiveness compared to the protocol that utilises the complete retinal extraction (explant).

5.3 The effect of hyperglycaemia on the morphology of pericytes and astrocytes within the retinal vasculature in normo- and hyperglycaemic *ex vivo* conditions over time

Structural changes to pericytes and astrocytes within the retinal vasculature were examined using multi-immunofluorescence labelling after superfusion and culture of rat retinal tissue in the hyperglycaemic medium. Structural changes to pericytes and astrocytes in the retinal blood vessels were observed after 3 hours of superfusion in the hyperglycaemic medium.

Retinal blood vessel width was reduced in the eyecup group, and the fluorescence intensity of NG2-immunolabelled pericytes was diminished as well as reduction in the number of the pericyte nuclei bulge in the lower vascular bed of the eyecup group (3-hour) and 48-hour cultured retinal explants. Similar to these findings, Weerasekera et al., Toh et al., Li et al. and Mizutani et al. found pericyte loss and increased acellular capillaries in diabetic rat retinae.[64, 85, 104, 105] Pericytes are perivascular cells that play an essential role in maintaining the BRB by regulating vascular tone and capillary bed integrity, blood flow, vessel permeability and stabilization, and its substantial loss or degeneration along with endothelial cell loss result in BRB functional disruption with acellular capillaries.[55, 56, 106] This is supported by studies that have reported an increased number of acellular capillaries in the retina of humans and rodents with diabetes mellitus.[60, 105]

Astrocytes are macroglial cells that provide structural support to the BRB and play an important role in blood vessel growth and function.[67] Alteration or loss of astrocytes in diabetes may result in retinal vascular changes such as hyperpermeability that is seen in diabetic retinopathy.[76, 107, 108] In this study, although the signal intensity of GFAP-immunolabelled astrocytes and area coverage show no substantial change. Retraction of astrocyte processes and signs of cellular disintegration were more evident in the hyperglycaemic eyecup group at the 3-hour time point. This may be indicative of astrocyte cell death. The study by Rungger-Brändle et al. demonstrated a significant reduction in astrocyte number in the central and peripheral retina of diabetic rats at 4 weeks which is consistent with the finding of astrocyte loss in 8-week old hyperglycaemic rat retina seen in the retinae cultured for 48 hours in this study using.[109] The findings of this study suggest that hyperglycaemia may be associated with more significant pericyte, astrocyte and blood vessel alterations in rat retinae in both superfused eyecups (3-hour) as well as severe astrocyte loss and blood vessel narrowing in tissue culture model at 48 hours. These findings may be explained partly by the influence of experimental conditions such as impaired nutrient supply and availability of oxygen leading to mitochondrial dysfunction in the eyecup retina during superfusion as previously postulated by Tsantilas et al., when they demonstrated decreased glutamine metabolism in mouse eyecups despite metabolic stability of the retina and eyecup *ex vivo*.[110] Following the preliminary investigation on retinae cultured for 48 hours in the present study, narrowing of blood vessels, loss of pericytes and disintegration of astrocytes was more pronounced in the hyperglycaemic group. These findings are consistent with those of Ly et al., who found retraction of astrocyte processes in 4-week diabetic rat retinae but differ from findings by Rungger-Brändle et al., Lechuga-Sancho et al. and Garcia-Caceres et al., who reported astrocyte loss in rat retinae (between 4-6 weeks), the cerebellum and the hypothalamus, respectively, in the streptozocin-induced diabetes mellitus model.[109, 111-113] Similarly, Weerasekera et al. reported astrocyte loss or death in a mouse model

of type 2 diabetes mellitus.[64] Contrastingly, Kumar et al. and Xia et al., found increased GFAP staining in astrocytes in diabetic mouse retinae and rhesus monkey retinae, respectively.[114, 115] The significant retraction of astrocyte processes and/or cell death may alter the functional integrity of the BRB, particularly at the 3-hour time point in hyperglycaemic rat retinae, suggesting this as one of the earliest signs of hyperglycaemic-associated BRB disruption.

5.4 Hyperglycaemia effect on retinal vascular endothelial glycocalyx

Whole-mount immunofluorescence and western blotting were used to determine the expression of syndecan-1 protein, a significant component of the endothelial glycocalyx, following superfusion and or culture of the retina in normoglycaemic and hyperglycaemic conditions. To the best of our knowledge, the present study is the first to demonstrate the presence of syndecan-1 protein in retinal blood vessels using immunofluorescence. Overall, the syndecan-1 fluorescence intensity was significantly higher in the hyperglycaemic groups i.e. rat retina at 1-hour superfusion, and eyecup at 1 and 3 hours of superfusion) compared to the controls, but lower syndecan-1 protein expression in the hyperglycaemic 48-hour cultured rat retina. Furthermore, ganglionic fibres, being the bulk syndecan-1-labelled structure in the retina, demonstrated no significant difference in syndecan-1 protein signal intensity between control and hyperglycaemia after 3 hours of superfusion. Syndecan-1 protein expression in 3-hour superfused retinal explants was significantly higher in the hyperglycaemic group than in the control as determined by western blotting, but whether this includes the additive effect of syndecan-1 positive structures such as neuronal processes of retinal cells, requires further evaluation. Consistent with our findings, Kaur et al., reported higher syndecan-1 protein expression in the retina of diabetic rats with western blotting, though his findings were from an *in vivo* study at 8 weeks after treatment with streptozotocin. They further found an increase in syndecan-1 protein in the plasma of diabetic rats and supernatant from endothelial cell

cultures, indicating shedding.[51] As hypothesised by Kaur et al., the findings in the present study suggest that apart from the altered retinal glycocalyx occurring in diabetes mellitus as a result of syndecan-1 shedding, increased retinal syndecan-1 expression in the hyperglycaemic state perhaps suggests a compensatory response of the retina to hyperglycaemia in early diabetic retinopathy.[51] In this study, although we could not determine objectively syndecan-1 shedding in hyperglycaemic retina by measuring plasma syndecan-1 levels, we hypothesise that the increase in retinal syndecan-1expression could be due to the clumping of shed syndecan-1 and lack of blood flow to wash away shed syndecan-1 protein that is closely associated with endothelial glycocalyx. Furthermore, the insertion of syndecan-1 from the intracellular stores or Golgi apparatus to the cell surface by the endothelial cells due to compensation for shed syndecan, could be another possible explanation for our findings. However these hypotheses require further interrogation in future studies. Syndecan-1 regulates the BRB by inhibiting angiogenesis and leukocyte-endothelial interactions in the retinal vasculature; hence, syndecan-1 loss in the retina may result in retinal endothelial dysfunction.[116] It has been reported that cellular syndecan-1 loss and a rise in soluble syndecan-1 is associated with endothelial junction and epithelial cell disruption leading to hyperpermeability in hyperglycaemic states.[101] In the present study, a weaker syndecan-1 signal intensity was observed in the hyperglycaemic retinal explant compared to the control after 48 hours in culture which is consistent with the finding by Wang and Yu, who reported decreased syndecan-1 in the retinal ganglionic fibre layer, outer and inner plexiform layers and in the rods and cones of 9-week diabetic rat and proliferative diabetic retinopathy.[117] These findings suggest that although there is a possible compensatory upregulation of syndecan-1 in the hyperglycaemic retina at the early time point, prolonged exposure of the retina to hyperglycaemia will result in cellular or tissue syndecan-1 loss or shedding. This hypothesis may be supported by the increased vitreous syndecan-1 levels in proliferative diabetic retinopathy patients compared to

their non-diabetic counterparts.[53] Similarly, a study reported higher serum syndecan-1 levels in patients with type 2 diabetes mellitus compared to the controls using an enzyme-linked immunosorbent assay.[52] However, this may not be attributable to retinal syndecan-1 shedding only as other cells or tissues such as intestinal epithelial cells, intestinal tissue, human umbilical vein endothelial cells, and human renal glomerular endothelial cells have been reported to express syndecan-1 and usually show syndecan-1 loss under hyperglycaemic conditions.[101, 118, 119] Syndecan-1 expression has been reported by others to be found in rod photoreceptor cells, glial cells, bipolar cells, and horizontal cells, hence there is reduced certainty that retinal syndecan-1 loss is directly reflective of endothelial cell disruption.[51, 117] Also, the present study demonstrated the presence of nonvascular cells which are likely to be the cytoplasmic processes of the cells in the lower layer of the retina which may correlate with the inner/outer plexiform layer that could possibly be affected by hyperglycaemia (Appendix 7). Therefore, future studies examining the effect of hyperglycaemia on the expression of syndecan-1 in other retinal cell types, and to determine whether retinal endothelial glycocalyx or ganglionic fibres is responsible for increased syndecan-1 signal intensity in the retina, will be critical.

5.5 Expression of potential signalling factors such as heat shock proteins in the retina in acute exposure to hyperglycaemia

Heat shock proteins (stress proteins) are significantly expressed in both human and animal retina in response to pathological and pathophysiological conditions such as hyperglycaemia, hypoxia, ischaemia and endotoxins mainly to prevent tissue damage.[78, 83, 120, 121] Oxidative stress, one of the pathophysiological mechanisms implicated in diabetic retinopathy, initiates the process of heat shock protein expression.[122, 123] Consistent with findings by Kumar et al., Kandpal et al. and Losiewicz et al., the present study showed higher expression of heat shock proteins in hyperglycaemic rat retina compared to the normoglycaemic group in the 3-hour

superfusion model.[124-126] Furthermore, Reddy et al. demonstrated higher heat shock protein mRNA expression in the diabetic rat retina than in the controls.[78] However, Reddy et al. and Simkhovich et al. reported decreased heat shock protein 27 expression in diabetic rat retina and ischaemic hearts, respectively.[78, 127] While this preliminary data and the sample size were limited, the findings of this study suggest heat shock proteins may play a role in protecting retinal cells of diabetic rats in response to hyperglycemia-induced oxidative stress.

5.6 Strengths of the study

To the best of our knowledge, this is the first study to use retinae which were harvested from rats, superfused *ex vivo* and cultured to develop a diabetes model. In addition, no single study has examined the retina for syndecan-1 changes, pericytes and astrocyte loss, as well as vascular changes altogether at very early time points.

5.7 Limitations of the study

While the isolated enucleated eye is a valuable model in studying histological and morphological changes in the retina, enucleating the eye, and superfusing the dissected-out retina in a continuous oxygen organ chamber may not provide an adequate milieu to regulate the body's normal physiology, and metabolic function. Again, since the retina is an extremely soft and delicate organ, extra dexterity is required during dissection as minor physical damages could occur, leading to breakage of the retina that may be associated with some of the changes found in the control samples. Furthermore, Krebs buffer, a crystalloid, was used for superfusion and can potentially prevent adequate tissue oxygenation; hence, the possibility of compromised tissue viability over time beyond 3 hours is likely. However, oxygen deprivation in the 48-hour cultured whole retina may be more of a factor with regards to compromising tissue quality as observed in the present study, as the retina is comprised mainly of neuronal cells which have a

high metabolic requirement. Finally, using a live animal model to induce diabetes will provide a clearer understanding of the disease process. Recently, Kaur et al. used the streptozotocin-induced type 1 diabetic rat model for assessing changes in the retinal glycocalyx *in vivo*, while glycocalyx shedding was studied in the plasma and culture medium using western blotting.[51] Finally, the sample size in the present study was limited, which could have led to a consequent low statistical power.

5.8 Future studies

Future studies investigating later time points may provide further insights into the understanding of mechanisms underpinning early changes to the BRB in diabetes mellitus. Also, investigating the effect of hyperglycaemia on the structures that make up the BRB using a diabetic rat model for *in vivo* studies will provide additional information to early changes in diabetic retinopathy; this may provide a better physiological environment and allow the metabolic process to occur for a more clinically relevant study. Hyperglycaemia was seen to have an effect on syndecan-1 levels. This effect could be due to compensation by the endothelial cells which may or may not result from shedding of syndecan-1. This concept can be explored in further studies. In addition, future studies utilizing the perfusate to assess shedding of syndecan-1 before and after superfusion will provide interesting insight.

5.9 Conclusion

This study revealed that there is no significant difference between the retinal preparations (explants vs eyecup) and that the BRB is still structurally intact up to 3 hours *ex vivo*. The subtle morphological changes of the BRB (blood vessels, pericytes, and astrocytes) induced by hyperglycaemia which were more apparent in the deeper vascular layers, suggests that this *ex vivo* model is suitable to study the early pathogenesis of diabetic retinopathy. Furthermore, this

study established that in response to hyperglycaemia, changes in syndecan-1 levels occurred at an earlier timepoint to the morphological changes of the other BRB structures which supports the notion that syndecan-1 plays a role in the pathophysiology of diabetic retinopathy. Findings of these preliminary data suggest that heat shock proteins may play a role in response to hyperglycemia-induced oxidative stress.

References

1. Centers for disease control and prevention. National diabetes fact sheet: national estimates and general information on diabetes and prediabetes in the United States, 2011. Atlanta, GA: US department of health and human services, centers for disease control and prevention. 2011;201(1):2568-9.

2. Saeedi P, Petersohn I, Salpea P, Malanda B, Karuranga S, Unwin N, et al. Global and regional diabetes prevalence estimates for 2019 and projections for 2030 and 2045: Results from the International Diabetes Federation Diabetes Atlas. *Diabetes Res Clin Pract*. 2019;157:107843.

3. Trends in adult body-mass index in 200 countries from 1975 to 2014: a pooled analysis of 1698 population-based measurement studies with 19.2 million participants. *Lancet*. 2016;387(10026):1377-96.

4. Ley SH, Hamdy O, Mohan V, Hu FB. Prevention and management of type 2 diabetes: dietary components and nutritional strategies. *Lancet*. 2014;383(9933):1999-2007.

5. Colagiuri R, Colagiuri S, Yach D, Pramming S. The answer to diabetes prevention: science, surgery, service delivery, or social policy? *Am J Public Health*. 2006;96(9):1562-9.

6. ADA. 11. Microvascular Complications and Foot Care: Standards of Medical Care in Diabetes-2019. *Diabetes Care*. 2019;42(Suppl 1):S124-s38.

7. Holman RR, Paul SK, Bethel MA, Matthews DR, Neil HA. 10-year follow-up of intensive glucose control in type 2 diabetes. *N Engl J Med*. 2008;359(15):1577-89.

8. Nathan DM. The diabetes control and complications trial/epidemiology of diabetes interventions and complications study at 30 years: overview. *Diabetes Care*. 2014;37(1):9-16.

9. Chawla A, Chawla R, Bhasin G, Soota K. Profile of adolescent diabetics in North Indian population. *J Clin Diabetol*. 2014;1:1-3.

10. Antonetti DA, Klein R, Gardner TW. Diabetic retinopathy. *N Engl J Med*. 2012;366(13):1227-39.

11. Leasher JL, Bourne RR, Flaxman SR, Jonas JB, Keeffe J, Naidoo K, et al. Global Estimates on the Number of People Blind or Visually Impaired by Diabetic Retinopathy: A Meta-analysis From 1990 to 2010. *Diabetes Care*. 2016;39(9):1643-9.

12. Lieth E, Gardner TW, Barber AJ, Antonetti DA. Retinal neurodegeneration: early pathology in diabetes. *Clin Exp Ophthalmol*. 2000;28(1):3-8.

13. Naylor A, Hopkins A, Hudson N, Campbell M. Tight Junctions of the Outer Blood Retina Barrier. *Int J Mol Sci*. 2019;21(1).

14. Abbott NJ, Rönnbäck L, Hansson E. Astrocyte-endothelial interactions at the blood-brain barrier. *Nat Rev Neurosci*. 2006;7(1):41-53.

15. World Health Organization. Definition, diagnosis and classification of diabetes mellitus and its complications: report of a WHO consultation. Part 1, Diagnosis and classification of diabetes mellitus. Geneva: World Health Organization; 1999.

16. Fowler MJ. Microvascular and macrovascular complications of diabetes. *Clin Diabetes*. 2008;26(2):77-82.

17. Fong DS, Aiello LP, Ferris FL, 3rd, Klein R. Diabetic retinopathy. *Diabetes Care*. 2004;27(10):2540-53.

18. Nentwich MM, Ulbig MW. Diabetic retinopathy - ocular complications of diabetes mellitus. *World J Diabetes*. 2015;6(3):489-99.

19. Solomon SD, Chew E, Duh EJ, Sobrin L, Sun JK, VanderBeek BL, et al. Diabetic retinopathy: a position statement by the American Diabetes Association. *Diabetes care*. 2017;40(3):412-8.

20. Klein R, Klein BE, Moss SE, Davis MD, DeMets DL. The Wisconsin epidemiologic study of diabetic retinopathy. IV. Diabetic macular edema. *Ophthalmology*. 1984;91(12):1464-74.

21. Wang W, Lo ACY. Diabetic Retinopathy: Pathophysiology and Treatments. *Int J Mol Sci*. 2018;19(6):1896.

22. Diabetic retinopathy study. Report Number 6. Design, methods, and baseline results. Report Number 7. A modification of the Airlie House classification of diabetic retinopathy. Prepared by the Diabetic Retinopathy. *Invest Ophthalmol Vis Sci*. 1981;21(1 Pt 2):1-226.

23. Domingueti CP, Dusse LM, Carvalho M, de Sousa LP, Gomes KB, Fernandes AP. Diabetes mellitus: The linkage between oxidative stress, inflammation, hypercoagulability and vascular complications. *J Diabetes Complications*. 2016;30(4):738-45.

24. Goldberg RB. Cytokine and cytokine-like inflammation markers, endothelial dysfunction, and imbalanced coagulation in development of diabetes and its complications. *J Clin Endocr Metab*. 2009;94(9):3171-82.

25. Gabbay KH. Hyperglycemia, polyol metabolism, and complications of diabetes mellitus. *Annu Rev Med*. 1975;26:521-36.

26. Gabbay KH. The sorbitol pathway and the complications of diabetes. *N Engl J Med*. 1973;288(16):831-6.

27. Hohman TC, Nishimura C, Robison WG, Jr. Aldose reductase and polyol in cultured pericytes of human retinal capillaries. *Exp Eye Res*. 1989;48(1):55-60.

28. Chakrabarti S, Sima AA, Nakajima T, Yagihashi S, Greene DA. Aldose reductase in the BB rat: isolation, immunological identification and localization in the retina and peripheral nerve. *Diabetologia*. 1987;30(4):244-51.

29. Dagher Z, Park YS, Asnaghi V, Hoehn T, Gerhardinger C, Lorenzi M. Studies of rat and human retinas predict a role for the polyol pathway in human diabetic retinopathy. *Diabetes*. 2004;53(9):2404-11.

30. Cheung AK, Fung MK, Lo AC, Lam TT, So KF, Chung SS, et al. Aldose reductase deficiency prevents diabetes-induced blood-retinal barrier breakdown, apoptosis, and glial reactivation in the retina of db/db mice. *Diabetes*. 2005;54(11):3119-25.

31. Simo R, Ballarini S, Cunha-Vaz J, Ji L, Haller H, Zimmet P, et al. Non-traditional systemic treatments for diabetic retinopathy: an evidence-based review. *Curr Med Chem*. 2015;22(21):2580-9.

32. Klaassen I, Van Noorden CJ, Schlingemann RO. Molecular basis of the inner blood-retinal barrier and its breakdown in diabetic macular edema and other pathological conditions. *Prog Retin Eye Res*. 2013;34:19-48.

33. Bucolo C, Drago F, Lin L-R, Reddy VN. Sigma receptor ligands protect human retinal cells against oxidative stress. *Neuroreport*. 2006;17(3):287-91.

34. Sweeney MD, Ayyadurai S, Zlokovic BV. Pericytes of the neurovascular unit: key functions and signaling pathways. *Nat Neurosci*. 2016;19(6):771-83.

35. Abbott NJ, Rönnbäck L, Hansson E. Astrocyte–endothelial interactions at the blood–brain barrier. *Nat Rev Neurosci*. 2006;7(1):41-53.

36. Rangasamy S, McGuire PG, Das A. Diabetic retinopathy and inflammation: novel therapeutic targets. *Middle East Afr J Ophthalmol*. 2012;19(1):52-9.

37. Heng L, Comyn O, Peto T, Tadros C, Ng E, Sivaprasad S, et al. Diabetic retinopathy: pathogenesis, clinical grading, management and future developments. *Diabet Med*. 2013;30(6):640-50.

38. Adamis AP, Miller JW, Bernal MT, D'Amico DJ, Folkman J, Yeo TK, et al. Increased vascular endothelial growth factor levels in the vitreous of eyes with proliferative diabetic retinopathy. *Am J Ophthalmol*. 1994;118(4):445-50.

39. Qaum T, Xu Q, Joussen AM, Clemens MW, Qin W, Miyamoto K, et al. VEGF-initiated blood-retinal barrier breakdown in early diabetes. *Invest Ophthalmol Vis Sci*. 2001;42(10):2408-13.

40. Salmon AH, Satchell SC. Endothelial glycocalyx dysfunction in disease: albuminuria and increased microvascular permeability. *J Pathol*. 2012;226(4):562-74.

41. van den Berg BM, Nieuwdorp M, Stroes ES, Vink H. Glycocalyx and endothelial (dys) function: from mice to men. *Pharmacol Rep*. 2006;58 Suppl:75-80.

42. Götte M. Syndecans in inflammation. *FASEB J*. 2003;17(6):575-91.

43. Mali M, Jaakkola P, Arvilommi AM, Jalkanen M. Sequence of human syndecan indicates a novel gene family of integral membrane proteoglycans. *J Biol Chem*. 1990;265(12):6884-9.

44. Wang JB, Zhang YJ, Zhang Y, Guan J, Chen LY, Fu CH, et al. Negative correlation between serum syndecan-1 and apolipoprotein A1 in patients with type 2 diabetes mellitus. *Acta Diabetol*. 2013;50(2):111-5.

45. Chelazzi C, Villa G, Mancinelli P, De Gaudio AR, Adembri C. Glycocalyx and sepsis-induced alterations in vascular permeability. *Crit care*. 2015;19(1):26.

46. Kolářová H, Ambrůzová B, Švihálková Šindlerová L, Klinke A, Kubala L. Modulation of endothelial glycocalyx structure under inflammatory conditions. *Mediators Inflamm*. 2014;2014.694312.

47. Drake-Holland AJ, Noble MI. Update on the important new drug target in cardiovascular medicine - the vascular glycocalyx. *Cardiovasc Hematol Disord Drug Targets*. 2012;12(1):76-81.

48. Adamis AP. Is diabetic retinopathy an inflammatory disease? *Br J Ophthalmol*. 2002;86(4):363-5.

49. Noda K, Nakao S, Ishida S, Ishibashi T. Leukocyte adhesion molecules in diabetic retinopathy. *J Ophthalmol*. 2012;2012:279037.

50. Leskova W, Pickett H, Eshaq RS, Shrestha B, Pattillo CB, Harris NR. Effect of diabetes and hyaluronidase on the retinal endothelial glycocalyx in mice. *Exp Eye Res*. 2019;179:125-31.

51. Kaur G, Rogers J, Rashdan NA, Cruz-Topete D, Pattillo CB, Hartson SD, et al. Hyperglycemia-induced effects on glycocalyx components in the retina. *Exp Eye Res*. 2021;213:108846.

52. Wang JB, Guan J, Shen J, Zhou L, Zhang YJ, Si YF, et al. Insulin increases shedding of syndecan-1 in the serum of patients with type 2 diabetes mellitus. *Diabetes Res Clin Pract*. 2009;86(2):83-8.

53. El-Asrar AMA, Nawaz MI, De Hertogh G, Alam K, Siddiquei MM, Van den Eynde K, et al. S100A4 is upregulated in proliferative diabetic retinopathy and correlates with markers of angiogenesis and fibrogenesis. *Mol Vis*. 2014;20:1209-24.

54. Wanjare M, Kusuma S, Gerecht S. Perivascular cells in blood vessel regeneration. *Biotechnol J*. 2013;8(4):434-47.

55. Kutcher ME, Herman IM. The pericyte: cellular regulator of microvascular blood flow. *Microvasc Res*. 2009;77(3):235-46.

56. von Tell D, Armulik A, Betsholtz C. Pericytes and vascular stability. *Exp Cell Res*. 2006;312(5):623-9.

57. Ogura S, Kurata K, Hattori Y, Takase H, Ishiguro-Oonuma T, Hwang Y, et al. Sustained inflammation after pericyte depletion induces irreversible blood-retina barrier breakdown. *JCI insight*. 2017;2(3):e90905.

58. Yang Y, Schmidt EP. The endothelial glycocalyx: an important regulator of the pulmonary vascular barrier. *Tissue barriers*. 2013;1(1):1217-23.e23494.

59. Kim SJ, Kim SA, Choi YA, Park DY, Lee J. Alpha-Smooth Muscle Actin-Positive Perivascular Cells in Diabetic Retina and Choroid. *Int J Mol Sci*. 2020;21(6):2158.

60. Hammes HP. Pericytes and the pathogenesis of diabetic retinopathy. *Horm Metab Res*. 2005;37 Suppl 1:39-43.

61. Roy S, Kim D, Lim R. Cell-cell communication in diabetic retinopathy. *Vision Res*. 2017;139:115-22.

62. Rucker HK, Wynder HJ, Thomas WE. Cellular mechanisms of CNS pericytes. *Brain Res Bull*. 2000;51(5):363-9.

63. Shepro D, Morel NM. Pericyte physiology. *FASEB J*. 1993;7(11):1031-8.

64. Weerasekera LY, Balmer LA, Ram R, Morahan G. Characterization of Retinal Vascular and Neural Damage in a Novel Model of Diabetic Retinopathy. I*nvest Ophthalmol Vis Sci*. 2015;56(6):3721-30.

65. Chung YR, Choi JA, Koh JY, Yoon YH. Ursodeoxycholic Acid Attenuates Endoplasmic Reticulum Stress-Related Retinal Pericyte Loss in Streptozotocin-Induced Diabetic Mice. *J Diabetes Res*. 2017;2017:1763292.

66. Choi YK, Kim KW. Blood-neural barrier: its diversity and coordinated cell-to-cell communication. *BMB Rep*. 2008;41(5):345-52.

67. Fletcher EL, Downie LE, Ly A, Ward MM, Batcha AH, Puthussery T, et al. A review of the role of glial cells in understanding retinal disease. *Clin Exp Optom*. 2008;91(1):67-77.

68. Bringmann A, Pannicke T, Grosche J, Francke M, Wiedemann P, Skatchkov SN, et al. Muller cells in the healthy and diseased retina. *Prog Retin Eye Res*. 2006;25(4):397-424.

69. Barber AJ. A new view of diabetic retinopathy: a neurodegenerative disease of the eye. *Prog Neuropsychopharmacol Biol Psychiatry*. 2003;27(2):283-90.

70. Zeng XX, Ng YK, Ling EA. Neuronal and microglial response in the retina of streptozotocin-induced diabetic rats. *Vis Neurosci*. 2000;17(3):463-71.

71. Sorrentino FS, Allkabes M, Salsini G, Bonifazzi C, Perri P. The importance of glial cells in the homeostasis of the retinal microenvironment and their pivotal role in the course of diabetic retinopathy. *Life Sci*. 2016;162:54-9.

72. Rowitch DH, Kriegstein AR. Developmental genetics of vertebrate glial-cell specification. *Nature*. 2010;468(7321):214-22.

73. Venkatesh K, Srikanth L, Vengamma B, Chandrasekhar C, Sanjeevkumar A, Mouleshwara Prasad BC, et al. In vitro differentiation of cultured human CD34+ cells into astrocytes. *Neurol India*. 2013;61(4):383-8.

74. Schnitzer J. Chapter 7 Astrocytes in mammalian retina. *Prog Retin Eye Res*. 1988;7:209-31.

75. Ridet JL, Malhotra SK, Privat A, Gage FH. Reactive astrocytes: cellular and molecular cues to biological function. *Trends Neurosci*. 1997;20(12):570-7.

76. Klaassen I, Van Noorden CJ, Schlingemann RO. Molecular basis of the inner blood-retinal barrier and its breakdown in diabetic macular edema and other pathological conditions. *Prog Retin Eye Res*. 2013;34:19-48.

77. Giacco F, Brownlee M. Oxidative stress and diabetic complications. *Circ Res*. 2010;107(9):1058-70.

78. Reddy VS, Raghu G, Reddy SS, Pasupulati AK, Suryanarayana P, Reddy GB. Response of small heat shock proteins in diabetic rat retina. *Invest Ophthalmol Vis Sci*. 2013;54(12):7674-82.

79. Kappé G, Franck E, Verschuure P, Boelens WC, Leunissen JA, de Jong WW. The human genome encodes 10 α-crystallin–related small heat shock proteins: HspB1–10. *Cell Stress Chaperones*. 2003;8(1):53-61.

80. Arrigo A-P. Chaperons moléculaires et repliement des protéines: l'exemple de certaines protéines de choc thermique. *Med Sci*. 2005;21(6-7):619-25.

81. Sun Y, MacRae TH. Small heat shock proteins: molecular structure and chaperone function. *Cell Mol Life Sci*. 2005;62(21):2460-76.

82. Pirkkala L, Nykanen P, Sistonen L. Roles of the heat shock transcription factors in regulation of the heat shock response and beyond. *FASEB J*. 2001;15(7):1118-31.

83. Reddy VS, Kumar CU, Raghu G, Reddy GB. Expression and induction of small heat shock proteins in rat heart under chronic hyperglycemic conditions. *Arch Biochem Biophys*. 2014;558:1-9.

84. Reddy VS, Raghu G, Reddy SS, Pasupulati AK, Suryanarayana P, Reddy GB. Response of small heat shock proteins in diabetic rat retina. *Invest Ophthalmol Vis Sci*. 2013;54(12):7674-82.

85. Toh H, Smolentsev A, Bozadjian RV, Keeley PW, Lockwood MD, Sadjadi R, et al. Vascular changes in diabetic retinopathy—a longitudinal study in the Nile rat. *Lab Invest*. 2019;99(10):1547-60.

86. Allen CL, Malhi NK, Whatmore JL, Bates DO, Arkill KP. Non-invasive measurement of retinal permeability in a diabetic rat model. *Microcirculation*. 2020;27(6):e12623.

87. Littlewood R, Mollan SP, Pepper IM, Hickman SJ. The Utility of Fundus Fluorescein Angiography in Neuro-Ophthalmology. *Neuroophthalmology*. 2019;43(4):217-34.

88. Semwogerere D, Weeks ER. Confocal microscopy. Encyclopedia of biomaterials and biomedical engineering, Taylor & Francis.2005;23:1-10.

89. Finkleman B. On the nature of inhibition in the intestine. *J Physiol*. 1930;70(2):145-57.

90. Fresta CG, Fidilio A, Caruso G, Caraci F, Giblin FJ, Marco Leggio G, et al. A new human blood–retinal barrier model based on endothelial cells, pericytes, and astrocytes. *Int J Mol Sci*. 2020;21(5):1636.

91. Gaddum J. The technique of superfusion. *Br J Pharmacol*. 1997;120(Suppl 1):82-7.

92. Hornof M, Toropainen E, Urtti A. Cell culture models of the ocular barriers. *Eur J Pharm Biopharm*. 2005;60(2):207-25.

93. Mishra A, Hamid A, Newman EA. Oxygen modulation of neurovascular coupling in the retina. *Proc Natl Acad Sci*. 2011;108(43):17827-31.

94. Reiter CE, Sandirasegarane L, Wolpert EB, Klinger M, Simpson IA, Barber AJ, et al. Characterization of insulin signaling in rat retina in vivo and ex vivo. *Am J Physiol Endocrinol Metab*. 2003;285(4):E763-74.

95. Abuhaiba SI, Cordeiro M, Amorim A, Cruz Â, Quendera B, Ferreira C, et al. Occipital blood-brain barrier permeability is an independent predictor of visual outcome in type 2 diabetes, irrespective of the retinal barrier: A longitudinal study. *J Neuroendocrinol*. 2018;30(1).e12566.

96. Nakagawa S, Deli MA, Nakao S, Honda M, Hayashi K, Nakaoke R, et al. Pericytes from brain microvessels strengthen the barrier integrity in primary cultures of rat brain endothelial cells. *Cell Mol Neurobiol*. 2007;27(6):687-94.

97. Wurbel H. Ideal homes? Housing effects on rodent brain and behaviour. *Trends Neurosci*. 2001;24(4):207-11.

98. Araibi H, van der Merwe E, Gwanyanya A, Kelly-Laubscher R. The effect of sphingosine-1-phosphate on the endothelial glycocalyx during ischemia-reperfusion injury in the isolated rat heart. *Microcirculation*. 2020;27(5):e12612.

99. Rasband WS. Image J, US National Institutes of Health, Bethesda, Maryland, USA. http://imagej nih gov/ij/. 2011.

100. Chelazzi C, Villa G, Mancinelli P, De Gaudio AR, Adembri C. Glycocalyx and sepsis-induced alterations in vascular permeability. *Crit Care*. 2015;19:26.

101. Qing Q, Zhang S, Chen Y, Li R, Mao H, Chen Q. High glucose-induced intestinal epithelial barrier damage is aggravated by syndecan-1 destruction and heparanase overexpression. *J Cell Mol Med*. 2015;19(6):1366-74.

102. Naidoo VL, Lang DM, Van der Merwe, EL. Addressing the Challenges of Multi-Immunofluorescent Deep Tissue Imaging of Islets and Vasculature in the Rat Pancreas. J Mol Biol & Mol Imaging. 2015;2(2):1022.

103. Piña R, Santos-Díaz AI, Orta-Salazar E, Aguilar-Vazquez AR, Mantellero CA, Acosta-Galeana I, et al. Ten Approaches That Improve Immunostaining: A Review of the Latest Advances for the Optimization of Immunofluorescence. *Int J Mol Sci.* 2022;23(3):1426.

104. Li W, Yanoff M, Liu X, Ye X. Retinal capillary pericyte apoptosis in early human diabetic retinopathy. *Chin Med J*. 1997;110(9):659-63.

105. Mizutani M, Kern TS, Lorenzi M. Accelerated death of retinal microvascular cells in human and experimental diabetic retinopathy. *J Clin Invest*. 1996;97(12):2883-90.

106. Cunha-Vaz J. Blood-retinal barrier and its relevance in retinal disease. *Medical Retina*. 2012:6-10.

107. Metea MR, Newman EA. Glial cells dilate and constrict blood vessels: a mechanism of neurovascular coupling. *J Neurosci*. 2006;26(11):2862-70.

108. Mulligan SJ, MacVicar BA. Calcium transients in astrocyte endfeet cause cerebrovascular constrictions. *Nature*. 2004;431(7005):195-9.

109. Rungger-Brändle E, Dosso AA, Leuenberger PM. Glial reactivity, an early feature of diabetic retinopathy. *Invest Ophthalmol Vis Sci*. 2000;41(7):1971-80.

110. Tsantilas KA, Cleghorn WM, Bisbach CM, Whitson JA, Hass DT, Robbings BM, et al. An Analysis of Metabolic Changes in the Retina and Retinal Pigment Epithelium of Aging Mice. *Invest Ophthalmol Vis Sci*. 2021;62(14):20.

111. Ly A, Yee P, Vessey KA, Phipps JA, Jobling AI, Fletcher EL. Early inner retinal astrocyte dysfunction during diabetes and development of hypoxia, retinal stress, and neuronal functional loss. *Invest Ophthalmol Vis Sci*. 2011;52(13):9316-26.

112. García-Cáceres C, Lechuga-Sancho A, Argente J, Frago LM, Chowen JA. Death of hypothalamic astrocytes in poorly controlled diabetic rats is associated with nuclear translocation of apoptosis inducing factor. *J Neuroendocrinol*. 2008;20(12):1348-60.

113. Lechuga-Sancho AM, Arroba AI, Frago LM, Pañeda C, García-Cáceres C, Delgado Rubín de Célix A, et al. Activation of the intrinsic cell death pathway, increased apoptosis and modulation of astrocytes in the cerebellum of diabetic rats. *Neurobiol Dis*. 2006;23(2):290-9.

114. Kumar S, Zhuo L. Longitudinal in vivo imaging of retinal gliosis in a diabetic mouse model. *Exp Eye Res*. 2010;91(4):530-6.

115. Xia Y, Luo Q, Chen J, Huang C, Jahangir A, Pan T, et al. Retinal astrocytes and microglia activation in diabetic retinopathy rhesus monkey models. *Curr Eye Res*. 2021;47(2):297-303.

116. Götte M, Joussen AM, Klein C, Andre P, Wagner DD, Hinkes MT, et al. Role of syndecan-1 in leukocyte-endothelial interactions in the ocular vasculature. *Invest Ophthalmol Vis Sci*. 2002;43(4):1135-41.

117. Wang J-B, Yu H-L. Expression of syndecan-1 in the retina of diabetes. *Int Eye Sci*. 2013;13(4):660-62.

118. Gharagozlian S, Borrebæk J, Henriksen T, Omsland TK, Shegarfi H, Kolset SO. Effect of hyperglycemic condition on proteoglycan secretion in cultured human endothelial cells. *Eur J Nutr*. 2006;45(7):369-75.

119. Qiu H, Fan W, Huang S, Liu F, Tang W, Zuo C. effect of high concentration of glucose on thickness of glycocalyx and expression of syndecan-1 and glypican-1 in cultured human renal glomerular endothelial cells. *J Sichuan UnivMed Sci Ed*. 2010;41(6):980-5.

120. Tanaka Y, Kobayashi K, Kita M, Kinoshita S, Imanishi J. Messenger RNA expression of heat shock proteins (HSPs) during ocular development. *Curr Eye Res*. 1995;14(12):1125-33.

121. Ochoa GH, Clark YM, Matsumoto B, Torres-Ruiz JA, Robles LJ. Heat shock protein 70 and heat shock protein 90 expression in light- and dark-adapted adult octopus retinas. *J Neurocytol*. 2002;31(2):161-74.

122. Morimoto RI. Regulation of the heat shock transcriptional response: cross talk between a family of heat shock factors, molecular chaperones, and negative regulators. *Genes Dev*. 1998;12(24):3788-96.

123. Wu C. Heat shock transcription factors: structure and regulation. *Annu Rev Cell Dev Biol*. 1995;11:441-69.

124. Kandpal RP, Rajasimha HK, Brooks MJ, Nellissery J, Wan J, Qian J, et al. Transcriptome analysis using next generation sequencing reveals molecular signatures of diabetic retinopathy and efficacy of candidate drugs. *Mol Vis*. 2012;18:1123-46.

125. Kumar PA, Haseeb A, Suryanarayana P, Ehtesham NZ, Reddy GB. Elevated expression of αA-and αB-crystallins in streptozotocin-induced diabetic rat. *Arch Biochem Biophys*. 2005;444(2):77-83.

126. Losiewicz MK, Fort PE. Diabetes impairs the neuroprotective properties of retinal alpha-crystallins. *Invest Ophthalmol Vis Sci*. 2011;52(9):5034-42.

127. Simkhovich BZ, Marjoram P, Poizat C, Kedes L, Kloner RA. Brief episode of ischemia activates protective genetic program in rat heart: a gene chip study. *Cardiovasc Res*. 2003;59(2):450-9.

Appendix 1

UNIVERSITY OF CAPE TOWN
Faculty of Health Sciences
Animal Ethics Committee

Room E52-24 Old Main Building
Groote Schuur Hospital
Observatory 7925
Telephone [021] 406 6492
Email: sumayah.ariefdien@uct.ac.za
Website: www.health.uct.ac.za/fhs/research/animalethics/forms

02 July 2018

Dr A Gwanyanya
Human Biology
4.10 Anatomy Building
FHS

Dear Dr Gwanyanya

PROTOCOL TITLE: The investigation of the mechanisms underlying cardiac remodelling and vascular changes in diabetes

FHS AEC REF NO: 018_021

Thank you for submitting your protocol to the Faculty of Health Sciences (FHS) Animal Ethics Committee (AEC) for review.

I am pleased to inform you that the FHS AEC has **approved** your protocol, which will terminate on **30 July 2021.**

Number of animals & species: 260 Wistar Rats

Please quote the FHS AEC REF NO (above) in all future correspondence.

Please note that the approval of this protocol imposes the following obligations on the principal investigator (PI):

1. To submit an annual mandatory progress report. The first annual report for this protocol is due on **28 February 2019**. The forms can be accessed from http://www.health.uct.ac.za/fhs/research/animalethics/forms
2. To submit a final mandatory report on the **30 July 2021**, please access the final report form from: http://www.health.uct.ac.za/fhs/research/animalethics/forms
3. Ensuring that all study participants perform within the confines of the procedures and experimental design of the protocol as approved, or as amended.

4. Ensuring that all study participants comply with all applicable national legislation, UCT policies, FHS AEC policies and standard operating procedures (SOPs) and national standards (SANS 10386: 2008).
5. Ensuring that you as the PI immediately alert the FHS AEC to any event involving the welfare of the animals which has occurred during the course of the study, as well as the actions that were taken to respond to these events.
6. Ensuring that you as the PI alert the FHS AEC to any new or unexpected ethical issues that arose during the course of the study, and how these issues were addressed.
7. Ensuring that all study participants are registered with or have been authorised by the South African Veterinary Council (SAVC) to perform the procedures on animals, or will be performing the procedures under the direct and continuous supervision of SAVC-registered veterinary professionals or SAVC-registered para-veterinary professionals.
8. If the PI or any study participant is in any way uncertain how to respond to any of these obligations or deal with any of the issues referred to above, they must consult with FHS AEC.
9. All animals found dead must be reported to the RAF on the appropriate form: http://www.health.uct.ac.za/fhs/research/animalethics/forms
10. All animals found in distress must be reported to the RAF on the appropriate form.

My best wishes for a successful research and /or teaching endeavour.

Yours sincerely

singed by the chair

PROF PJ COMMERFORD
CHAIR, FHS AEC

AEC REF# 018_021

UNIVERSITY OF CAPE TOWN
Faculty of Health Sciences
Animal Ethics Committee

Room E53-46 Old Main Building
Groote Schuur Hospital
Observatory 7925
Telephone [021] 406 6492
Email: sumayah.ariefdien@uct.ac.za
Website: www.health.uct.ac.za/fhs/research/animalethics/forms

30 May 2019

Prof E van der Merwe
Division of Cell Biology
Room 6.02.3
Anatomy Building-FHS

Dear Prof van der Merwe

PROTOCOL TITLE: Request to harvest eyes from surplus rat carcasses euthanised at RAF

FHS AEC REF NO: 019_021

Thank you for submitting your request for approval of use of animal material for scientific purposes to the Faculty of Health Sciences (FHS) Animal Ethics Committee (AEC).

I am pleased to inform you that the FHS AEC EXCO has **approved** your request, which will terminate on **30 April 2022.**

Number of animal material & species: Rats eyes -30-40

Please quote the FHS AEC REF NO (above) in all future correspondence.

Please note that the approval of this protocol imposes the following obligations on the principal investigator (PI):

1. To submit an annual mandatory progress report. The first annual report for this protocol is due on **28 February 2020**. The forms can be accessed from http://www.health.uct.ac.za/fhs/research/animalethics/forms
2. To submit a final mandatory report on the **30 April 2022**, please access the final report form from: http://www.health.uct.ac.za/fhs/research/animalethics/forms
3. Ensuring that all study participants perform within the confines of the procedures and experimental design of the protocol as approved, or as amended.
4. Ensuring that all study participants comply with all applicable national legislation, UCT policies, FHS AEC policies and standard operating procedures (SOPs) and national standards (SANS 10386: 2008).

My best wishes for a successful research and /or teaching endeavour.

Yours sincerely

signature removed

PROF PJ COMMERFORD
CHAIR, FHS AEC

AEC REF# 019_021

Appendix 2

Standard whole-mount (Retinal tissue) immunohistochemistry protocol for Liz's lab:

1. Harvest the eyes, remove the lens, dissect out retina
2. Fix in 4% PFA overnight
3. Wash in 1 x PBS 3x 20 min each using a belly dancer or nutator
4. Permeabilise in 0.5% Tween 20/PBS for 2 hours at room temperature on a belly dancer or nutator or in methanol for 1.5hours at 37^{o}C in an incubator
5. Block in 0.1% tween/3% BSA for 3 hours or overnight on a rocker at 4^{o}C
6. Incubate in primary antibody overnight
7. Wash in PBS 3x 20 min each using a belly dancer or nutator
8. Incubate in secondary antibody x 5hours or overnight at 4^{o}C
9. Wash in PBS 3x 20 min each using a belly dancer or nutator
10. Put sample into DABCO/glycerol for 2 hours at room temperature then into fridge overnight
11. Mount on coverslips
12. Store in fridge in DABCO/glycerol after microscopy.

Mounting

1. Use two clean cover slips (22x50 and 22x32mm size)
2. Place a drop of DABCO/glycerol on the small slide
3. Using the dissecting microscope for guidance, mount the retina using a forceps and stick
4. Mount the retina facing upwards
5. Cover with the larger cover slip

6. When placing on the microscope stage , turn the coverslips so that the larger one is below while the smaller one is on top so that superficial surface of the retina faces downwards towards the microscope objective.

Appendix 3

Image analysis using image J software

Image J instructions for syndecan

1. Upload image into image J
2. Separate the channels
3. Run a macro which convert the images to 8 bits gray scale
4. Create individual image from the image stack
5. Then select the 1st or 2nd image in the stack (based on the clarity of vessels in the 3D stack of lectin stained vessels) and compare syndecan channel with the blood vessel layer
6. Draw a line on the ROI on that and then generate the line plot
7. Take a maximum and minimum plot profile values and find the average

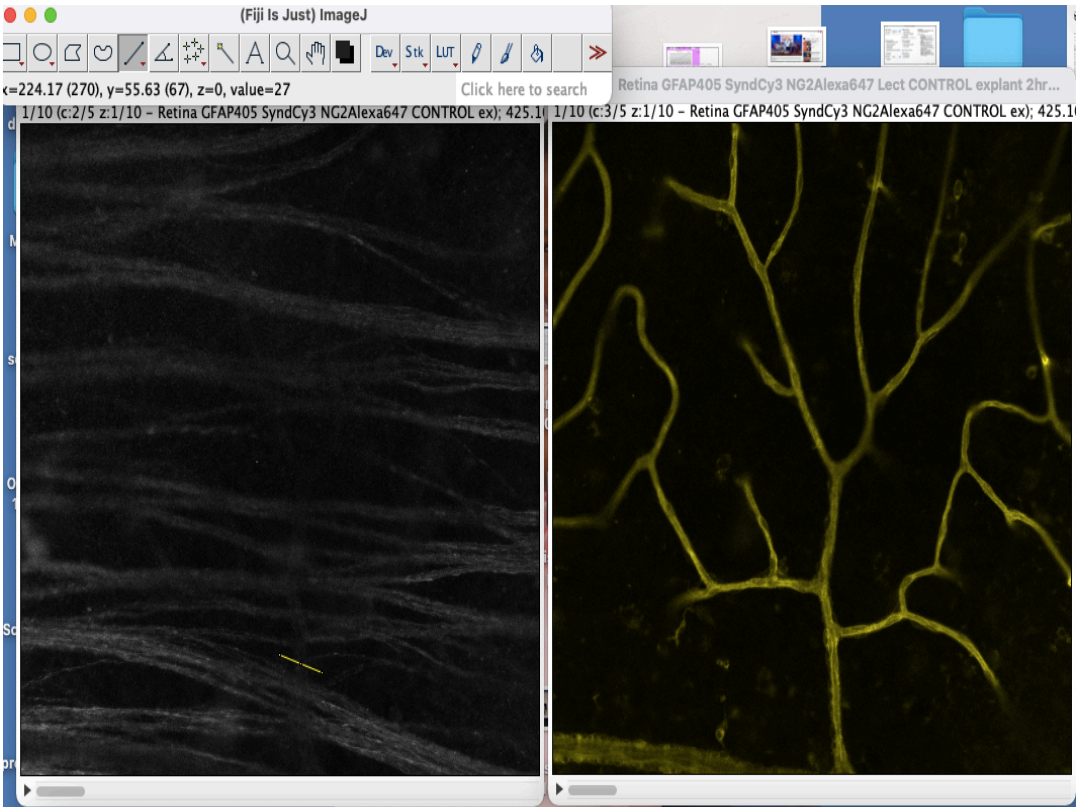

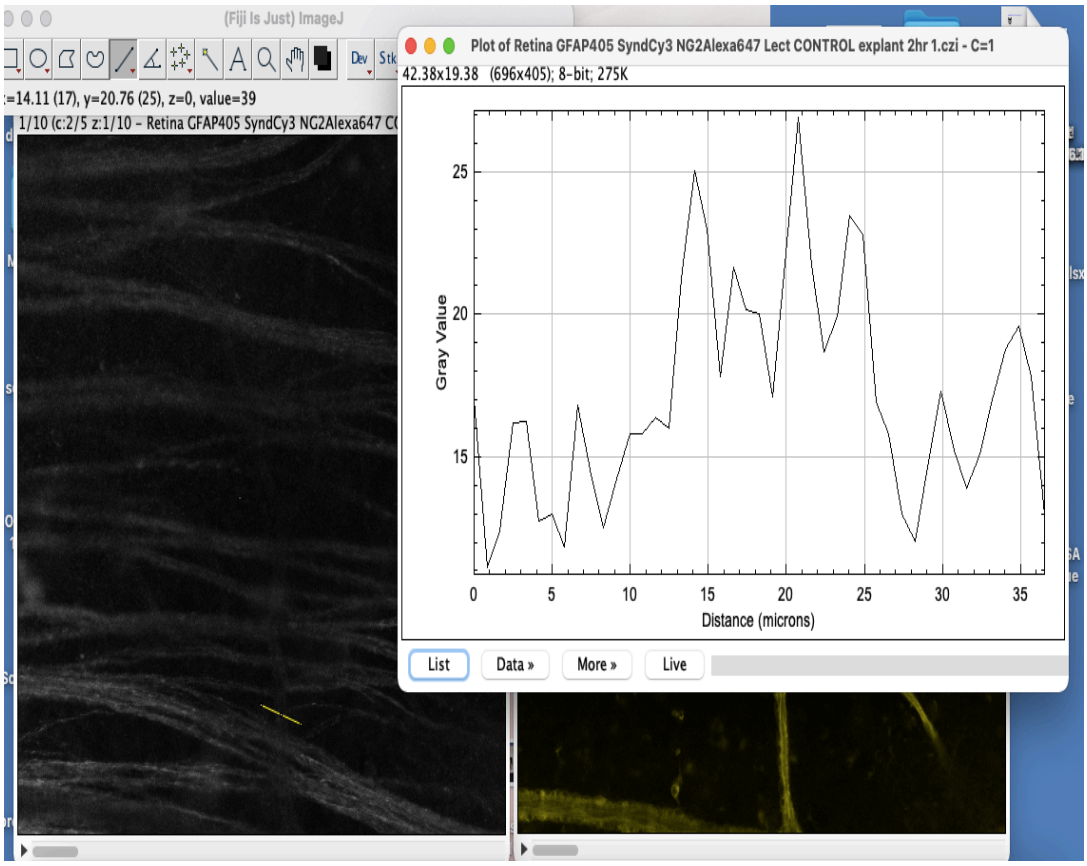

Note: For analysis of astrocyte area , steps 1-5 above were used followed by an extended focus image. The ROI was the frame of the whole image and a second macro was run which included the threshold and area analysis.

Astrocyte Macro for area analysis:

```
run("Duplicate...", " ");
run("Measure");
setAutoThreshold("Huang dark");
//run("Threshold...");
setAutoThreshold("Huang dark");
run("Measure");
```

Appendix 4

Western blot protocol

(Standard protocol being used in our laboratory)

1. Preparation of buffers
2. Sample preparation
3. Protein Quantification
4. Gel preparation and electrophoresis
5. Transfer process
6. Blocking of the membrane and antibody probing
7. Enhanced Chemiluminescence (ECL) detection
8. Stripling and re-probing
9. Scanning and analysis

1. Preparation of buffers: The following buffers are required for western blot analysis:

A- Radioimmunoprecipitation assay buffer (RIPA buffer): recipe for 50 ml include: NaCl (5 molar) 1.5 ml, Triton X -100 (100%) 500 ul, SDS (10%) 500 ul, Tris (1molar, Ph 7.5), Deoxycholate sodium 0.5 g and distilled water 46.5 ml.

B- Phosphate Buffered Saline-Tween (PBS-T×1): 8 g NaCl, 0.2 g KCl, 1.44 g Na2HPO4, 0.24 g KH2PO4, 2 ml Tween 20 and up to1000 ml distilled water, stir for 20 minutes and adjust the pH to 7.4.

C- Running (tank) buffer: using a Bio-Rad buffer (10× Tris/Glycine/SDS TGS Buffer, Bio-Rad SA). Mix 100 ml of TGS with 900 ml of distilled water.

D- Transfer buffer: using Bio-Rad buffer (Trans -Blot Turbo ×5 Transfer buffer, Bio-Rad SA). Mix 200 ml of 5× transfer buffer with 600 ml of distilled water and 200 ml of ethanol.

E- Stripling buffer: 8 g NaOH in 1liter distilled water.

2. Sample preparation: A. Retrieve the frozen retinal samples from -80°C freezers. The tissue weighed and placed in new labelled Eppendorf tube and calculate the amount of RIPA extraction buffer (weigh of tissue in gram ×19), this gives the volume of RIPA needed 86 to add to tissue before homogenisation. Add protease and phosphatase inhibitor cocktail (Halt protease &phosphatase inhibitor, ThermoScientific, USA) 2 ul of cocktail inhibitor per 1 ml of RIPA buffer.

B. Tissue homogenisation by sonication (Soniprep 150, UK). The Eppendorf tube with tissue and RIPA inside are placed in fetched place in the sonicator and allow the Soniprep probe just touch the tissue inside the Eppendorf and sonicate at 180 watts for 20 seconds until all tissue get homogenised in the buffer.

C. Centrifuge the samples in a centrifuge (Labnet International, NJ07095 USA), at 15 000 relative centrifugal force at 4°C for 30 minutes then transfer the supernatant into well labelled Eppendorf tube and make aliquot of 20 ul for protein assay and store at -80°C.

3. Protein quantification: BCA protein assay using the Pierce protein assay kit (Thermo Scientific, Rockford, USA).

A. Preparation of diluted bovine serum Albumin (BSA) standards using RIPA buffer as diluent and standard Bovine serum solution as follows:

Vial volume of diluent (µl) volume of BSA (µl): A 0 300 of stock, B 125 375 of stock, C 325 325 of stock, D 175 175 of vial B dilution, E 325 325 of vial C dilution, F 325 325 of vial E dilution, G 325 325 of vial F dilution, H 400 100 of vial G dilution

B. Preparation of BCA working reagent

To calculate the amount of working reagent required use the following formula: Number of standards used + number of samples ×2 (for duplicate) +1 for pipetting error ×200 (amount required per well). To prepare WR mix 50 parts of reagent A and on I 400 part of reagent B giving a clear green solution.

C. For a microplate procedure using a flat bottom 96 wells plate, pipette 25 µl of standards in duplicate, 10 µl of samples in duplicate. Add 50 µl of RIPA buffer to the samples and 200 µl of working reagent to both standards and samples. Shake the microplate briefly and cover with parafilm and incubate in the oven at 37°C for 30 minutes.

D. Measure the absorbance in plate reader (RT-2100C, Microplate Reader, Germany) at 562 nm. Create a standard curve and calculate the volume of protein sample required and other recipe, which include RIPA buffer, Lammli dye (Bio-Rad, SA) and diethyltritroil as shown below:

Appendix 5

Retinal blood vessels

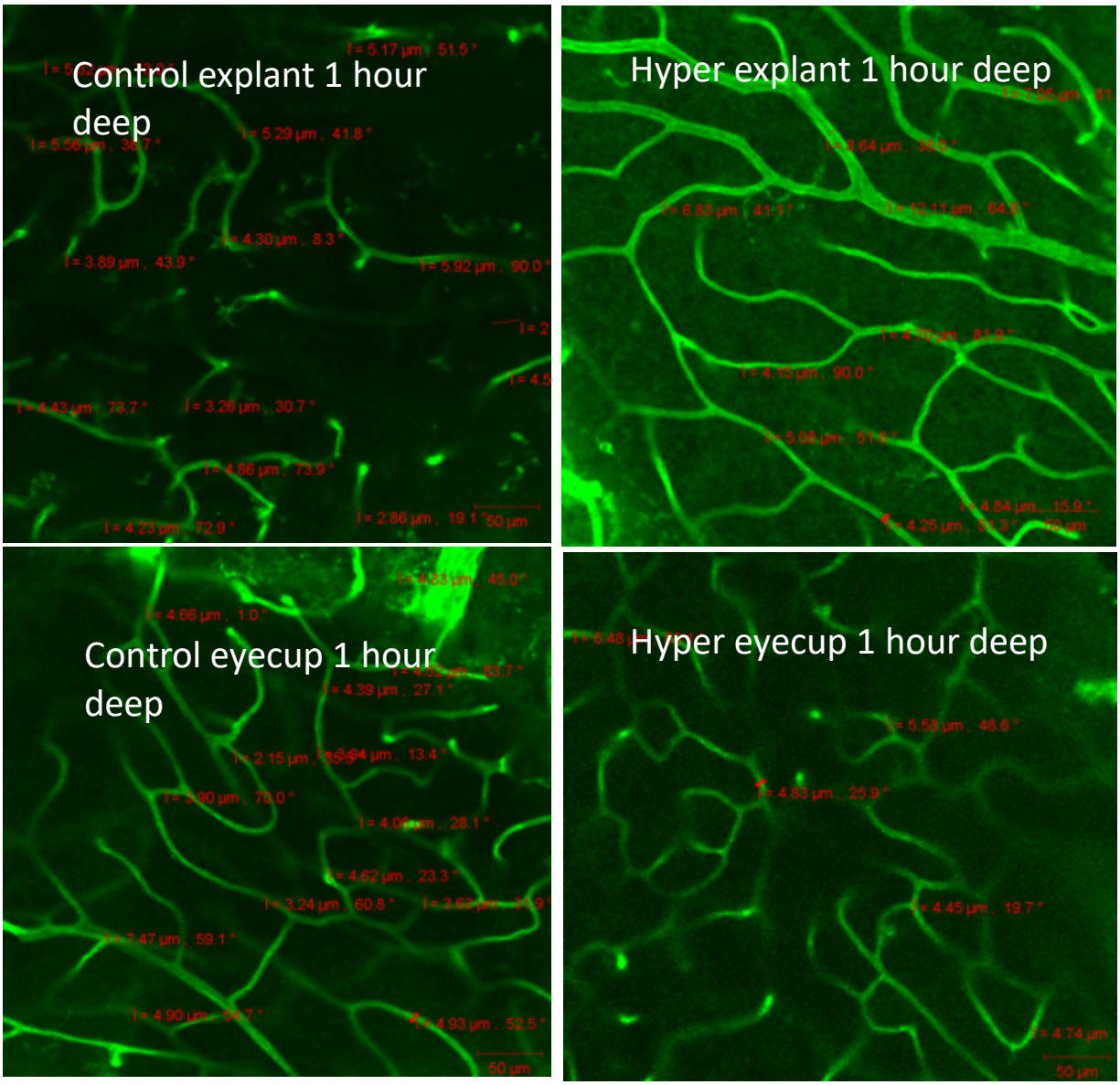

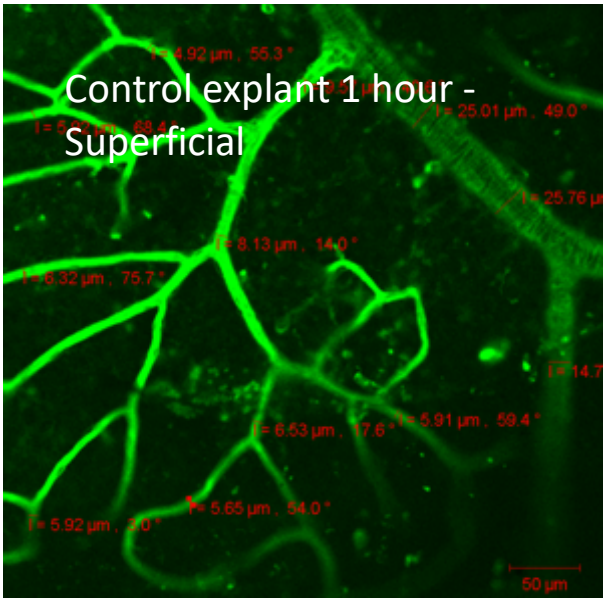
Control explant 1 hour - Superficial

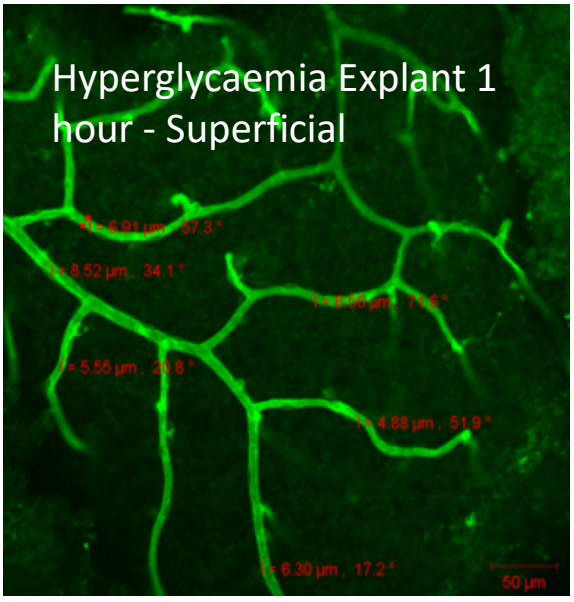
Hyperglycaemia Explant 1 hour - Superficial

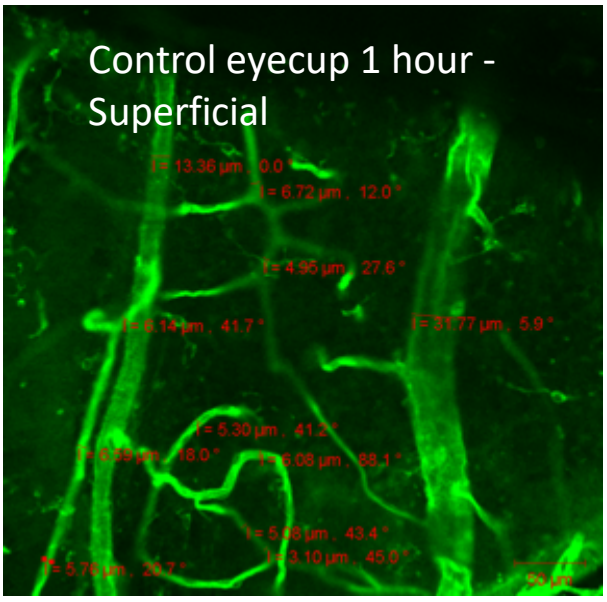
Control eyecup 1 hour - Superficial

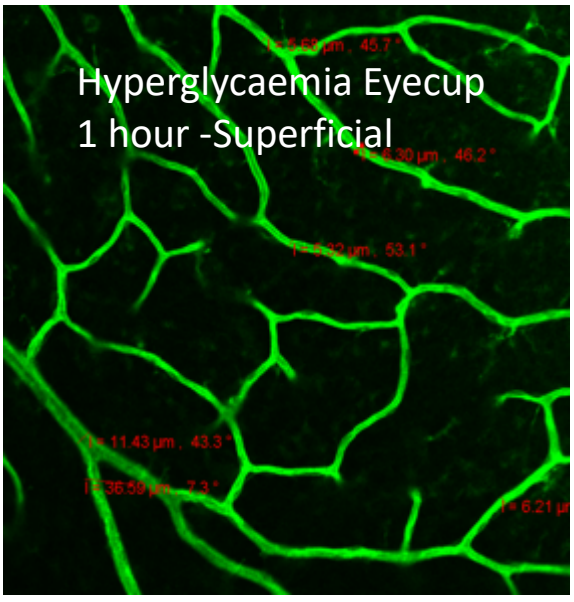
Hyperglycaemia Eyecup 1 hour -Superficial

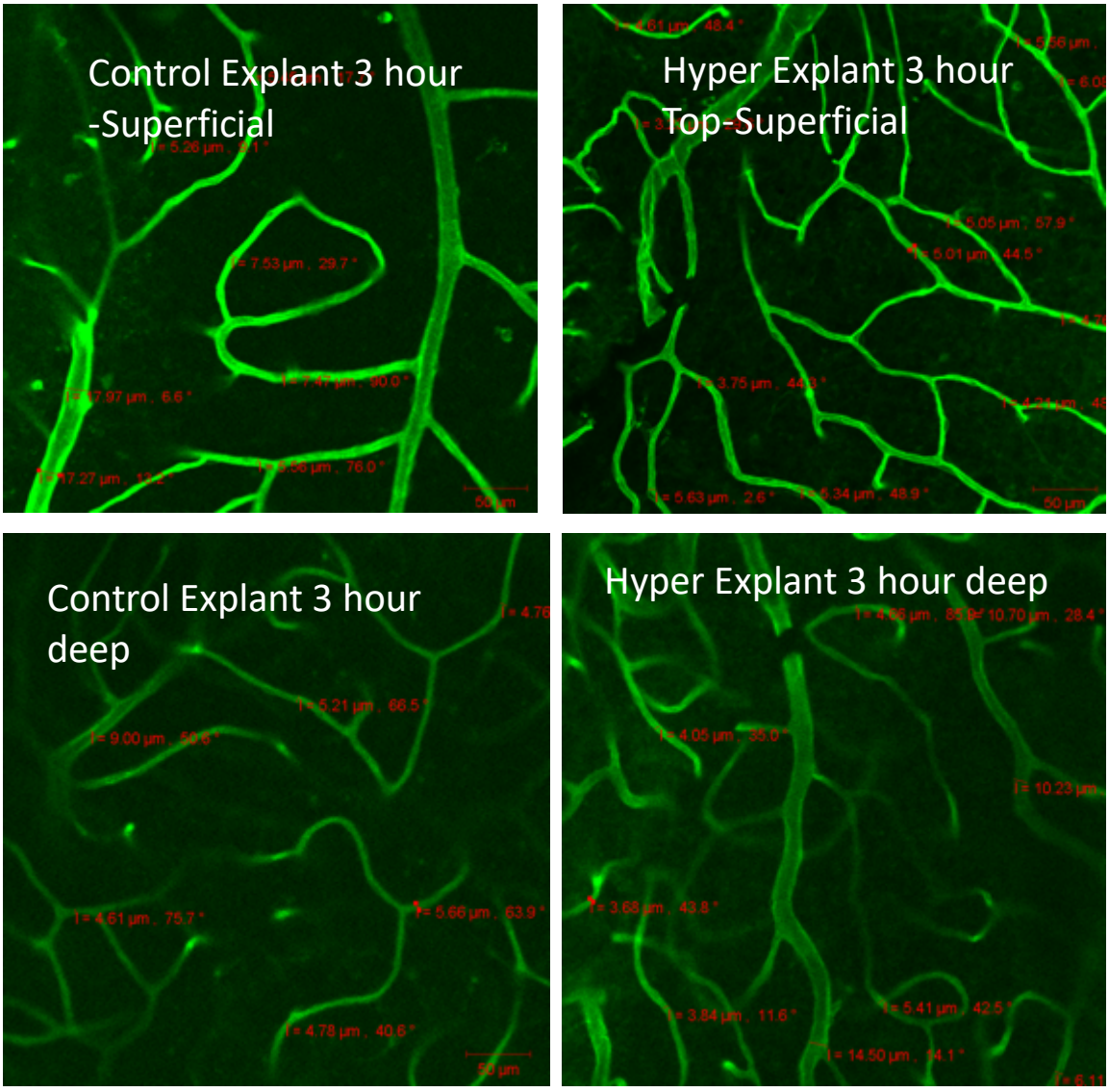

Superficial and deep optical planes showing the effect of hyperglycaemia on rat retinal blood vessels after 48 hours in culture: Superficial and deep layers of retinal explants and eyecups in control and hyperglycaemic conditions.

Appendix 6

Pericytes

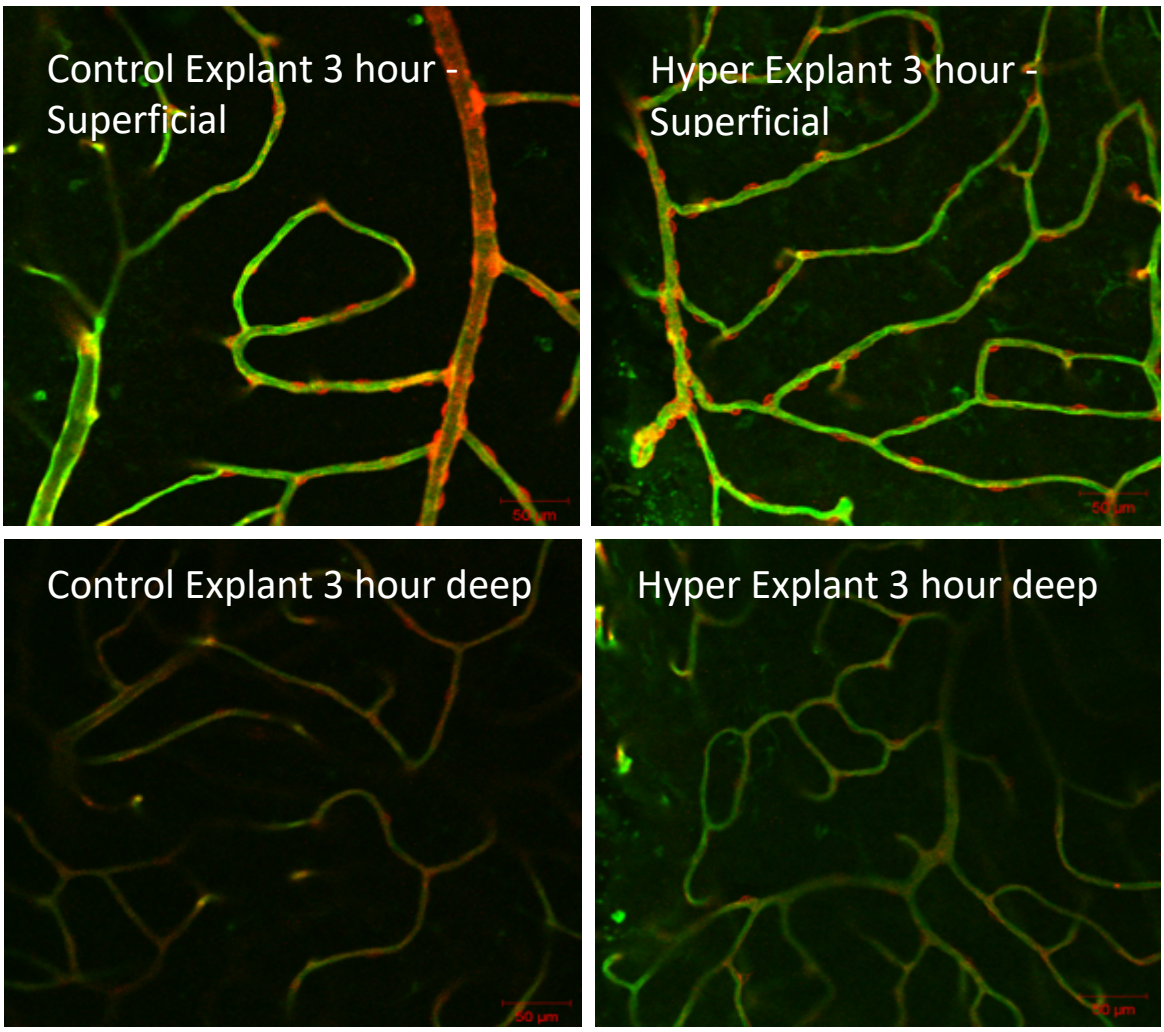

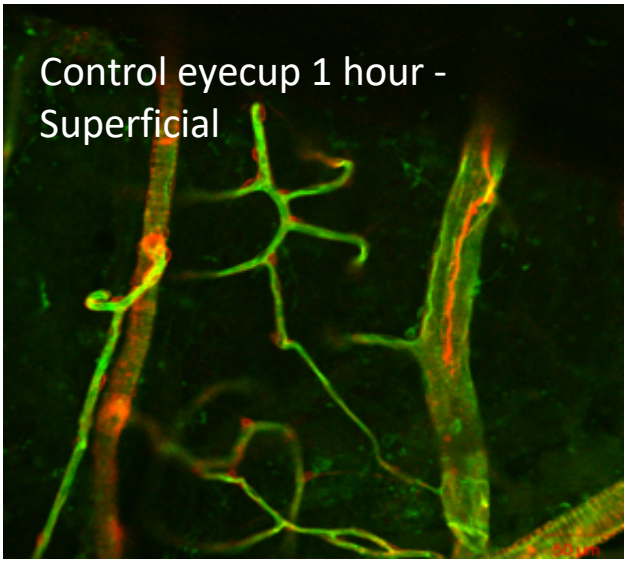
Control eyecup 1 hour -
Superficial

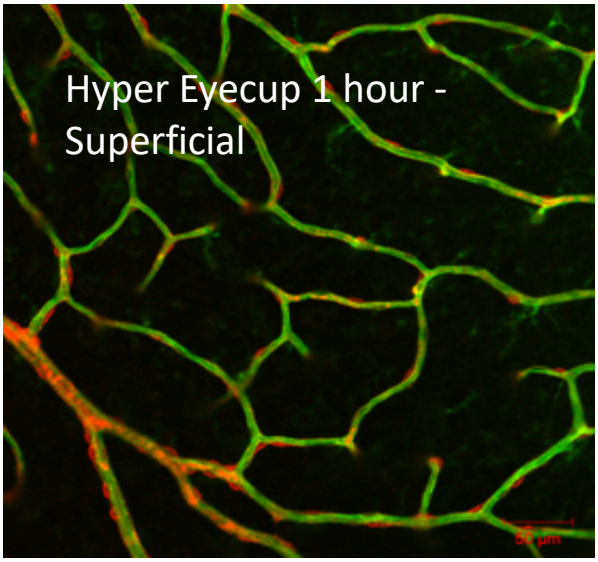
Hyper Eyecup 1 hour -
Superficial

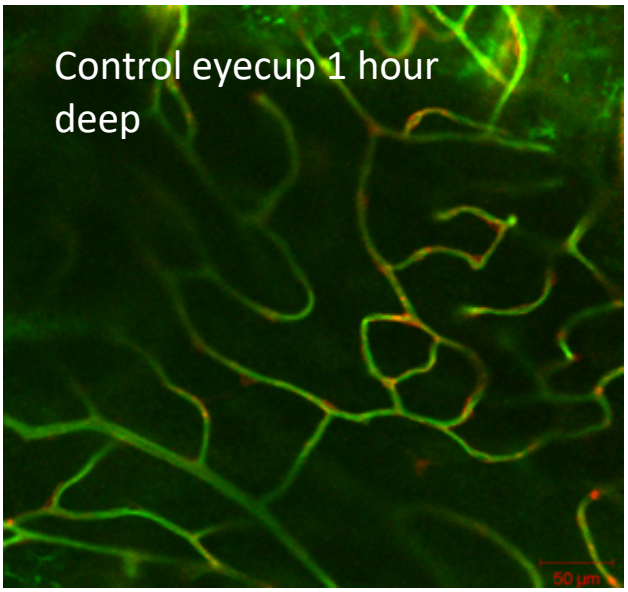
Control eyecup 1 hour
deep
50 µm

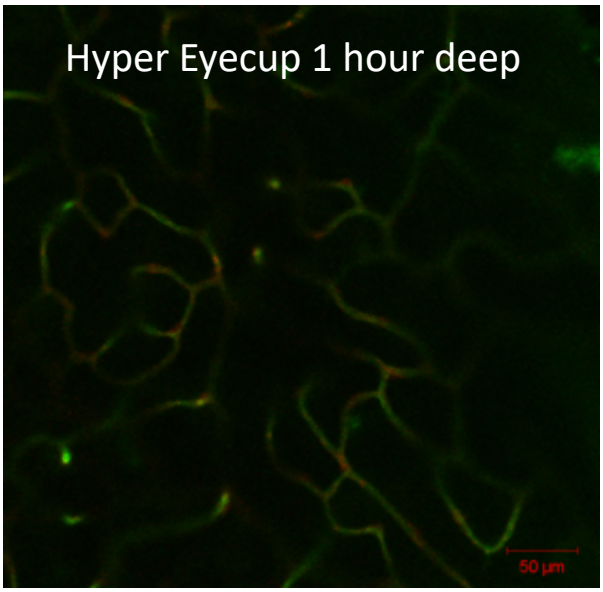
Hyper Eyecup 1 hour deep
50 µm

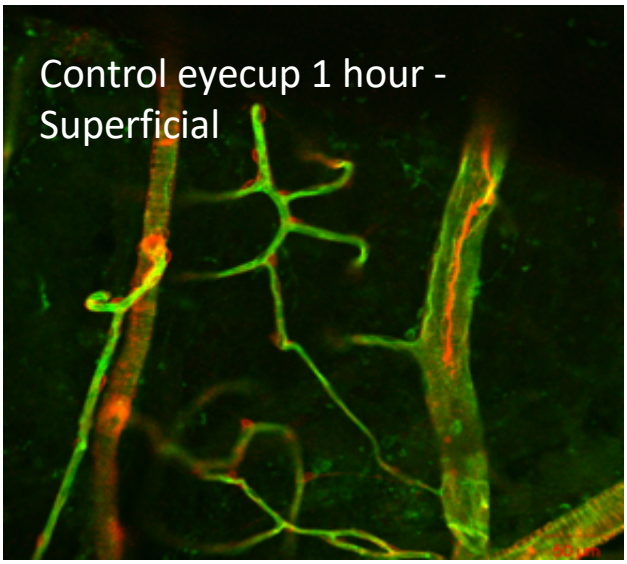
Control eyecup 1 hour -
Superficial

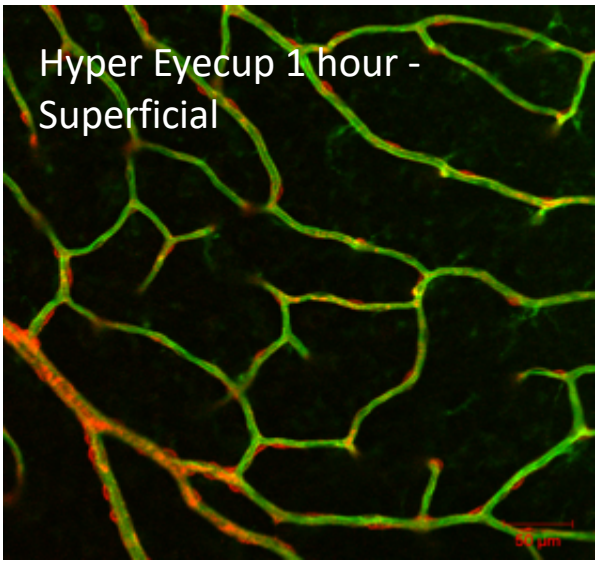
Hyper Eyecup 1 hour -
Superficial

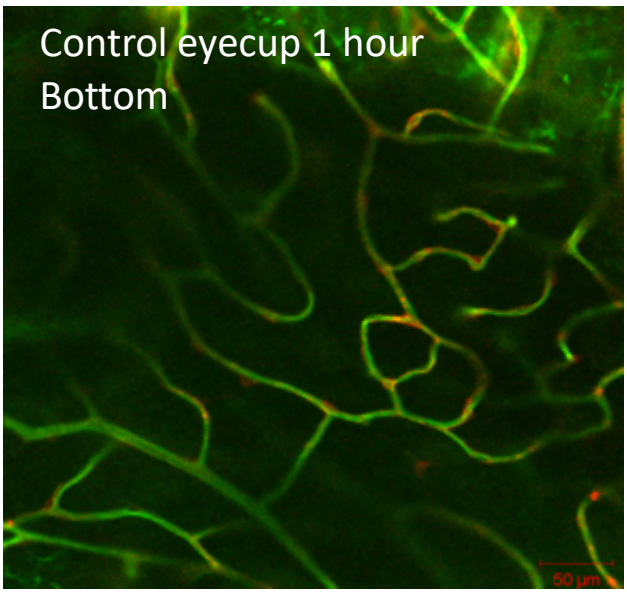
Control eyecup 1 hour
Bottom

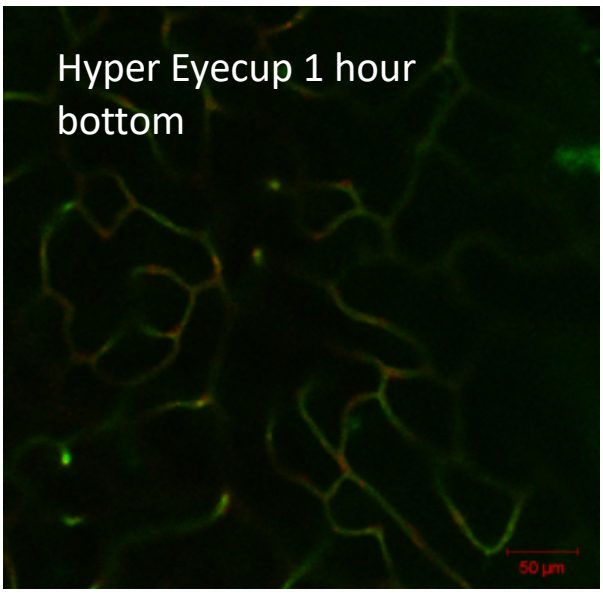
Hyper Eyecup 1 hour
bottom

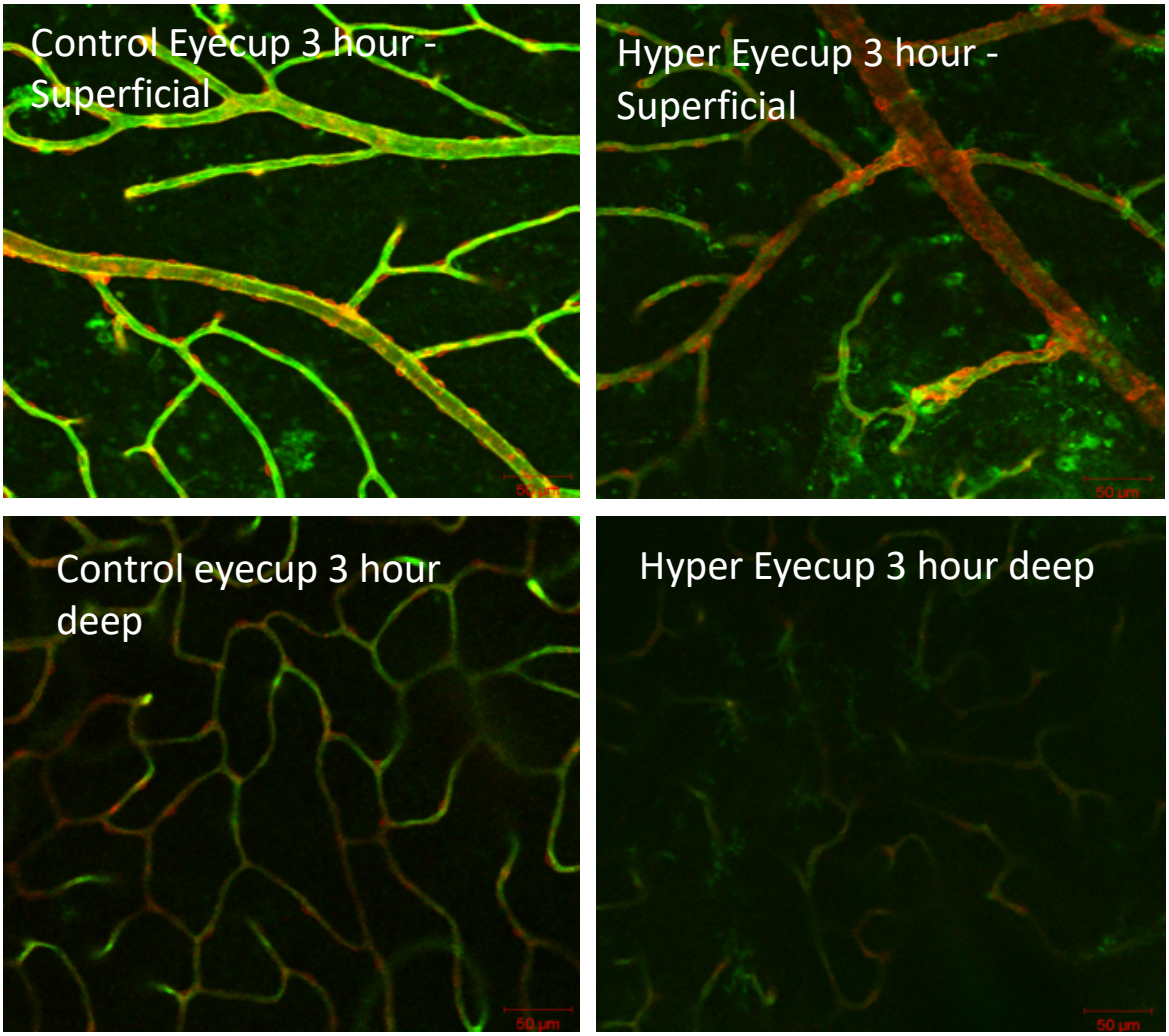

Appendix 6. Single image planes of the superficial and deep layers of the retinal vessels showing the effect of hyperglycaemia on pericytes: Superficial and deep layers of retinal explants and eyecup in control and hyperglycaemic conditions.

Appendix 7

Syndecan-1 expression in the lower layers of the retina

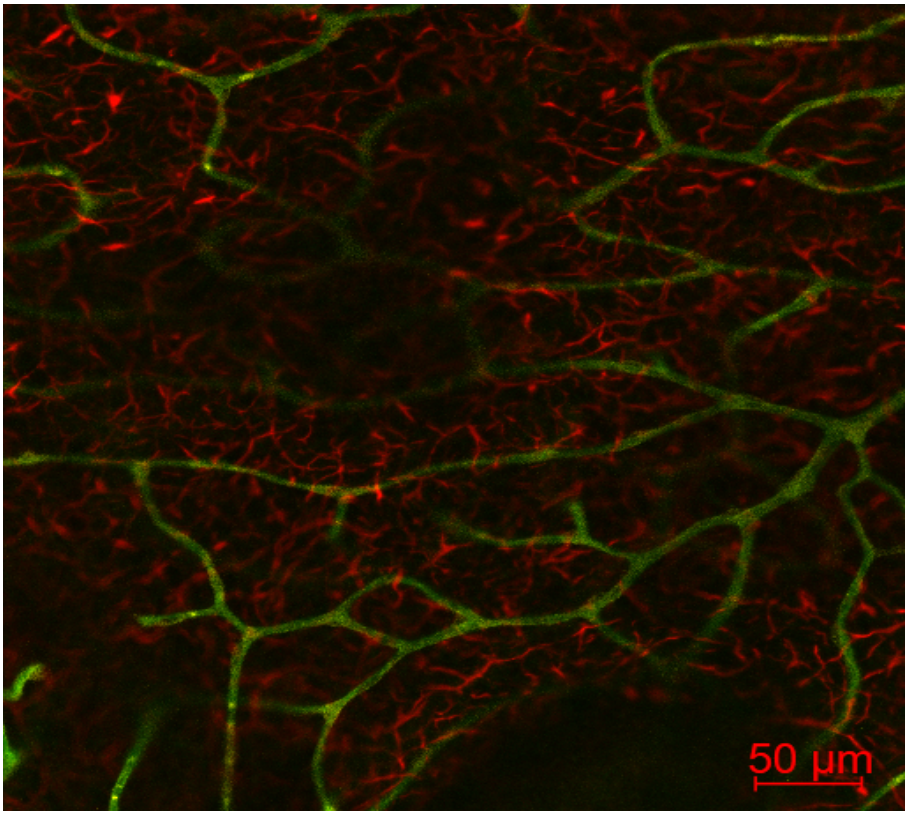

Appendix 7 : Split image showing syndecan-1 and lectin staining in the lower layers of the retina. The syndecan-1 staining at 3 hours showing up a network-like pattern which may be the connecting processes of the cells in the outer nuclear layer and plexiform layer (the cells would be the bipolar cells, and amacrine cells).